UNIVERSIDADE DE LISBOA

FACULDADE DE CIÊNCIAS

Departamento de Física

Study of the Interactions of Surface-Modified Particles with Membrane Model Systems

Mestrado Integrado em Engenharia Biomédica e Biofísica
Perfil em Engenharia Clínica e Instrumentação Médica

Melissa Margarete Jessen Sirage

Dissertação orientada por:
Professor Doutor Hugo Alexandre Ferreira

Doutora Liana C. Silva

2016

Acknowledgements

The realization of this master thesis was only possible under strong teamwork and individual dedication. At the end of this journey, there are some people I want to express my gratefulness.

First of all, I want to thank to Professor Hugo Alexandre Ferreira his supervision and support.

A great thank to my supervisor Doctor Liana C. Silva for all the support and supervision. Her precious meetings of discussion of results and all exigencies during the writing of this master thesis was of extreme importance.

Thanks to Professor Helena Florindo for accepting me in IntraCell_ADD group. Thanks for all the advices and supervision on the work done in microparticles. Thanks also for reviewing my master thesis.

I am grateful to all my colleagues for teaching, advice and guidance during laboratory work. Thanks a lot to João Oliveira Conniot, Carina Peres, Joana Silva and Eva Zupančič for accompanying me on my first steps on the laboratory formulating microparticles. A very special thanks goes to Ana Varela, Ester Ventura, Ana Carreira and also Andreia Giro dos Santos for supporting me during the confocal experiments and vesicles' formulation. Overall, thanks to all my colleagues for making IntraCell_ADD a lovely special group to work with!

Thanks to Ana Matos for the strong friendship, advices and gaiety. I am very greatful for all your advice.

A very special thanks to my lovely and exceptional family: parents, brothers, sister and sister in law. Thanks for all your unconditional support, all love and for teaching me and inspiring me so much. Thank you, thank you, thank you!!!

An extra special thanks to Fábio Mogas for all love, unconditional support and for helping me untangle when all seems complicate.

This master thesis marks the end of my Biomedical and Biophysics Engineering course. So I want to thank to all my wonderful colleagues from the course that at the same time became friends for live. Many thanks to Marina Costa, Neuza Silva, Carolina Vale, Gil Braz, André Girão, Mariana Trincão, Tiago João Ferro and Andreia Cândido e Silva. Mainly without all of you, these six years of faculty wouldn't represent *Anos Dourados* to me.

Abstract

The complexity of cell membranes and the development of nano/micro drug delivery systems make the topic of interactions between these two structures challenging. Studies point that the surface properties of these carriers like size, surface charge, shape and hydrophobicity largely influence such interactions. This project aims to study the interactions of surface modified Poly(lactic-co-glycolic acid) (PLGA) Microparticles (MPs) with Giant Unilamellar Vesicles (GUVs).

MPs were formulated by the double emulsion solvent evaporation method and surface modified using chitosan (CH) and alginate (ALG) in order to manipulate the surface charge. Five concentrations of coumarin-6 (0.04, 0.10, 0.20, 0.40 and 1.00 μg/mg) were entrapped into the PLGA matrix, after formulation optimization without probe. Phisichochemical characterization of MPs was made in terms of size, surface charge, coumarin-6 loading and morphology. Spectral properties of coumarin-6 were analyzed by fluorescence spectroscopy with the five different probe concentrations and five concentrations of MPs in suspension (0.10, 0.20, 0.25, 0.40, and 0.50 mg/mL). GUVs with different lipid composition and membrane properties, namely, homogeneously fluid GUVs and GUVs displaying gel-fluid and l_o-l_d phase separation were produced. Confocal microscopy was used to monitor the possible interactions between coumarin-6-loaded PLGA MPs and GUVs.

MPs size ($D_{50\%}$) of non-fluorescent and fluorescent coumarin-6-loaded PLGA MPs ranged between 1.4±0.3 to 3.8±0.2 μm. The span values ranged between 1.1±0.2 to 4.8±1.1, demonstrating polidisperse populations. The surface modification did not demonstrate a statistically significant impact on the $D_{50\%}$ values. In addition, the presence of coumarin-6 did not demonstrate a statistically significant impact on the $D_{50\%}$ values, except for PLGA ALG MPs loaded with 0.4 and 1.0 μg/mL of coumarin-6 ($p < 0.01$). As expected, the surface modification produced a statistically significant impact on the surface charge ($p < 0.001$). Negative surface charges were displayed for non-fluorescent and fluorescent PLGA PVA MPs (-17.8±0.9 to -19.9±0.2 mV) and for non-fluorescent and fluorescent PLG ALG MPs (-30.8±2.3 to -36.8±4.4 mV). PLGA MPs containing CH PLGA showed a highly positive surface charge (50.8±2.7 and 58.7±3.4 mV). The presence of coumarin-6 did not demonstrate statistically significant impact on surface charge.

Spectral studies showed that once increasing the MPs concentration in suspension no spectral changes were detected, suggesting that coumarin-6 did not change the partition environment to the surface and so remains on the hydrophobic matrix. In addition, this observation was further supported by the mainly linear variation of fluorescence intensity maximum upon increasing the concentration of the coumarin-6-loaded PLGA-C6 MPs, independently of their surface modification. At coumarin-6 concentrations above 0.2 μg/mg, the increase of the non-encapsulated molecules localized in the surface of the MPs or even aqueous medium was mainly evidenced by the decrease of anisotropy values. Regardless of MP composition, the red shift in probe emition of an aproximately 15 nm once increasing probe concentration from 0.04 to 1.00 μg/mg also account that observation.

Studies on the MPs-membranes interaction studies were performed under the following experimental conditions: i) concentration of coumarin-6 0.2 μg/mg and ii) MPs concentration 0.25 mg/mL. Data showed that highly positive PLGA CH-C6-3 MPs and highly negative PLGA ALG-C6-3 MPs interacted with GUVs and were mainly directed to the gel phase and interface of fluid-gel phases.

Results show that the MP surface modification plays an important role on surface charge. Entrapment of the fluorescent dye coumarin-6 conducts to a probe/MPs stable system. It was

demonstrated that surface charge and biophysical membrane behaviour are important on interactions of surface modified MPs and GUVs.

Keywords: Poly(lactic-co-glycolic acid) micoparticles, coumarin-6, surface charge, giant unilamelar vesicles, interactions.

Resumo

Os avanços feitos na área do transporte de agentes terapêuticos têm-se focado no desenvolvimento de sistemas à escala nano/micrométrica. Uma das vantagens desses sistemas promissores prende-se com a sua especificidade e eficiência na entrega do agente terapêutico à célula, tecido ou órgão alvo, permitindo a manutenção da concentração terapêutica desejada durante o tempo requerido. Deste modo, a quantidade de agente terapêutico no alvo será apenas a necessária e os efeitos secundários serão mínimos. Por outro lado, os estudos das membranas biológicas e dos sistemas modelo de membrana têm demonstrado que a membrana celular não é uma mera barreira entre o meio extra e intracelular. Na verdade, as evidências apontam para uma grande complexidade das membranas celulares, tanto ao nível da sua compartimentação estrutural e funcional bem como no papel activo dos lípidos na manutenção do equilíbrio celular. É na junção destes dois contextos – membranas celulares e sistemas de entrega à escala nano/micrométrica – que o tópico das interacções entre estes dois sistemas se torna tão desafiante e de grande interesse biológico.

Os estudos nesta área apontam que as características superficiais de nano/micro sistemas impactam significativamente as interacções entre estes dois sistemas. Características como tamanho, carga superficial, forma e hidrofobicidade de nano/micro sistemas parecem estar na base do mecanismo de interacção. Além do mais, alguns estudos apontam que aquando da interacção, estes nano e micro vectores podem interferir com a sinalização celular, induzir danos estruturais, alterar a expressão génica bem como modificar as características biofísicas das membranas celulares. No entanto, diversos estudos têm também demonstrado resultados contraditórios sobre quais dos factores primeiramente influenciam a interacção de nano/micro partículas. De facto, esta dependência pode também estar relacionada com o tipo de célula. Porém, o tópico das interacções ainda continua pouco estudado. A percepção clara dos factores que determinam o sucesso da interacção bem como do efeito imediato produzido na membrana celular irão permitir um desenho preciso destes sistemas de entrega de medicamentos. Além do mais, também irão possibilitar a modulação com melhor precisão do sucesso terapêutico e diminuir efeitos indesejáveis, como toxicidade. Assim, o objectivo deste projecto é desenvolver micropartículas (MPs) poliméricas modificadas à superfície para o estudo das interacções com sistema de modelo membranares.

O poli(ácido láctico-co-glicólico) (PLGA) foi usado como matriz polimérica das MPs. Estas foram formuladas usando o método modificado de dupla emulsão por evaporação do solvente. A superfície destas MPs foi modificada usando ácido polivinílico (PVA), quitosano (CH) e alginato (ALG), para que se obtivessem partículas com carga superficial neutra, positiva e negativa, respetivamente. A composição e processo de produção das MPs foram optimizados de forma a obter características físico-químicas desejadas, nomeadamente *span* (medida da dispersão das populações) menor que 1. Posteriormente, as MPs foram marcadas com a sonda fluorescente cumarina-6. Esta sonda foi encapsulada na matriz polimérica usando cinco concentrações de cumarina-6: 0.01, 0.10, 0.20, 0.40 e 1.00 μg/mg (μg/mg expressa a concentração de coumarina-6/polímero). Assim, as PLGA MPs não fluorescentes e fluorescentes foram caracterizadas tendo em conta o seu tamanho, carga superficial, forma, eficiência de encapsulação, capacidade de carga e características espectrais através de Difracção Laser, Dispersão Electroforética da Luz, Espectroscopia de Absorção e Microscopia Confocal (respectivamente).

De forma estudar a estabilidade e localização da sonda na matriz, foram preparadas cinco concentrações de MPs em suspensão: 0.10, 0.20, 0.25, 0.40, and 0.50 mg/mL. O estudo espectral, através de Espectroscopia de Fluorescência, permitiu também a optimização das condições

experimentais (em termos de concentração de cumarina-6 e de concentração de MPs em suspensão) da última etapa do projecto. Para o efeito, foram adquiridos espectros de emissão/excitação e os valores de anisotropia de fluorescência em estado estacionário foram medidos. Posteriormente, Vesículas Gigantes Unilamelares (GUVs) contendo diferentes composições lipídicas e propriedades biofísicas foram preparadas por electroformação e marcadas com rodamina. Assim, foram preparadas GUVs homogeneamente fluídas (POPC), GUVs com separação de fases gel-fluído (POPC/DPPC 1:1 mol/mol) e separação de fases líquido ordenado–líquido desordenado (POPC/SM/Chol 1:1:1 mol/mol/mol). Finalmente, para o estudo das interacções recorreu-se a microscopia confocal.

Os resultados demonstraram que as PLGA MPs não fluorescentes e fluorescentes têm diâmetros médios $D_{50\%}$ entre 1.4±0.3 e 3.8±0.2 μm. A presença da cumarina-6 não produziu diferenças estatisticamente significativas, excepto para PLGA ALG MPs carregadas com 0.4 and 1.0 μg/ml de cumarin-6 ($p < 0.01$). Os valores de *span* variaram entre 1.1±0.2 e 4.8±1.1, o que demonstra heterogeneidade. Os resultados de carga superficial (medida pelo valor de ZP) variaram significativamente com a modificação à superfície ($p < 0.001$). Tanto para MPs fluorescentes como para não fluorescentes, a carga superficial situou-se nos intervalos de [(-17.8±0.9)-(-19.9±0.2)] mV, [50.8±2.7-58.7±3.4] mV e [(-30.8±2.3)- (-36.8±4.4)] mV para MPs modificadas com PVA, CH e ALG, respectivamente. A introdução da sonda não produziu alterações significativas nos valores de ZP. A caracterização morfológica revelou que as MPs são esféricas, podendo adoptar, nalguns casos, forma de foice (indicador de instabilidade). A caracterização espectral de cumarina-6 demonstrou que os comprimentos de onda de excitação/emissão máximos ($\lambda_{ex\ max}$ e $\lambda_{em\ max}$) não variam significativamente com a concentração de suspensão de MPs e com o surfactante usado na formulação. Do mesmo modo, à medida que a concentração de MPs na suspensão aumenta, a intensidade máxima de fluorescência (F.I.) aumenta de maneira aproximadamente linear. Estes resultados demonstram que a sonda está essencialmente localizada na matriz polimérica e, deste modo, a sua partição entre o ambiente polimérico hidrofóbico e o ambiente hidrofílico que a rodeia, não é alterada. No entanto, com o aumento da concentração de cumarina-6 observou-se, no espectro de emissão da sonda, um ligeiro desvio de 15 nm para o vermelho. Os resultados das medidas de anisotropia mostram que para concentrações de sonda abaixo de 0.2 μm/mg, os valores são de aproximadamente 0.35, decrescendo para valores de 0.15, quando a concentração de sonda aumenta de 0.2 μm/mg para 1.00 μm/mg. A alteração dos valores de anisotropia e de desvio no espectro de emissão observado sugerem que, para altas concentrações, houve um aumento de moléculas não encapsuladas localizadas na superfície das MPs ou até mesmo na água. Tendo em conta o estudo espectral, a combinação de concentração de sonda/concentração de suspensão escolhida foi de [0.2 μg/mg; 0.25 mg/ml], pois representaram os valores medianos e os parâmetros analisados variarem linearmente. Além do mais, nessa concentração as imagens microscópicas adquiridas não teriam demasiada fluorescência.

Os sistemas de modelo membranares, GUVs, foram preparados com sucesso. As GUVs compostas por POPC apresentaram uma distribuição homogénea de Rodamina-DOPE (1,2-Dioleoil-sn-glicero-3-fosfaetanolamina-N-(lissamina rodamina B Sulfonil), demonstrando a sua fluidez. Por outro lado, as vesículas compostas de POPC/DPPC (1:1 mol/mol) apresentaram separação de fases gel-fluído. A mistura ternária POPC/SM/Chol (1:1:1 mol/mol/mol) mostrou separação de fases fluído-fluído. No entanto, nalgumas POPC/SM/Chol (1:1:1 mol/mol/mol) GUVs, também se verificou a separação de fases gel-fluído. Finalmente, os estudos das interacções demonstraram nenhuma aproximação às vesículas homogeneamente fluidas. As observações feitas demonstraram que apenas as PLGA MPs marcadas com sonda com carga superficial altamente positivas e negativas interagiram com as GUVs compostas por POPC/DPPC (1:1 mol/mol), na fase gel e interface das fases gel-fluído.

Resultados semelhantes foram obtidos com a mistura de POPC/SM/Chol, na qual as PLGA MPs modificadas com CH direccionaram-se para a fase líquida-ordenada.

Os resultados descritos mostram que o tipo de surfactante usado produz uma clara distinção de carga superficial. A sonda cumarina-6 demonstrou ser adequada para marcação deste tipo de MPs pois a sua encapsulação permitiu a produção de um sistema sonda/MPs estável. Os estudos de interacção revelaram que a carga superficial das MPs e fase biofísica das GUVs determinam as interacções entre estes sistemas.

Palavras-chave: Micropartículas ácido poli(láctico-co-glicólico), cumarina-6, carga superficial, vesículas unilamelares gigantes, interacções

Table of Contents

List of Figures

List of Tables

List of Acronyms

λ_{em} emission maxima wavelength

λ_{ex} excitation maxima wavelength

A absorbance

ALG Alginate

c concentration

CH chitosan

Chol Cholesterol

Coumarin-6 3-(2'-benzothiazolyl)-7-N,N-diethylaminocoumarin

DCM dichloromethane

DNA deoxyribonucleic acid

DPPC 1,2-dipalmitoyl-*sn*-glycero-3-phosphocholine

E.E. Entrapment Efficiency

EPC ethanolaminephosphoryl ceramide

G α-L-guluronic acid

GPI glycosylphosphatidylinositol

GUVs Giant Unilamellar Vesicles

$\mathbf{H_I}$ Hexagonal Phase

$\mathbf{H_{II}}$ Inverted Hexagonal Phase

l optical length

L Lamellar Phase

LUVs Large Unilamellar Vesicles

$\mathbf{L_\alpha}$ Fluid Phase

$\mathbf{L_\beta}$ gel state

$\mathbf{l_d}$ liquid disordered

$\mathbf{l_o}$ liquid ordered

λ_{max} adsorption maxima wavelength

ε molar absorptivity

L.C. Loading Capacity

M β-D-mannuronic acid

MPs microparticles

MRI Magnetic Resonance Imaging

NPs nanoparticles

(O) oil phase

PA phosphatidic acid

PE phosphatidylethanolamine

PEG poly(ethylene glycol)

PI phosphatinositol

PC phosphatidylcholine

PCL poly(*ε*-caprolac-tone)

PET Positron Electron Tomography

PG phosphatiglycerol

PGA Polyglycolic acid

PLA Poly(lactic acid)

PLGA *poly(lactic-co-glycolic acid*)

POPC 1-palmitoyl-2-oleoyl-*sn*-glycero-3-phosphocholine

PVA polyvinyl alcohol

PS phosphatidylserine

RGD Arg-Gly-Asp

Rho-DOPE 2-Dioleoyl-*sn*-Glycero-3-Phosphoethanolamine-N-(Lissamine Rhodamine B Sulfonyl)

RNA ribonucleic acid

SM sphingomyelin

SUVs Small Unilamellar Vesicles

Src proto-oncogene tyrosine-protein *kinase*

US-FDA United States Food and Drug Administration

T_m main transition temperature

TMC N-trimethyl CH

ZP zeta potential

(W) Water phase

CHAPTER 1: Introduction

In the last three decades, nanotechnology has become a promising approach in diverse research areas, like electronics, material engineering, biomedical engineering and pharmaceutics. The wide range specific surface area, size, shape, surface chemistry and crystalline structure provide nanostructures with unique properties and promising applications in drug delivery (1).

The efficient delivery of therapeutic agents that target specific sub-cellular compartments such as cytoplasm, nucleus, and mitochondria is crucial for their therapeutic success (2). Nano and micro drug delivery systems must cross one or various biological membranes (e.g. mucosa, epithelium, endothelium) and, after interacting with the plasma membrane, can thus be internalized by a process called endocytosis **(Figure 1.1)** (2,3). During endocytosis, the drug delivery system is first engulfed inside the plasma membrane through endosomes, invaginations of the plasma membrane. The carrier can then follow different intracellular trafficking pathways and reach specific sub-cellular compartments. Part of the therapeutic agent can be removed to the extracellular medium or to other cells, in the case of polarized cells.

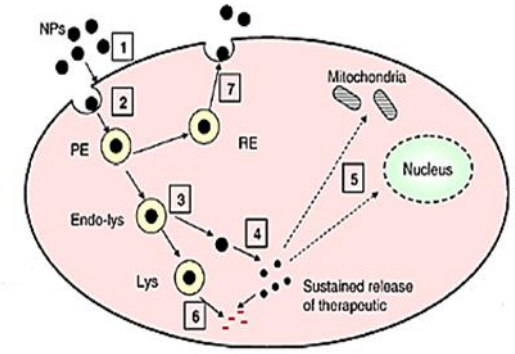

Figure 1.1 Representation of the uptake and internalization by endocytosis of the drug carrier systems, in this case, nanoparticles, NPs. (1) Plasma membrane association with the NPs (2) Internalization of the NPs by endocytosis. (3) Endosomal escape of the NPs (4) Release of the therapeutic agent in the cytoplasm (5). Transport of the therapeutic agent to the target sub-cellular compartment. (6) Degradation of the therapeutic agent in the lysosomes and cytoplasm. (7) Exocytosis of the NPs. PE: primary Endosome; Endo-Lys: Endo-lysossome; Lys: Lysossome; RE: reticulum endoplasmic. Adapted from (2)

Overall, during the endocytic process, drug carrier systems have some barriers to overcome until it reaches the target sub-cellular site: association with the plasma membrane and internalization through endocytosis; intracellular trafficking and delivery of the therapeutic agent or the drug carrier system in the cytoplasmic medium; and translocation to the nucleus or other cellular organelle (2,3). During the association with the plasma membrane, the interactions between the drug carriers and the

plasma membrane largely determine the successful passage to the interior of the cell. However, such interactions are still poorly studied. Due to the complexity of the plasma membrane and the properties of nano and micro drug delivery systems, the clear perception of how they interact is very important to control and understand the mechanisms of uptake by the target cells. As so, some features like size, morphology, surface charge (zeta potential, ZP) and surface chemistry of the nano and micro drug delivery systems, are widely acceptable as critical factors that control their interaction and further uptake by the biomembranes (4–6).

This dissertion is divided in 8 chapters:

Chapter 1 - Introduction
Chapter 2 – Literature Review contains a review on the properties of the polymeric microparticles and the surface-related features critical to the interactions with the cells. This chapter also includes an overview of historical perspective, structure, function and dynamics of the biomembranes.
Chapter 3 - Aims
Chapter 4 – Materials and Methods
Chapter 5 – Results includes a detailed description of the main results of the physicochemical characterization of the surface-modified microparticles. Also provides a detailed study on the spectral characterization of coumarin-6 entrapped into the MPs. Finally, this chapter contains the MPs-membrane interaction studies made under confocal imaging.
Chapter 6 – Discussion
Chapter 7 – Conclusion
Chapter 8 – Future Work Perspective

In aditition, suplementary data on spectral data is presented on Annexes.

CHAPTER 2: Literature Review

2.1 Drug Delivery Systems – Micro and Nano Systems

Modern drug delivery research is focused on the development of micro and nano delivery systems. These systems have the ability to deliver therapeutic entities to the target cell, tissue or organ in a more controlled, specific and reproducible way, while maintaining the release of the desired therapeutic concentration in a controlled rate and for an appropriate period of time (5). These systems provide minimal side effects by increasing the delivery of the therapeutic agent to the target site, thus requiring lower amount of therapeutic entity.

Nano and micro drug delivery systems should be biocompatible, non-toxic, non-allergic or non–inflammatory. In addition, several key parameters should be considered such as: size of the drug delivery system, entrapment method, stability of the therapeutic entity, mechanism of degradation of the matrix and the release kinetics of the therapeutic agent (6). The materials used as matrix can be diverse, including ceramic, gold, carbon, lipidic or polymers. Matrices that are biodegradable and bioabsorbable are the most preferred as will not require removal surgical operations. Therapeutic entities can be entrapped, protecting their functional properties, decreasing the risk of inactivation and toxicity for prolonged time. The release stimuli of the therapeutic agent includes activation of drug release by signals as pH variations, temperature, electric field and ultrasound or by degradation of the polymeric matrix (5). Additionally, release mechanisms include diffusion of the therapeutic agent and erosion of the matrix.

Examples of nano and micro delivery systems are micelles, liposomes, dendrimers, carbon nanotubes, solid-lipid nanoparticles, gold nanoparticles, polymeric nanoparticles (NPs) and polymeric microparticles (MPs).

2.1.1 Polymeric Microparticles

Polymeric MPs are spherical solid colloidal structures composed of a biodegradable polymeric matrix with more than 1 μm (7). Polymeric MPs are divided in microspheres and microcapsules, depending on their morphology, leading to distinct therapeutic agent distributions. In the first ones, the therapeutic agent is homogeneously dispersed or solubilized inside the polymeric matrix, while in microcapsules the drug is inside an individualized core surrounded by a polymeric membrane. The materials used in polymeric MPs formulation can be natural polymers like alginate (ALG), Chitosan (CH), collagen, dextran, gelatin and albumin. Regarding the synthetic polymers, these include the widely used Poly(lactic acid) (PLA), the copolymer poly(lactic-co-glycolic acid) (PLGA) and poly(ε-caprolactone) (PCL) (8). Polymeric MPs can be formulated using i) monomers by polycondensation or polymerization; or from ii) polymers by single or double emulsion with solvent evaporation, microfluid technology and spray-drying (8).

Regarding the single and double emulsion processes with solvent evaporation, both hydrophobic and hydrophilic molecules can be entrapped. Hydrophobic molecules are generally entrapped by single emulsion, while hydrophilic molecules are entrapped by double emulsion (9). Briefly describing the single emulsion method, the polymer is dissolved in an organic solvent such as

dichloromethane (DCM), oil phase (o) (10). The therapeutic entity is also added to that phase. Under appropriate stirring and temperature, this organic solution is emulsified in the presence of a large volume of aqueous surfactant solution, the water phase (w) (10). The resulting emulsion is an oil-in-water (o/w) emulsion. The organic solvent is allowed to evaporate under appropriate stirring and temperature conditions. The MPs are normally collected by centrifugation. Concerning to the double emulsion method (**Figure 2.1**), the polymer is dissolved in an organic solvent such as DCM, (o). The therapeutic entity is dissolved in the aqueous surfactant solution (w). The (w) is added to the (o) under appropriate stirring to allow the generation of the water-in-oil (w/o) emulsion (9,11). This emulsion is transferred to an aqueous surfactant solution, being then emulsified under strong stirring. The resulting emulsion is a water-in-oil-water (w/o/w) emulsion. The organic solvent is allowed to evaporate under stirring during several hours. The MPs are usually collected by centrifugation (9,11).

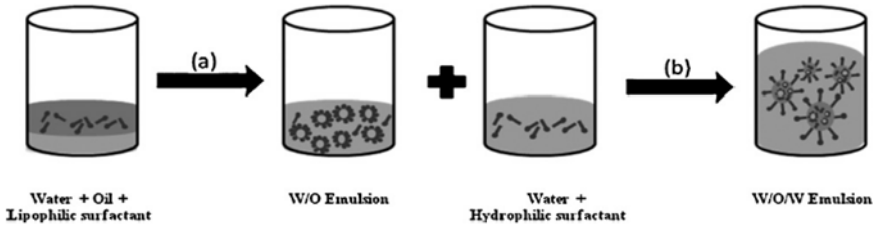

Figure 2.1 Double emulsion solvent evaporation method. (a) and (b) corresponds to emulsification steps (11).

2.1.1.1 PLGA Microparticles

PLGA is a synthetic biodegradable polymer widely studied in the last decades and used for several biomedical applications, namely in the fabrication of drug delivery devices such as NPs and MPs (10). PLGA-containing medicines have been approved by the United States Food and Drug Administration (US-FDA) for drug delivery due to polymers' high biocompatibility, biodegradability, and control of the drug release (12). PLGA can be implanted and carriers can be administrated by parenteral or non-invasive routes.

PLGA is polyester composed of the copolymers PLA and Poly(glycolic acid) (PGA) (**Figure 2.2**) and undergoes degradation through the hydrolysis of its ester linkages, producing those monomers that will be metabolized by the body via Krebs cycle. This phenomenon was demonstrated in various conditions *in vivo* and *in vitro* with different ratios of PLA and PGA and several types of bioactive molecules (10,13,14). The mechanism of degradation is the bulk degradation and so, the water penetration in the polymeric matrix is faster than the degradation, and therefore the erosion is uniform in the entire matrix surface. The release profile of drugs within the PLGA matrix is usually described by a biphasic curve, where initially the release is abrupt (called a burst) and the polymer molecular weight loss is not significant. The second phase consists on a slow release of the drug, commonly by diffusion (by passing water through the pores). The water inside the matrix hydrolyzes the polymer, leading to a significant loss of polymer molecular weight. Design factors like molar ratio of PLA and PGA, molecular weight of the PLGA, degree of crystallinity, drug hidrophilicity and pH of the environment determine the degradation rate.

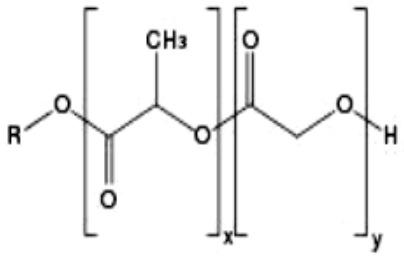

Figure 2.2 Chemical Structure of the copolymer PLGA. X represents the number of units of PLA and Y the number of PGA units (10).

The PLGA-based drug delivery systems have been studied to deliver proteins, peptides, deoxyribonucleic acid (DNA), ribonucleic acid (RNA) and drugs (10). PLGA MPs can be prepared by single or double emulsion with solvent evaporation, phase separation (coacervation) and spray-drying. Usually, these MPs are prepared by the emulsion solvent evaporation method. The polyvinyl alcohol (PVA) is the most widely used surfactant to stabilize the emulsion and to reduce the surface tension because it generally allows the formulation of MPs with uniform size distribution, it is easy to disperse in aqueous medium and easily washed (15). In fact, due to its amphiphilic nature, PVA has excellent emulsifying properties being also able to increase the viscosity of the continuous phase. However, the use of PVA has raised some concerns regarding its carcinogenic potential and toxicity (16). Complications like anemia and infiltration in various tissues and organs were reported when subcutaneously injecting 5 % (w/v) PVA aqueous solutions in rats (17).

The biomedical applications PLGA MPs include the diagnostic and treatment of cancer, cardiovascular disease and diabetes, development of vaccines, among others.

In tumor imaging, the use of imaging techniques like Magnetic Resonance Imaging (MRI), ultrasounds and Positron Electron Tomography (PET) in combination with PLGA MPs entrapped imaging contrast agents is an important approach for the diagnostic and study of the tumoral area *in vivo*. Lavisse *et al.* developed PLGA MPs with size distributions of 1 to 15 μm to acoustically characterize and select the most suitable to encapsulate the ultrasound contrast agent and then, perform a preliminary *in vivo* study in melanoma grafted mice using Doppler ultrasonography. PLGA MPs of 3 μm showed the best results, inducing an enhancement of 47% of intratumoral vascularization visualization after the MPs injection (18). In cancer disease treatment, PLGA MPs linked with antibodies or targeting ligands such as cytokines, hormones, vaccines and chemotherapeutic agents are employed to treat malignant tumors with high specificity and affinity (12). Yemisci *et al.* developed PLGA MPs loaded with mitoxantrone to treat malignant glioma (19). In this study, wister were divided into three groups: i) rat glioma (RG2) cells and blank PLGA MPs were simultaneously implanted, ii) RG2 cells and mitoxantrone loaded-PLGA MPs were simultaneously implanted and iii) RG2 cells was implanted and mitoxantrone loaded-PLGA MPs were injected after 7 days. Results demonstatred that mitoxantrone loaded-PLGA MPs reduced significantly the tumor volume of the rats belonging to group iii). No tumor formation was observed in rats belonging to group ii). In addition, results showed no systemic side effects or parenchymal inflammatory infiltration in either groups .

PLGA MPs were also studied to deliver growth factors (such as cytokines) to the heart to treat cardiac failure after a myocardial infarct, in a rat model of myocardial infarction. The results showed a high angiogenic and arteriogenic effect (8).

Regarding the development of vaccines, PLGA is the most studied polymer in this field because it is a promising candidate to deliver antigens and adjuvants to the target site with a controlled release profile (12,20,21). PLGA MPs have been used as a delivery vehicle of antigens in injectable administration (20). Peyere *et al.* developed PLGA MPs prepared by spray-drying or coacervation loaded with tetanus or diphtheria toxins, acting as a multivalent vaccine. The PLGA MPs were administrated subcutaneously by single injection in guinea pigs and the results showed a high immunogenic effect compared with the same dose injected with the licensed divalent vaccine (20).

2.1.1.2 Surface modification of PLGA Microparticles

PLGA NPs and MPs can be surface-modified by functionalization with target ligands and antibodies, or alternatively by coating with hydrophobic and hydrophilic polymers. Surface modification can be used in order to manipulate several chemical surface properties, such as hydrophobicity, hydrophilicity and surface charge (22). In this way, surface modification will help to modulate the entrapment efficiency and the release of the therapeutic entities and also to improve the interactions between the PLGA NPs/MPs systems with the cells (23). This section will briefly review the properties of the polymers CH and ALG, which can be used to modify the surface of PLGA NPs and MPs.

CH is a natural polymer used in the pharmaceutical field since 1990. It is very attractive to use in drug delivery systems because of its biocompatibility, "non-toxicity" and cationic properties due to the presence of the primary amino groups. In fact, the presence of its amino groups is responsible for important properties such as controlled release and the mucoadhesion. The mucoadhesion is achieved due to the interaction of positively charged CH MPs and the negative charge of mucosal surfaces (24). As a drug carrier system, CH has been used in the fabrication of membranes, tablets, NPs and MPs which can be administrated via oral, nasal, ocular, vaginal, buccal, parenteral and intravesical routes (24). CH is obtained by the deacetylation at high temperatures of chitin, which is the main constituent of the exoskeleton of crustaceans. Structurally, it is a linear polyaminosaccharide, composed of the copolymers of β-(1–4) linked 2-acetamido-2-deoxy- β-D-glucopyranose and 2-amino-2-deoxy- β-D-glycopyranose (**Figure 2.4**) (24–26). CH is soluble in aqueous acidic solutions and insoluble in water and organic solvents. However nowadays there are some derivates such as N-trimethyl CH (TMC) that are water soluble (27).

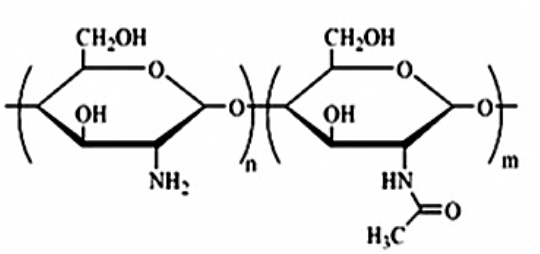

Figure 2.3 Chemical structure of CH (26).

It is known that the entrapment efficiency of the therapeutic agent in CH MPs increases with the increase of CH concentration (25). Typically, solutions with high concentrations of CH have higher viscosity and avoid the formation of drug crystals from leaving the droplets (25). Additionally, it is known that the molecular weight of CH influences the release of the therapeutic agent from the MPs. A decrease in the release velocity is observed with increasing of the CH molecular weight

because of the higher viscosity of the gel layer in the drug delivery system, which affects the diffusion of the therapeutic agent (25).

Some of the biomedical applications of PLGA NPs and MPs surface modified with CH include the diagnostic and treatment of cancer and development of vaccines. Chandy *et al.* developed PLA MPs and PLGA MPs coated with CH or PVA loaded with 5-Fluorouracil (a hydrophilic antimetabolite used in cancer therapy), prepared by double emulsion solvent evaporation. Results from scanning electron microscopy revealed that CH-coated MPs had less surface pores than the PVA-coated MPs. This was reflected in the drug release profile, which was slower in CH MPs than in the PVA MPs. This work demonstrated that PLGA MPs coated with CH are promising carriers for a prolonged release of anti-tumor drugs (28). The high mucoadhesive properties of CH increase significantly the amount of macromolecules absorbed in mucosal barriers when administrated with this polymer (26,29–31). Kawashima *et al.* prepared PLGA NPs surface modified with CH, poly(acrylic acid) and sodium alginate for oral administration (31). These NPs systems entrapped the peptide elcatonin. By measuring the PLGA NPs adsorbed to a rat everted instestinal sac (*in vitro*), their mucoadhesive properties were evaluated. Results showed that surface modified CH PLGA NPs showed higher mucoadhesion to the everted intestinal tract in saline than the other PLGA NPs (31).

ALG is a natural, biocompatible, biodegradable and "non-toxic" polymer used in several biomedical applications such as tissue engineering and drug delivery (32). In drug delivery, alginate has been used to prepare gels, matrices (as an encapsulating material to cell culture and transplant), membranes, NPs and MPs (32,33). ALG is approved by the US-FDA as a safe material for use in the alimentary field, having the designation of "Generally Referred as Safe" (34). Structurally, alginate is a linear polysaccharide composed by residues of α-L-guluronic acid (G) and β-D-mannuronic acid (M) linked by 1-4 linkages, which generates homopolymeric MM and GG segments interposed by heteropolymeric segments of MG or GM (**Figure 2.4**) (32,33). ALG is pH-sensitive due to the pendent acid groups that, in different pH, accept or release protons.

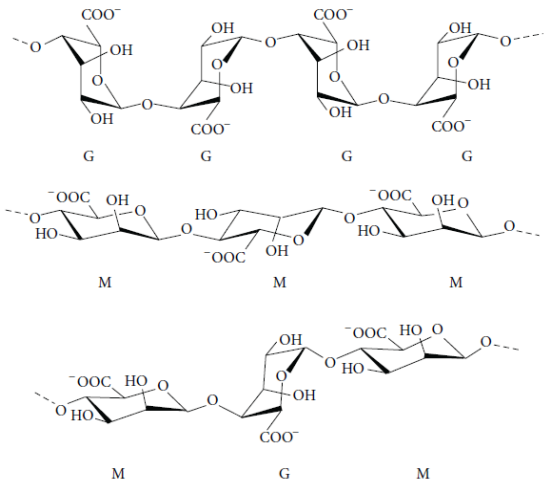

Figure 2.4 Structure of Alginate: GG, MM and MG segments (34).

The production of ALG can be from two sources: algae and bacteria. Regarding the extraction from bacteria, it is important to mention that it is normally restricted to some research studies, due to the high cost of the process. Hence, commercial ALG is mainly extracted by alkaline extraction, from brown algae: the algae is collected, dried and submitted to chemical treatments to remove undesired

substances like heavy metals, endotoxins and proteins, and is converted to a powder material in the acid or salt form (33).

The biomedical applications of ALG-surface modified PLGA NPs and MPs include e.g. the development of vaccines. Mata *et al.* developed PLGA MPs and ALG surface modified PLGA MPs to malaria vaccination (35). These microparticulate systems entrapped the malaria synthetic peptides SPf66 and S3 and the humoral and cellular immune responses were evaluated after intradermal immunization. Results showed that the incorporation of ALG caused higher humoral and cellular immune responses (35). Additionally, the administration of PLGA MPs coated with Arg-Gly-Asp (RGD)-modified ALG showed higher cellular responses such as interferon-γ secretion and lymphoproliferation. Actually, this observation was an evidence of cell targeting (35). ALG has also been described as mucoadhesive polymer, improving the delivery of molecules to the mucosal tissues (23,36). Ungaro *et al.* developed PLGA NPs surface modified with ALG or CH to the production of dry powders for the tobramycin antibiotic inhalation (36). PLGA NPs were embedded in an inert microcarrier made of lactose. Results showed that surface modified ALG PLGA NPs allowed efficient antibiotic entrapment and achieved its release up to one month. The *in vivo* biodistribution studies demonstrated that plain PLGA NPs and ALG surface modified PLGA NPs reached up the deep lung. On other side, CH surface modified PLGA NPs reached the upper airways, the lining lung epithelial surfaces (36).

2.1.2 Impact of Physicochemical Surface Properties of Nano and Micro Systems in Cellular Uptake – size, surface charge, shape and chemistry

Understanding the mechanism of interaction between cell and the nano and micro drug delivery systems is essential to the efficient design and safe application of drug targeting strategies (37). The cellular uptake can be described as a combination of attractive and adhesive interactions between the carrier and the plasma membrane and the driving force for wrapping (38,39). The driving force for wrapping can be described as the amount of free energy required to produce the deformation and drive the carrier to the internal medium of the cells (38). This process is dependent of some factors such as the size, shape, surface charge and surface chemistry of the carrier, rigidity of the plasma membrane and receptor abundance (38,39). Thus, the study and optimization of the impact of these parameters can lead to the development of smarter and safer drug delivery systems. This section is focused on the significance of the characteristics of the surface of the nano and microcarriers in the context of their interaction with plasma membranes (**Figure 2.5**).

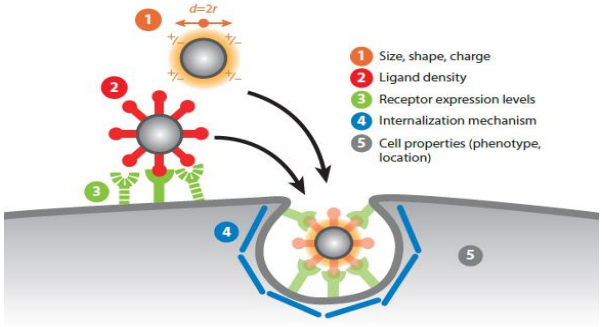

Figure 2.5 Factors that influence the cellular uptake of the nano and micro drug delivery systems. The cellular uptake is dependent of factors of the carrier such as size, shape, surface charge and chemistry. In the feature chemistry we can considerate the surface composition, ligand density, hydrophobicity and hidrophilicity. On the other side, cell properties like the receptor internalization levels, internalization mechanism, phenotype, localization and also the rigidity of the plasma membrane also affect the cellular uptake. (58)

It has being reported that the drug carrier size is not the only factor involved in the cellular uptake, however it is determinant to that process (1,4,37,40–43). Theoretical models and its supported experimental evidence have suggested that to achieve effective cellular uptake, NPs must have a minimum size of 30-50 nm (44–48). This minimum range of size seems to be necessary to produce the required driving force for wrapping, leading to the deformation and invagination of the plasma membrane. Each cell can have differential levels of expression of target receptors, leading to an enhancement of the recognition of certain ligands. It should be noted that the range of sizes above mentioned corresponds to the scenario where the concentration of ligand on the NPs surface, when present, and the receptor abundance are not limiting factors. In addition, it was observed in *Acanthamoeba* that large carriers roughly with 250 nm -3 μm are faster internalized than particles with diameters less than 250 nm (41,49) . The different mechanisms of internalization displayed by the cells also contribute to different uptake mechanisms of drug carriers in terms of size (1,3,42). Actually the nonphagocytic mechanism allows the internalization of fluids and soluts. The phagocytic mechanism allows the internalization of large particles i.e more than 0.5 μm. In this way, NPs are preferently internalized by other endocytic processes that are not restricted to phagocytic cells (42,50). However, MPs are preferentially internalized by phagocytosis in phagocytic cells such as macrophages, neutrophils, monocytes and dendritic cells. MPs can be also non-specifically internalized by macropinocytosis, when their diameters range from 0.5 μm to 10 μm (3). There is evidence that other types of cells, referred as nonprofessional phagocytes like fibroblasts, epithelial and endothelial cells can display the phagocytic mechanism but at a lower extent (3,41). Dendritic cells have shown an optimal uptake of particles with diameters up to 10 μm (37). Regarding macrophages, they have shown that the optimal diameter of particles is up to 30 μm (37). Considering the efficient permeation in biological barriers, the nano sized drug delivery systems are usually more efficient than the larger ones and so NPs have higher rate of uptake compared to MPs (15,51). NPs penetrate throughout the submucosal layers while MPs stay mainly in the epithelial lining; some NPs can cross the blood-brain barrier through the opening of tight junctions by hyperosmotic mannitol, passing through the capillaries after their injection and achieving the stability in blood circulation (15,51). Thus, for targeted drug delivery, the size of 100 nm or less are usually preferred (15,51).

Polymeric particle surface charge is a parameter that highly affects the uptake and therefore, the selectivity and efficiency of all drug delivery systems (50). Surface charge is the result of the chemical nature of the polymer matrix, the stabilizing agent and the pH of the dispersant medium (37). Evidence suggests that cells preferentially take up charged micro and nanocarriers instead of the neutral ones (3,42,52,53). To the positive carriers is associated a high rate of uptake and internalization, that can be explained by the ionic interactions between cationic polymers of the particles and the negative charge of the plasma membrane of the target cells (37). MPs and NPs containing cationic polymers, like stearylamine-coated PEG-co-PLA, PLGA modified with PLL and CH, are a good example of this finding (42) . Yue *et al.* prepared positive, negative and neutral CH NPs with an average diameter of 215 nm and showed that positive charged CH NPs (ZP≈39.25 mV) allowed a significant increase of the amount and rate of cellular uptake in all the cell lines tested (54). However, there is also evidence of the uptake of negative nano and microcarriers. This mechanism is associate to a slower internalization, as compared with the positive counterparts (1,3). The involvement of non-specific interactions with non-specific receptors by electrostatic interactions can explain the uptake of negatively charged carriers. Electrostatic interactions with the positive site of the proteins of the plasma membrane can trigger their uptake (55). In addition, phenomenon like oxidative stress to the plasma membrane can favor the adhesion of negatively charged carriers (56). Lao *et* al. demonstrated that under normal conditions, fullerene NPs are repulsed by cerebral microvessel

endothelial cells. Under oxidative conditions, the negative charge of the cell surface is decreased and these NPs adhere (56).

The shape of two interacting bodies can significantly affect the superficial adhesion (57). Actually, the nano and micro drug delivery systems, specially the polymeric ones, are centered in spherical shapes (58). Champion *et al.* developed polystyrene MPs of various sizes and shapes, as spheres, oblate ellipsoids, prolate ellipsoids and rectangular discs. They demonstrated that, instead of size, the shape is a highly significant parameter in the uptake of these MPs by alveolar macrophages (59). The orientation of the MPs in the point of contact with the cell also plays an important role in the internalization – this local shape dictates the actin structure that must be created to initiate the internalization process, allowing the membrane moving over the MPs. When the required actin structure is not created, the internalization does not happen and there is just a spreading. It must be emphasized that size is more important than shape when the volume of the particle exceeds the volume of the cell (59). Other studies have suggested that cells display selectivity in terms of the shape of the drug carrier captured. Hutter *et al.* prepared rod, spherical and spiky shaped gold NPs and showed that spiky gold NPs are preferentially taken up by microglia cells (60). However, only rods are internalized by the nonphagocytic neuron cells. It should be noted that some studies have shown that these new shaped drug delivery devices are associated to significant toxic effects due to its accumulation (61).

Chemical properties such as surface composition, functionalization, hydrophobicity and hydrophilicity play an important role in cellular uptake of MPs and NPs (22). Evidence shows that nano and microcarriers with different surface chemistry have increased uptake when they are more hydrophobic (37). In PLGA NPs and MPs, it was shown that hydrophobicity affects the cellular uptake due to the fraction of PVA that remains on the particle surface. PLGA NPs and MPs are more hydrophilic when they have a greater amount of PVA associated to its surface and so, the cellular uptake of these particles is reduced (15). Y. L. Chiu *et al.* demonstrated that NPs prepared with a hydrophobically-modified CH with more palmitoyls groups present on the surface of the particles have higher interaction with cell membranes (62). The surface of the nano and micro drug delivery devices can be functionalized with some target ligands - biomolecules like peptides or chemical groups - to confer a more specific delivery of the target cell and enhance the uptake. Surface functionalization can reduce the surface reactivity, the toxicity or enhance the stability. In fact, the surface adsorption of proteins, like transferrin, or other molecules, such as citric-acid, by the nano and micro drug delivery devices can lead to a higher uptake by the cells. Coating with cell penetration peptides such as poly(L-lysine) and arginine-rich peptides or cell-fusogenic peptides like the ones found in some viruses, is an efficient approach to increase the uptake by the cells. Some cell penetration peptides have hydrophilic residues interchanging with hydrophobic residues, which can be an interesting approach in the modulation of cell uptake (1). On other side, the surface modification with the hydrophilic non-ionic polymer poly(ethylene glycol) (PEG) is a common approach to promote the escape of NPs from the reticulo-endothelial system, increasing their time in the blood circulation (42).

2.2 Biomembranes – structure and importance

Biomembranes are complex and dynamic organization of lipids and proteins and glycids that surround the cells and create a boundary between the intracellular medium and the extracellular medium (63–65). Biomembranes act as a matrix for the organization and to the dynamic interactions

between their molecules, connecting its different compartments (66). Eukaryotic cells have a plasma membrane and intracellular membranes that encase cellular organelles, while prokaryotic cells have just the plasma membrane.

Plasma membrane regulates the type of molecules that cross the cell and the amount of each molecule. This barrier function of biomembranes underlies the formation, maintenance and use of the transmembranar solute gradients, essential to cell metabolism and production of energy (64). Biomembranes are also responsible for the selection and release of molecules via endocytosis and exocytosis, and are sensitive to chemical changes in the environment such as pH, temperature, pressure, salinity, ionic strength and hydration state (64). The accumulated evidence have suggested that the function of the cell membranes is achieved by interactions among the membrane components that build functional compartments with specific lipid and protein composition and biophysical properties (63). Their lipids can be bioactive entities (67). The bioactive lipids can act as first or second messengers in signal transduction (67). On other hand, bioactive lipids can act as regulators of the biomembrane organization, allowing the aggregation or segregation of certain proteins (67).

2.2.1 Historical Perspective

The investigation of the structure of the biomembranes started on the 19th century, when Charles Ernest Overton (1895) during his doctoral degree, investigated substances that freely passed into cell plants (68). He found that the membrane has a selective permeability and that this is related to the partition coefficient between water and oil and the chemical nature of each substance. Overton suggested that the cells were surrounded by membranes composed by lipids and cholesterol. Later, in 1917, Irving Langmuir, during his research in molecular monolayers of lipids, studied the interaction between oil films and water. He proposed that a monolayer is composed by molecules of fatty acids oriented vertically with the polar headgroups to the surface of the water and the hydrocarbon chains oriented to the air phase (68). In 1925, Gorter and Grendel proposed that cell membranes are composed by a lipid bilayer where the polar headgroups were oriented to the aqueous medium. Danielli and Davson proposed the first membrane model accepted by the majority of the scientific community – arrangement of an amphiphilic phospholipid bilayer covered on both sides with proteins - the Sandwich Model. With the development of the electron microscopy, J. David Robertson confirmed the experimental findings of Gorter and Grendel and Danielli and Davson (68). In fact, he extended the concept of cell membranes to subcellular organelles like mitochondria and nucleus and concluded that there was evidence for a common structure for all biomembranes. In 1972, Singer and Nicolson proposed the Fluid Mosaic Model (**Figure 2.6**) which describes that biomembranes are fluid entities composed by a supporting matrix of a phospholipid bilayer that act as a solvent for proteins (69). The model also highlighted the distinction between integral proteins, as the ones that penetrate to the core of the lipid bilayer, and peripheral proteins, as the ones that are attached to the plasma membrane surface on the cytoplasmic side (69). This model considers that lipids and proteins can freely diffuse laterally in the biomembrane. Additionally, the model also considers that some lipids may interact specifically with the membrane proteins (69).

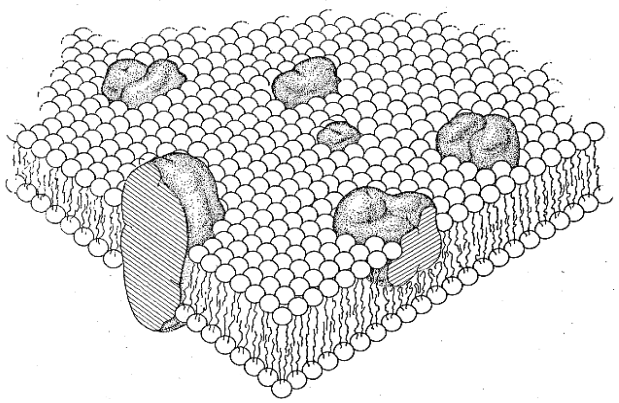

Figure 2.6 Schematic representation of the Fluid Mosaic Model, proposed by Singer and Nicolson. This model proposes a non-compartmented perspective of biomembranes composed by a lipid bilayer and integral and peripheral proteins, non-homogenously distributed along the biomembrane. (69)

Although the Fluid Mosaic Model is still the main concept that explains the basis of the structure of biomembranes, the subsequent research supported by new experimental techniques provided novel structural features. Taking into account the asymmetric distribution of the different lipid species along the inner and outer leaflet of biomembranes proposed before, in 1997 Kai Simons and Elina Ikonen, in the Raft Model, proposed the existence of specialized lipid domains that appear in a time and space-dependent manner (70). This model also proposes that these specific domains are responsible for lipid-lipid and lipid-protein interactions (70). In fact, currently biomembranes are viewed as highly compartmentalized entities due to the heterogeneities in organization, asymmetric distribution of lipids and protein organization (**Figure 2.7**). In addition, biomembranes are also currently viewed as dynamic entities due to its components interactions.

In 2005, Kusumi *et al.* proposed the Fence Model that describes that the cell membranes compartments are delineated by the cytoskeleton meshwork that act as "fences" anchored to the intrinsic proteins acting as the "pickets" to the lipid movement (71). This protein arrangement confines the lipids for a certain time in a compartment, serving as a diffusion barrier, where molecules diffuse rapidly by Brownian motion and escape from one compartment to the next by hop diffusion or through transient gaps in the barrier (71)**.**

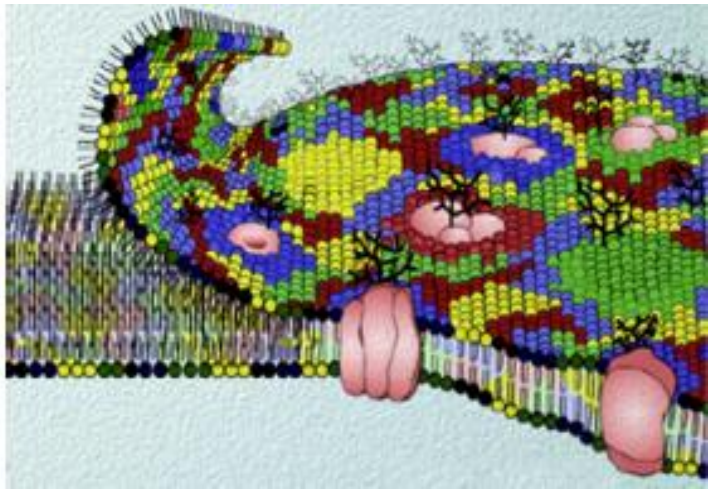

Figure 2.7 Schematic representation of the update view of the Fluid Mosaic Model. Lipid bilayer is highly compartmentalized, due to the heterogeneous lipid distribution along the bilayer. Like in the first version of this model, proteins here appear with a non-homogeneous distribution and are also classified as integral and peripheral. Adapted from (80)

2.2.2 Types of Biomembrane Lipids

Biomembranes are composed by lipids, proteins and glycids, these last always in the form of glycolipids or glycoproteins. The major components of biomembranes are lipids and they exist with a high variety that, in eukaryotic cells, can be achieved through modifications in the hydrophilic head group and the hydrophobic carbon chains (67,72). Biomembranes lipids can be divided in three main classes of lipids:

- **Glycerolipids –** mainly the glycerophospholipids (65). They are composed of fatty acyl chains of a number of carbon atoms ranging from 14 to 22. These acyl chains can be saturated or unsaturated with variable degree of unsaturation, in the *sn-1* and *sn-2* positions (stereospecific number, *sn*) (67,72). The *cis* isomer is the most common isomer but the *trans* isomer can also be present (67,72). The two nonpolar chains compose the hydrophobic part and are linked to a glycerol via ester or alkyl ether or alkenyl ether bond (67). In the *sn-3* position of the glycerol backbone, is placed the phosphate group that can be linked to different chemical groups (hydrophilic part), leading to different glycerophospholipids, including: phosphatidylcholine (PC), phosphatidylethanolamine (PE), phosphatidylserine (PS), phosphatiglycerol (PG), phosphatinositol (PI), and the unmodified, phosphatidic acid (PA) (67,72). PC is the most abundant in eukaryotic cells, accounting more than 50% of the total glycerophospholipids of biomembranes (64,67). In fact, the chemical headgroups define the charge of the whole lipid. Accordingly, at physiological pH, PA, PS and PG are anionics, whereas PC and PE are zwitterionic (65); (**Figure 2.8**)
- **Sphingolipids –** are composed of a shingoid base that is amine linked to a fatty acid (73). The sphingoid base, in mammalians, is typically sphingosine or sphinganine. Sphingosine has 18 or 20 carbon atoms, a *trans* double bound between the carbons 4 and 5 and two hydroxyl groups placed at carbons 1 and 3 (73). Sphinganine is the saturated form of sphingosine. The fatty acid has typically 16-24 carbon atoms and can be saturated or monosaturated. Ceramide is the simplest sphingolipid and the backbone of all complex sphingolipids. Ceramide can be phosphorylated to yield Ceramide 1-Phosphate; glycosylated to form complex glycosphingolipids; or form sphingomyelin (SM) or ethanolaminephosphoryl ceramide (EPC) through the addition of a phosphocholine or phosphoethanolamine headgroup to the ceramide backbone, respectively (72,73). **(Figure 2.8)**
- **Sterols –** composed of a steroid ring (hydrophobic part) linked to a hydroxyl group (hydrophilic part). Cholesterol (Chol) is the most common in mammalian cells (65,67). **(Figure 2.8)**

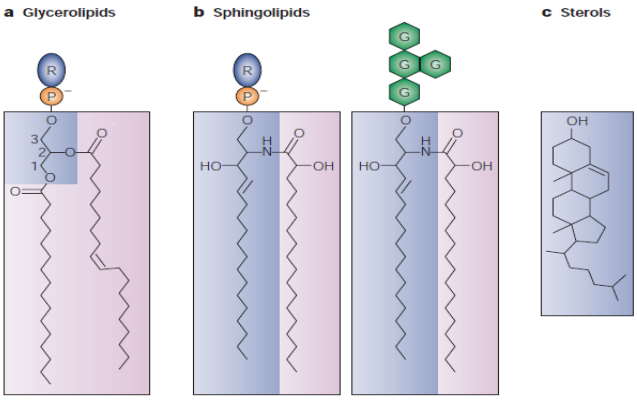

Figure 2.8 Schematic representation of the three main types of lipids in eukaryotic membranes. (a) Glycerophospholipids. They are composed of two fatty acyl chains, represented in pink that are linked to the glycerol (blue shading). In the *sn-3* position of the glycerol is placed the phosphate group, represented by the orange circle. The phosphate group can be associated to serine, inositol, ethanolamine, choline and glycerol, leading to phosphatidylserine (PS), phosphatinositol (PI), phosphatidylethanolamine (PE), phosphocholine (PC) and phosphatiglycerol (PG), respectively. These substitutions on the phosphate group are symbolized by the R blue circles. Glycerophospholipids without the headgroup form the phosphatidic acid (PA). (b) Sphingolipids. They are composed of a sphingoid base represented in blue shading, amine linked to a fatty acid (pink shading). This is the constitution of Ceramide (Cer), the simplest sphingolipid. The introduction of phosphocholine or phosphoethanolamine (blue circles) to the headgroup of the ceramide backbone yields sphingomyelin (SM) and to ethanolaminephosphoryl ceramide (EPC), respectively. The introduction of glucose or galactose groups (green hexagons) gives rise to the formation of complex glycosphingolipids. (c) Sterols. They are composed of a sterol ring linked to a hydroxyl group. In mammalians, cholesterol is present, ergosterol in fungi and stigmasterol and sitosterol in plants. Adapted from (120).

2.2.3 Membrane Lipid Phases

Lipids can adopt different supramolecular structures, which are influenced by a number of factors like temperature, pressure, pH, salinity, ionic strength, hydration state and shape (64,67). Lipid phases can be divided in lamellar (L) and non-lamellar (67). The main L phases are: i) gel or solid ordered (L_β) ii) fluid (L_α) that is further divided in liquid ordered (l_o) and liquid disordered (l_d). The main non-lamellar phases are the hexagonal and cubic.

The L is the most representative in cell membranes under normal conditions. Structurally, the headgroups face the aqueous medium in both sides of the biomembrane and the acyl chains oppose each other, forming a lipid bilayer (74). The thickness of the bilayer is roughly similar to the hydrocarbon length (74). The presence of unsaturations along the acyl chains reflects a decrease in the thickness of the bilayer. When a *cis* double bound is introduced, it produces a permanent kink in the acyl chain, increasing the cross-sectional area of the lipid and decreasing the average length of the acyl chain, in order to maintain the total volume (74).

In the gel phase, L_β, the hydrocarbon chains of the phospholipids are in the all *trans* configuration and so, are fully extended. Thus, this leads to a small cross-sectional area per lipid molecule and a maximum bilayer thickness (**Figure 2.9**) (75). The hydrocarbon chains with small headgroups are aligned perpendicular to the surface of the lipid bilayer, being ordered side-to-side. To optimize the packing of the lipids, the ones with larger headgroups (like PC) have their hydrocarbon chains tilted (75). In this phase, the lipid motion is greatly restricted, giving rise to a highly

impermeable ordered structure. It is noted that L_β is formed at low temperatures and in presence of low amount of water.

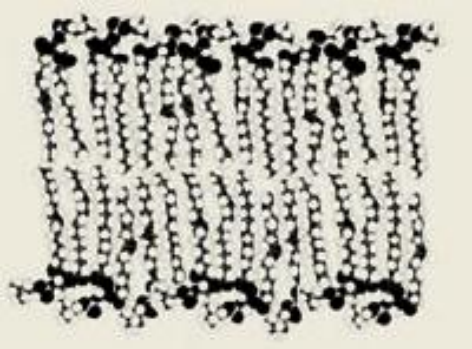

Figure 2.9 Schematic representation of the gel phase where is noted the maximal bilayer thickness and the high packing of the lipids. Adapted from (67)

The fluid phase,L_α, occurs in the presence of higher water content, the thickness of the bilayer and the order of the acyl chains decreases relatively to the L_β phase (76). In fact, due to the separation distance and the increase of the cross sectional area of the chains, the fatty acyl chains are arranged parallel to the bilayer surface and in lipids with larger headgroups, its hydrocarbon chains do not need to be tilted. Lipids display a fast lateral diffusion and move freely within the membrane leaflet with a direction perpendicular to the plane of the membrane. In other words, L_α is a two dimensional fluid (66,74). According to the degree of internal freedom, L_α can be further divided into liquid ordered (l_o) and liquid disordered (l_d) phases (**Figure 2.10**) (77). In l_o phase, the hydrocarbon chains are highly ordered and extended (as in the L_β) and exhibits high lateral mobility, characteristic of fluid states (65,67)**.** This lipid arrangement is adopted in the presence of cholesterol, which is able to insert in the free spaces between the acyl chains, acting as a stabilizer of this phase (66). Cholesterol has a preferential partition to the l_o phase, where the highly ordered acyl chains of the lipids provide a tighter packing of the sterol ring. In the l_d phase, the acyl chains are highly disordered and the motion of the acyl chains of the lipids is higher than in the l_o phase. l_d is mainly composed of glycerophospholipids with unsaturated acyl chains (65,67).

Besides all the controversy, the accumulated studies consider that biomembranes are normally in the fluid phase (l_o phase l_d) (65). It should be noted that the actual literature considers that the L_β is not physiologically relevant (76). Actually, it was argue that the high lipid packing is not consistent to the proper function of proteins. However, some studies point that L_β is physiologically relevant (78).

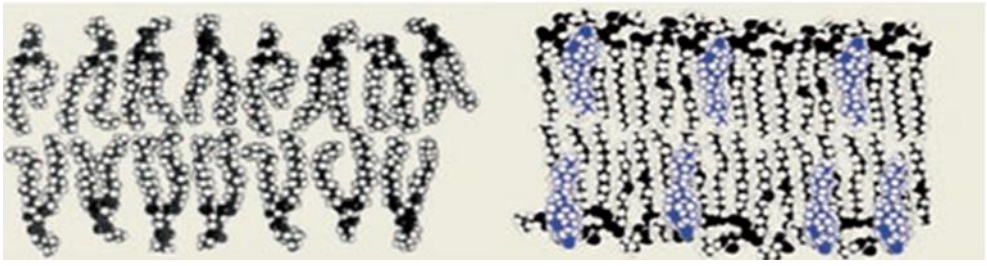

Figure 2.1 0 Schematic representation of the liquid disordered (l_d) (on the left) and the liquid ordered (l_o) (on the right) phases. The l_o phase just occurs in the presence of cholesterol (represented in blue) and has a high order (like in gel phase) and a high translational mobility, characteristic of fluid phases. The l_d phase is mainly composed by phospholipids and the order of the acyl chains is lower and the degree of freedom of the lipids is higher, comparatively to l_o phase. Adapted from (67)

Non-lamellar phases are present in transient biomembrane phenomena like membrane fusion, fission, pore formation and formation of tight junctions (67). In the Hexagonal Phase (H_I) lipids are organized as many micelles joined to form long tubes, where the polar headgroups are facing out and the acyl chains the interior. This phase is formed under low hydration (74).In the Inverted Hexagonal Phase (H_{II}), lipids are packed inversely in relation to H_I – the polar headgroups are facing the interior of the long tube and the acyl chains the outside (**Figure 2.11**). Because of this arrangement, the center of the tube is aqueous, surrounded by the hydrophilic polar headgroups and the surface is hydrophobic, leading to aggregation of the tubes (giving rise to a hexagonal cross section) in order to exclude the water from the surface (74). In the Cubic Phase, lipids are arranged like short tubes joined in a hexagonal array. This phase can be found in mixtures passing from the L phase to the H_{II} (74)**.**

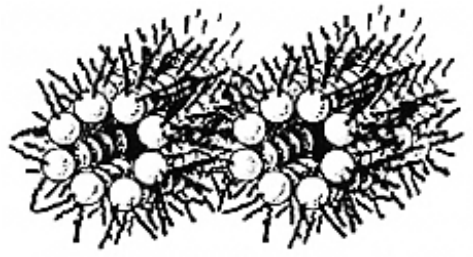

Figure 2.11 Schematic representation of the Inverted Hexagonal Phase. The hydrocarbon chains are facing the exterior and the polar headgroups the interior. Adapted from (74).

The main transition temperature (T_m) defines the temperature at which the transition between the gel and the fluid phase occurs. In homogenous systems, typically composed by a single lipid species, this transition occurs at a defined temperature, and so, bellow this temperature the system is in the gel phase, while at temperatures above T_m only fluid phase is present (79). T_m is highly dependent of the characteristics of the acyl chain, Van der Waals interactions and also the type of the headgroup. For longer acyl chains, the contact area is higher and so the strength of the Van der Waals interactions increases. This leads to an increase of T_m leading to a decrease of the lipid mobility (64,75). The presence of unsaturations is related to a decrease of T_m. In fact, the existence of a *cis* double bound give rise to free spaces, allowing additional flexibility in the adjacent hydrocarbon chains, abruptly decreasing the T_m. The *trans* double bonds also decrease the T_m, but not so abruptly (66).

In membrane model systems containing more than one type of lipids the melting occurs over a range of temperatures, and the midpoint of the transition, corresponds to the main transition temperature. Over the range of melting temperatures, different proportions of lipids in L_α and L_β coexist (75).

2.2.4 Membrane Lipid Domains

As referred in the above sections, biomembranes are fluid entities with nonhomogeneous lateral lipid and protein distribution, being therefore highly compartmentalized. These regions, also known as lipid domains, display specific lipid and protein composition that confer the characteristic biophysical properties of membrane domains (66). The existence of these compartments is directly

connected to different functional features of biomembranes, like transduction of signal, endocytosis and intracellular trafficking (66,80).

Lipid Rafts (**Figure 2.12**) are a good example of membrane domains. Lipid Rafts consist of ordered membrane regions, enriched in sphingolipids and cholesterol. These domains are thought to be small (nanosized) dynamic entities that exist transiently and that can be stabilized in response to a variety of stimuli. In fact, an important feature of lipid raft domains is the inclusion or exclusion of proteins. This feature has been considered as one of the essential factors for formation, maintenance and dynamics of lipids rafts domains (70). On other side, protein-protein interactions have been attributed as an important factor for raft stabilization (66). Proteins that have preferential partition into lipid rafts are glycosylphosphatidylinositol (GPI)-anchored proteins (or others with hydrophobic modifications) that partition into these domains due to preferential packing of their saturated membrane anchors (81). Other proteins are the double acylated proteins (such as proto-oncogene tyrosine-protein kinase (Src)-family kinases), cholesterol-linked and palmitoylated proteins and transmembrane proteins (specially the palmitoylated ones) (81). Nonetheless, the dynamic nature of lipid rafts, together with their small size, precludes their visualization under physiological conditions with the currently available technologies (81). Therefore, their existence in living cells is still controversial (73). Nonetheless, because lipid rafts have a lipid composition and properties different from the surrounding biomembrane – actually they are l_o regions dispersed in a l_d matrix of glycerophospholipids with unsaturated acyl chains, leading to a fluid-fluid phase separation – they are thought to be important modulators of cellular events (65,66,81).

The biological significance of lipid rafts domains is related, for example, with protein sorting and transduction of signal pathways like in the immune system during bacterial and viral infections of HIV and influenza (73,80).

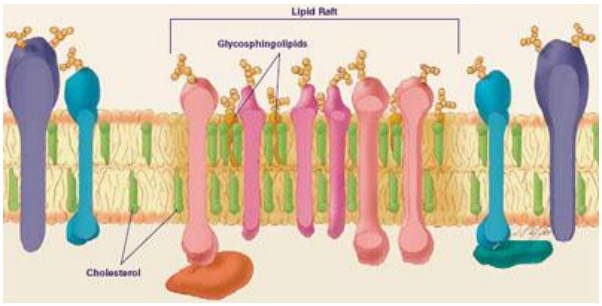

Figure 2.12 Schematic representation of Lipid Rafts. In the l_o phase it is visible an enrichment in Chol (green) and a high packing of the hydrocarbon chains of the lipids. Glycosphingolipids are represented in pink. The surrounded l_d phase has a lower content of cholesterol and lipids have a disordered arrangement of its hydrocarbon chains (121).

2.2.5 Membrane Model Systems

The complex nature of biomembranes that includes multiple lipid species and proteins, together with cellular events that constantly change the lipid and protein composition of biological membranes, is a major drawback for studies that aim to understand the biophysical principles underlying membrane organization and structure, as well as for studies that aim to evaluate the interaction of biologically relevant entities with the membrane (65). The use of artificial systems that mimic some features of biomembranes, constitutes a more controlled and simple manner to tackle

these subjects. Membrane model systems mimic the lipid organization of the biological membrane, and their composition can be selected according to the aim of the study (65). These models have been created to keep the bilayer structure, but simplifying the system to facilitate the study of the individual role of components. Lipid Monolayers, Supported Lipid Bilayers and Liposomes are examples of membrane model systems (65).

Liposomes (**Figure 2.13**) are approximately spherical lipid assemblies (as lipid bilayers) that enclose an aqueous compartment. Liposomes can be made of one or more lipid components, and might also contain peptides or proteins. These systems are widely used to study the biophysical properties of membranes, particularly to address specific lipid-lipid and lipid-protein interactions (65,82). The advantages of the use of liposomes are the easy formulation and the reproducible properties. On other side, some liposomes (mainly the multi bilayered ones) can display heterogeneity in terms of size distribution (74). In addition, liposomes display poor long-term stability (65). According to the number of bilayers, they are divided in Unilamellar Vesicles (just a single lipid bilayer) and Multilamellar Vesicles (MLVs) when there is more than one lipid bilayer. Regarding the diameter of the liposome, are designated as Small Unilamellar Vesicles (SUVs, 25-100 nm), Large Unilamellar Vesicles (LUVs, 100-1000nm) and Giant Unilamellar Vesicles (GUVs, 1-100 μm) (83).

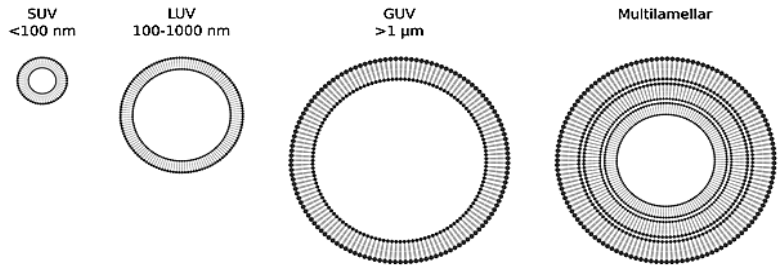

Figure 2.13 Schematic representation of the different types of liposomes, according to its size and number of bilayers. Adapted from (70).

GUVs are the membrane model systems that display a size similar to cells (82)**.** In fact, the membranes of GUVs are good approximations of the self-closed lipid structures of biomembranes. They are stable under different values of pH, pressure and temperature (84). When a fluorescent probe is properly incorporated during the vesicle preparation or after that, GUVs can be observed through fluorescence or confocal microscopy, allowing the real-time monitoring of its morphological changes and phase behaviour (82,84). These liposomes can be prepared by eight different methods such as fusion of SUVs or LUVs, transformation of a lipid stabilized water/oil/water double emulsion into GUVs, GUVs formed from micellized bilayer-forming lipids and electroformation, that is the most used (82).

CHAPTER 3: Aims

For the successful development of nano and micro drug delivery systems, a through knowledge of the surface-related physicochemical features that are determinant for the interaction of these carrier systems with cells is also needed. In the past few years, the study of the interactions between nano and micro drug delivery systems and biomembranes has been under focus (1,4,42,43,85). Notwithstanding, comprehensive studies on how the surface-related physicochemical properties influence the interaction of these systems with cell membranes and the consequent effects produced on these membranes are still missing. Such knowledge will contribute to the establishment of strategies and guidelines that allow a safer and more efficient design of nano and micro drug delivery systems.

This project aims to study how the surface-related physicochemical features of MPs modulate their interactions with GUVs, used as membrane model systems. To achieve this main goal, polymeric MPs were prepared, optimized to confer neutral, negative and positive surface charges and characterized for their physicochemical properties. MPs were then labeled with the fluorescent dye coumarin-6 to assess the interaction with GUVs, using confocal microscopy technique. Prior to the analysis of MPs-membrane interactions, a fundamental control was performed by studying the photophysical properties of coumarin-6-loaded MPs after the optimization of the experimental conditions regarding coumarin-6-loaded MPs (dye concentration and MPs:dye ratio). Finally, the effect of the MP surface charge on the MPs- membrane interactions were evaluated using GUVs with different lipid composition and membrane properties, namely, homogeneously fluid GUVs and GUVs displaying gel-fluid and l_o-l_d phase separation based on previous findings (86,87).

CHAPTER 4: Materials and Methods

4.1 Materials

Poly(D,L-lactide-co-glycolide) (PLGA) Resomer® RG 504 (lactide:glycolide 50:50) (batch 1042040), Polyvinyl alcohol (PVA) 13-23k 87-89 % hydrolyzed (batch MKBJ9294V), Alginic Acid Sodium Salt (batch 051M1864V), Coumarin-6 98 % (batch MKBJ5465V) and Cholesterol (Chol) >99 % (batch SLBC 7554V) were purchased from Sigma-Aldrich (St. Louis, MO, USA). CH Low Viscous (batch 131663) was obtained from Fluka (Buchs, Switzerland).

POPC (1-palmitoyl-2-oleoyl-*sn*-glycero-3-phosphocholine) and 16:0 SM (N-palmitoyl-D-erythro-sphingosylphosphorylcholine) were obtained from Avanti Polar Lipids (Alabarster, AL, USA). DPPC (1,2-dipalmitoyl-*sn*-glycero-3-phosphocholine) (batch 563098-01/131) from Lipoid. Avidin Egg White was purchased from Sigma Chemical Co. Rho-DOPE (1,2-Dioleoyl-*sn*-Glycero-3-Phosphoethanolamine-N-(Lissamine Rhodamine B Sulfonyl)) and DOPE-biotin (1,2-dioleoyl-sn-glycero-3-phosphoethanolamine-N-(biotinyl)) at a biotinylated/non-biotinylated lipid ratio of $1:10^6$ were obtained from Molecular Probes (Leiden, The Netherlands).

Dichloromethane (DCM) (for analysis) (batch K43751220236) and Chloroform Uvasol® grade were obtained from Merck. Acetic Acid from Hipersolv Chromanorm (batch 07B010521) was obtained from VWR Prolabo (Radnor, PA, USA). Deionized water was obtained in the equipment Merck Millipore (Darmstadt, Germany).

4.2 Methods

4.2.1 Lipids and probe stock solutions

Stock solutions of lipids and Rho-DOPE were prepared in chloroform and stored at -20 °C protected from the light. Depending on the application of coumarin-6, stock solutions were prepared in ethanol to produce PLGA MPs or DCM for absorption spectroscopy studies and stored at -20 °C protected from the light. The concentration of dye stock solutions was determined spectrophotometrically, measuring the absorption spectrum over a range of wavelengths and applying the Beer-Lambert law: $A = \varepsilon l c$ (**Equation 4.1**), where A is the absorbance, ε the molar absorption coefficient, l the optical length and c the concentration (88). Probe concentrations were determined using ε(Rho-DOPE λ_{max}=559 nm, chloroform)=95×10^3 $M^{-1}cm^{-1}$ (89) and ε(coumarin-6 λ_{max}=458 nm, ethanol)= 54×10^3 $M^{-1}cm^{-1}$ (90). An ε(coumarin-6 λ_{max}=455 nm, DCM)=55.6×10^3 $M^{-1}cm^{-1}$ was also determined using several dilutions of coumarin-6 stock solution in DCM. An absorption calibration curve was obtained from the plot absorption *vs* probe concentration, and the ε determined from the slope according to the Beer-Lambert law.

4.2.2 Surface-modified MPs preparation

Polymeric MPs with different compositions (**Table 4.1)** were prepared in triplicates using the w/o/w double emulsion solvent evaporation technique. Three different surface modifications of MPs were performed to manipulate MPs' surface charge: PVA, CH and ALG. PLGA MPs were first

optimized in terms of size and surface charge and then in terms of optimal loading of coumarin-6. Different initial amounts of coumarin-6 were used to prepare coumarin-6-loaded MPs: 10, 25, 50, 100 and 250 μg (for 250 mg of polymer). Coumarin-6 concentration was expressed as mass (μg) per mg of PLGA: 0.04, 0.10, 0.20, 0.40 and 1.00 μg/mg.

Briefly, 250 mg of PLGA were dissolved in 5 mL of DCM and emulsified with 1 mL of 5 % (w/v) PVA aqueous solution using an IKA UltraTurrax T10 Basic® at 3000 rpm for two minutes, resulting in a w/o emulsion. The 5 % (w/v) PVA aqueous solution was added drop-by-drop to the w/o emulsion. This emulsion was then added dropwise to 40 mL of 2.5 % (w/v) PVA aqueous solution, 0.75 % (w/v) CH aqueous solution or 0.75 % (w/v) ALG aqueous solution and emulsified during 5 minutes using a Yellowline DI25 Basic UltraTurrax® at 9500 rpm, resulting in a w/o/w emulsion. Formulations were then placed under magnetic stirring for 3 h at room temperature, to allow the organic solvent (or DCM) evaporation. PLGA MPs were collected by centrifugation at 6240 × g during 20 minutes at 4 °C (Centrifuge Mega Fuge 1.0R Heraeus) and washed three times with 20 mL of ultrapure water to remove the excess of PVA (or surfactant). PLGA MPs were finally resuspended in 5 mL of ultrapure water.

Coumarin-6-loaded MPs (PLGA-C6 MPs) were formulated using the same protocol and adding the mentioned solutions of coumarin-6 at different concentrations during the formulation procedure. A 5.56×10^{-4} M coumarin-6 stock solution was prepared in ethanol and different volumes (51, 128, 257, 514 or 1284 μL) were added to the oil phase. DCM was added to complete the 5 mL of the oil phase and 250 mg of PLGA were then dissolved in this organic phase. PLGA-C6 MPs were washed as mentioned above to remove the excess of PVA and the non-entrapped coumarin-6.

Table 4.1 Composition of the plain, CH surface modified MPs and ALG surface modified MPs.

	Formulation	**Concentration of coumarin-6 (μg/mg)**	**External Phase**
Non-surface modified MPs	PLGA PVA	0.00	2.5 % (w/v) PVA
	PLGA PVA-C6-1	0.04	
	PLGA PVA-C6-2	0.10	
	PLGA PVA-C6-3	0.20	
	PLGA PVA-C6-4	0.40	
	PLGA PVA-C6-5	1.00	
CH surface modified MPs	PLGA CH	0.00	0.75 % (w/v) CH
	PLGA CH-C6-1	0.04	
	PLGA CH-C6-2	0.10	
	PLGA CH-C6-3	0.20	
	PLGA CH-C6-4	0.40	
	PLGA CH-C6-5	1.00	
ALG surface modified MPs	PLGA ALG	0.00	0.75 % (w/v) ALG
	PLGA ALG-C6-1	0.04	
	PLGA ALG-C6-2	0.10	
	PLGA ALG-C6-3	0.20	
	PLGA ALG-C6-4	0.40	
	PLGA ALG-C6-5	1.00	

4.2.3 Physicochemical Characterization of the surface-modified microparticles

4.2.3.1 Microparticle size and ZP analyses

MP size parameters ($D_{10\%}$, $D_{50\%}$, $D_{90\%}$) were measured by laser diffraction using a Malvern Mastersizer Hydro 2000S. MP suspensions were diluted to 1:10 in ultrapure water, the obscuration window was set at 10-15 % and the target value was 12 %. Before each measurement, the device was washed with ultrapure water to attain a laser beam intensity above 80 %. The background was measured when the light energy was fewer than 60 %, fewer than 20 % and approximately 0 to detectors 0, 20 and 30, respectively. The size parameters represent an average of 6 measurements. MP sizes are represented as MP size distributions by volume and the span, which is a calculation of the width of the distribution of the volume in relation to the median diameter, was calculated by the expression

$$\frac{D_{90\%}-D_{10\%}}{D_{50\%}}$$ **Equation 4.2**

Results are expressed as the mean of three independent experiments measured in triplicate.

The MPs' surface charge was analyzed through ZP measurement by Laser Doppler Electrophoresis at 25 °C using a Malvern Zetasizer Nano ZS equipment. MP suspensions were diluted to 1:4 in ultrapure water (pH=5.7). Approximately 0.8 mL were used to fill the clear disposible capillary zeta cell (DTS060C). The ZP data represents an average of a triplicate measurement of 50 rounds with an equilibration time of 30 seconds. Results are expressed as the mean of three independent experiments measured in triplicate.

4.2.3.2 Confocal Microscopy

The size and shape of coumarin-6-loaded PLGA MPs containing 0.2 μg/mg of coumarin-6 was evaluated by confocal microscopy imaging. Each batch of MP suspension (initial concentration: 50 mg/mL) was diluted to 1:200 in ultrapure water (pH=5.7). The final concentration of MPs was 0.25 mg/mL. Samples were then analyzed using a Leica TSC SP5 (Leica Microsystems CMS GmbH, Mannheim, Germany) inverted microscope (DMI6000) with a 63x water (1.2 numerical aperture) apochromatic objective. The excitation of coumarin-6 fluorophore was performed through the 458 nm line of an Ar^+ laser beam and the emission collected beetween 480-530 nm wavelenghts. The confocal sections had a thickness bellow 0.5 μm. Three-dimensional (3D) projections were obtained using a galvanometric motor stage and processed using the Leica Application Suite-Advanced Fluorescence Software.

4.2.3.3 Coumarin-6 loading analysis

The Entrapment Efficiency (E.E., %) and the Loading Capacity (L.C., μg/mg) of coumarin-6 were determined through direct quantification, by absorption spectroscopy using a Hitachi U-2001 UV/Vis Spectrometer. For each batch of coumarin-6-loaded PLGA MPs containing 0.2 μg/mg of

coumarin-6, MPs were collected by centrifugation at 6240 × g during 20 minutes at 4°C, using the Centrifuge Mega Fuge 1.0R Heraeus. The supernatant was removed and the pellet dissolved in DCM. However the complete dissolution was not immediately attained once two different phases were observed. Therefore, the pellet in DCM was placed at strong magnetic stirring for 2 h to obtain a solution of coumarin-6 and PLGA polymer. The measurements were done in 1 cm quartz absorption cuvettes and the concentration was determined by measuring the absorption at 455 nm and using non-fluorescent MPs dissolved in DCM as blank. The absorption calibration curve was prepared using coumarin-6 solutions in DCM at different known concentrations. Using the Beer-Lambert law, the slope of the calibration curve was obtained and the ε(coumarin-6 λ_{max}=455 nm, DCM)=55.6×10^3 $M^{-1}cm^{-1}$ calculated. The E.E. (%) and the L.C. (μg/mg) for coumarin-6 were determined using the follows equations:

$$E.E.(\%) = \frac{Amount\ of\ the\ coumarin6\ in\ MPs}{Initial\ amount\ of\ coumarin6} \times 100 \qquad \textbf{Equation 4.3}$$

$$L.C.(\mu g\ /\ mg) = \frac{Amount\ of\ Coumarin6\ in\ MPs}{Initial\ polymer\ amount} \qquad \textbf{Equation 4.4}$$

4.2.3.4 Statistical Analysis

All experimental results are expressed as mean ± standard deviation (SD). Two-way ANOVA and Bonferroni's post test were performed in order to demonstrate statistical differences in size and ZP data. One-way ANOVA and Tukey's post test were performed in order to demonstrate statistical differences in E.E. (%) and L.C. (μg/mg) data. All the statistical analysis was made using the Graph Pad software (version 5.02) for Windows®. Differences were considered statistically significant at $p < 0.05$.

4.2.4 Spectral characterization of coumarin-6

For each batch of PLGA-C6 MPs, five dilutions (1:100, 1:125, 1:200, 1:250 and 1:500) were prepared in ultrapure water (pH=5.7) and achieving the following final concentrations of coumarin-6-loaded PLGA MPs: 0.50, 0.40, 0.25, 0.20 and 0.10 mg/mL.

Steady-state fluorescence measurements were performed at room temperature (23 °C) in a SLM Aminco 8100 series 2 spectrofluorimeter or in a Hitachi F-2000 Spectrofluorimeter, using 0.5 cm or 1.0 cm quartz cuvettes. Under the experimental conditions employed in this study the excitation and emission maxima wavelengths ($\lambda_{ex}/\lambda_{em}$) were determined to be 465 nm and 500 nm, respectively. However, due to partial overlay of the emission and excitation spectra and in order to collect the whole excitation and emission spectra of the probe, measurements were performed setting the emission wavelength to 510 nm during the acquisition of the excitation spectra, while the excitation wavelength was set to 445 nm during the acquisition of the emission spectra.

The steady-state anisotropy, < r >, was calculated according to the equation:

$$< r >= \frac{I_{VV} - G * I_{VH}}{I_{VV} + 2G * I_{VH}}$$ **Equation 4.5**

Where I_{VV} is the emission intensity measured parallelarly to the vertical polarized excitation, I_{VH} is the emission intensity measured perpendicularly and G is a correction factor calculated by the ratio between the emission intensity measured parallelarly and perpendicularly to the horizontal polarized excitation (91). Fluorescence anisotropy measurements were performed using $\lambda_{ex}/\lambda_{em}$=445/500 nm. An appropriate blank was subtracted from each intensity reading before calculation of the anisotropy value.

4.2.5 Giant unilamellar vesicles preparation

Three different lipid mixtures were prepared: POPC, POPC/DPPC (1:1 mol/mol) and POPC/SM/Chol (1:1:1 mol/mol/mol).

The lipid mixtures containing the adequate amount of lipids, DOPE-biotin (at a biotinylated:non-biotinylated lipid ratio of $1:10^6$), Rho-DOPE (at a probe:lipid ratio of 1:500) were prepared in glass amber vials. 3 μL of each lipid mixture were spread onto the platinum electrodes. The solvent was dried in vacuum and the electrodes were placed in 1 mL of 200 mM sucrose solution heated at 60 ˚C. GUVs were prepared by electroformation using an alternating electric field of a sinusoidal wave of 30 Hz and 0.2 V during 1 h 15 min. Prior to GUVs preparation, the wells of an 8-well μ-Slide from Ibidi® were coated with avidin at 0.1 mg/mL to facilitate the adhesion of the GUV to the plate by the reaction of avidin/biotin (84). The wells were then washed three times with 200 μL of ultrapure water (pH=5.7) to remove the excess of avidin. GUVs (150 μL) were transferred into the wells and 250 μL of glucose were then added to each well.

4.2.6 Impact of the surface properties in the interaction between surface-modified microparticles and giant unilamellar vesicles

The interaction between coumarin-6-loaded PLGA MPs and GUVs was evaluated by confocal microscopy imaging. Each suspension of coumarin-6-loaded PLGA MPs containing 0.2 μg/mg of coumarin-6 was diluted to 1:200 in ultrapure water (final concentration of 0.25 mg/mL, pH=5.7). 50 μL of PLGA MPs were added into the GUVs-containing wells of the 8-well μ-Slide. The excitation of coumarin-6 and Rho-DOPE was performed using the 458 and 514 nm lines of an Ar^+ laser, respectively. The emission was collected in the ranges of 480-530 nm and 530-650 nm for coumarin-6 and Rho-DOPE, respectively. By using the setting “smart offset” set bellow 0.5, the stray light was reduced. The confocal sections with a thickness bellow than 0.5 μm were obtained using a galvanometric motor stage. The three-dimensional (3D) projections were obtained using the Leica Application Suite-Advanced Fluorescence Software. Confocal microscopy imaging of GUVs interacting with MPs was performed during 3 h.

CHAPTER 5: Results

5.1 Characterization of the surface-modified MPs

Surface-modified MPs were characterized in terms of size ($D_{10\%}$, $D_{50\%}$, $D_{90\%}$), span, ZP and shape. Values of $D_{10\%}$, $D_{50\%}$, $D_{90\%}$ and span are summarized on **Table 5.1** according to MP surface modification with PVA, CH or ALG and to the coumarin-6 concentration. Histograms of MP size distribution in terms of Volume (%) are also represented on **Figure 5.1** for plain or non-fluorescent MPs (**Figure 5.1 A**) and coumarin-6-loaded MPs containing 0.2 μg/mL of coumarin-6 (**Figure 5.1 B**).

Unloaded and coumarin-6-loaded PLGA MPs presented median size ($D_{50\%}$) values ranging from 1.4±0.3 μm to 3.8±0.2 μm and span ranging from 1.1±0.2 to 4.8±1.1 (**Table 5.1**). Specifically, non-fluorescent MPs ranged from 2.9±0.3 μm and 3.8±0.1 μm, being the highest $D_{50\%}$ values obtained for PLGA PVA MPs and the lowest ones for PLGA ALG MPs. In fact, the differences observed in $D_{50\%}$ values of MPs were not statistically significant, suggesting that the different surface modifications did not have a significant impact on their median size values. Even though, slightly different size distribution patterns can be observed on the size distribution histograms for non-fluorescent MPs prepared according to the different surface modifications tested (**Figure 5.1 A**). PLGA PVA MPs showed the most homogeneous population in terms of size polydispersity, as can be seen by the narrower single peak of the histogram (blue line). PLGA CH MPs (red line) exhibited a slightly wider size distribution, with a $D_{50\%}$ value of 2.9±0.8 μm. PLGA ALG MPs (green line) presented the lowest $D_{50\%}$ value (2.9±0.3 μm) but also the most heterogeneous population, as can be observed by the presence of a wide subpopulation ranging from 10 μm to 50 μm, approximately.

Regarding coumarin-6-loaded MPs, the presence of the fluorescent probe at different concentrations did not demonstrate a statistically significant impact on $D_{50\%}$ values, except for PLGA ALG MPs containing 0.4 and 1.0 μg/mL of coumarin-6 (1.4±0.3 μm and 1.7±0.1 μm, respectively) that presented a significant ($p < 0.01$) lower $D_{50\%}$ values comparing to MPs containing 0.04 μg/mL (3.7±1.2 μm) (**Table 5.1**). PLGA PVA MPs and PLGA CH MPs did not demonstrate statistically significant differences for $D_{50\%}$ values regarding the different concentrations of coumarin-6 tested (**Table 5.1**). For PLGA ALG-C6-4 MPs and PLGA ALG-C6-5 MPs, $D_{10\%}$ values showed the presence of one subpopulation in the nanometer size.

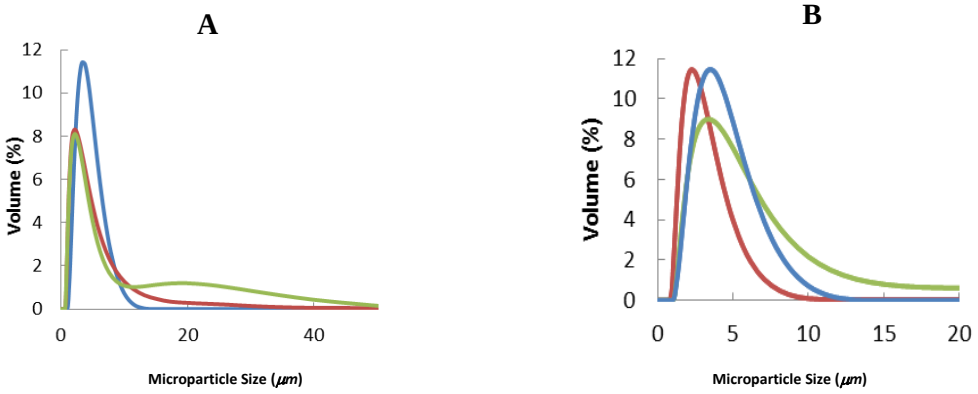

Figure 5.1 Microparticle Size Distribution by Volume. (A) PLGA MPs: PLGA PVA MPs (blue), PLGA CH MPS (red) and PLGA ALG MPs (green). (B) PLGA-C6 MPs (labeled with 0.2 μm /mg of coumarin-6): PLGA PVA-C6-3 MPs (blue), PLGA CH-C6-3 MPS (red) and PLGA ALG-C6-3 MPs (green).

Table 5.1 Physicochemical characterization of coumarin-6-loaded PLGA Microparticles. Size parameters of unloaded and coumarin-6 loaded PLGA PVA MPs, PLGA CH MPs and PLGA ALG MPs are presented as span, $D_{10\%}$, $D_{50\%}$ and $D_{90\%}$ (mean ± SD; $N \geq 3$, $n = 3$). Statistical analysis: two way ANOVA and Bonferroni's post test. $D_{50\%}$ **[a] significantly different ($p < 0.01$) comparing to PLGA ALG C6-5. $D_{50\%}$ **[b] significantly different ($p < 0.01$) comparing to PLGA ALG C6-4.

	Formulation	Concentration of coumarin-6 (μg/mg)	Span	$D_{10\%}$ (μm)	$D_{50\%}$ (μm)	$D_{90\%}$ (μm)
Non-surface modified MPs	**PLGA PVA**	0.00	1.3±0.1	2.1±0.1	3.4±0.1	6.9±0.4
	PLGA PVA-C6-1	0.04	1.9±0.3	1.6±0.4	3.5±0.4	8.0±0.1
	PLGA PVA-C6-2	0.10	1.8±0.3	1.5±0.2	3.5±0.4	7.8±0.5
	PLGA PVA-C6-3	0.20	1.5±0.3	1.6±0.2	3.4±0.8	6.5±0.3
	PLGA PVA-C6-4	0.40	3.2±0.4	1.7±0.3	2.8±0.3	10.6±1.9
	PLGA PVA-C6-5	1.00	1.6±0.3	1.8±0.2	3.8±0.2	7.6±0.6
CH surface modified MPs	**PLGA CH**	0.00	1.9±0.4	1.4±0.3	2.9±0.8	6.9±1.6
	PLGA CH-C6-1	0.04	1.3±0.0	1.5±0.1	2.6±0.1	4.7±0.2
	PLGA CH-C6-2	0.10	1.1±0.2	1.5±0.1	2.4±0.3	4.3±0.9
	PLGA CH-C6-3	0.20	1.3±0.2	1.5±0.0	2.6±0.2	4.9±0.8
	PLGA CH-C6-4	0.40	2.5±1.0	1.4±0.3	3.5±0.0	9.5±5.2
	PLGA CH-C6-5	1.00	1.9±0.4	1.0±0.1	2.5±1.2	5.8±3.7
ALG surface modified MPs	**PLGA ALG**	0.00	3.7±1.9	1.3±0.1	2.9±0.3	12.1±6.5
	PLGA ALG-C6-1	0.04	4.8±1.1	1.6±0.2	3.7±1.2	13.1±9.4
	PLGA ALG-C6-2	0.10	2.7±0.0	1.4±0.1	2.4±0.9	9.4±0.6
	PLGA ALG-C6-3	0.20	2.0±0.2	1.5±0.0	3.0±0.0	7.4±0.7
	PLGA ALG-C6-4	0.40	2.8±0.5	0.1±0.0	1.4±0.3**[a]	6.5±2.0
	PLGA ALG-C6-5	1.00	3.3±0.1	0.1±0.0	1.7±0.1**[b]	5.6±0.2

In order to study the impact of MP surface charge on the interaction between MPs and biomembrane models, three different polymers known to cause alterations on the surface charge of particles (24), were used in the formulation process. Surface charge of the different MPs was analyzed through the ZP measurement by Laser Doppler Electrophoresis, at 25 °C in ultrapure water. As expected, PLGA MPs prepared with distinct surface-modifier polymers clearly exhibited different surface charges. PLGA CH MPs showed a highly positive surface charge (50.8±2.7 mV). In contrast, negative surface charges were displayed for PLGA ALG MPs (-36.8±4.4 mV) and for PLGA PVA MPs (-19.6±1.1 mV) (**Table 5.2**). Surface charges results for non-fluorescent PLGA MPs were significantly affected ($p < 0.001$) by the different surface modifications (PVA, ALG or CH).

On the other hand, MP loading with coumarin-6 did not change the surface charge of MPs since no statistically significant differences were observed regarding the different coumarin-6 concentrations tested ($p > 0.001$) (**Table 5.2)**. PLGA CH-C6 MPs presented highly positive ZP values ranging from 53.6±4.5 mV to 58.7±3.4 mV and PLGA ALG-C6 MPs showed highly negative ZP values ranging from -30.8±2.3 mV to -36.2±3.3 mV. PLGA PVA-C6 MPs also presented negative ZP values ranged between -17.8±0.9 mV and -19.9±0.2 mV. Independently of the coumarin-6 concentration used, statistical differences were found for the surface charge values of the different surface-modified MPs ($p < 0.001$).

Table 5.2 Physicochemical characterization of the PLGA MPs. Table shows the Zeta Potential (ZP) of the unloaded and coumarin-6 loaded PLGA MPs. Data correspond to mean ± SD ($N \geq 3$, $n = 3$). Statistical analysis: two way ANOVA and Bonferroni's post test. Relative to the same coumarin-6 concentration *** $p < 0.001$.

	Formulation	Concentration of coumarin-6 (μg/mg)	ZP (mV)
Non-surface modified MPs	**PLGA PVA**	0.00	-19.6±1.1***
	PLGA PVA-C6-1	0.04	-19.9±0.2***
	PLGA PVA-C6-2	0.10	-18.8±2.0***
	PLGA PVA-C6-3	0.20	-17.8±0.9***
	PLGA PVA-C6-4	0.40	-19.0±1.1***
	PLGA PVA-C6-5	1.00	-18.5±0.8***
CH surface modified MPs	**PLGA CH**	0.00	50.8±2.7***
	PLGA CH-C6-1	0.04	54.0±3.9***
	PLGA CH-C6-2	0.10	56.9±6.3***
	PLGA CH-C6-3	0.20	55.1±3.5***
	PLGA CH-C6-4	0.40	53.6±4.5***
	PLGA CH-C6-5	1.00	58.7±3.4***
ALG surface modified MPs	**PLGA ALG**	0.00	-36.8±4.4***
	PLGA ALG-C6-1	0.04	-31.9±3.0***
	PLGA ALG-C6-2	0.10	-36.2±3.3***
	PLGA ALG-C6-3	0.20	-32.3±1.7***
	PLGA ALG-C6-4	0.40	-32.5±2.6***
	PLGA ALG-C6-5	1.00	-30.8±2.3***

Confocal microscopy was used to qualitatively characterize the size and shape of coumarin-6-loaded PLGA MPs and also to provide insights on the apparent probe distribution throughout the polymeric matrix of MPs. PLGA MPs containing 0.2 μg/mg of coumarin-6 were formulated with the different surface-modifying polymers (PVA, ALG and CH). MPs were then resuspended in ultrapure water and diluted to 1:200 to a final concentration of 0.25 mg/mL. Three-dimensional projections represented in **Figure 5.2** were obtained from confocal sections. In general, MPs presented a spherical shape, as can be seen on confocal images **(Figure 5.2)**. Notwithstanding, some PLGA PVA-C6-3 MPs and PLGA ALG-C6-3 appear with a sickle-like shape (**Figure 5.2 D and E**), probably resulting from the collapse of some MPs, apparently those with larger sizes. Since MPs were formulated and immediately observed, the results obtained might suggest that these types of MPs are slightly unstable under the experimental conditions used. Some MP aggregation was observed for PLGA PVA-C6-3

MPs (as pointed in **Figure 5.2 A**), which might be related to the surface hydrophobicity conferred by the hydrophobic nature of the polymeric matrix of the MPs and consequent instability in aqueous suspension. Confocal microscopy images showed that coumarin-6 seems to have a predominant uniform distribution as denoted by the dense green color noticed in the majority of the MPs observed. However, some of the PLGA PVA-C6-3 MPs (**Figure 5.2 A**) and PLGA ALG-C6-3 MPs (**Figure 5.2 C, E**) displayed small round-like dark areas that might correspond to coumarin-6-free regions.

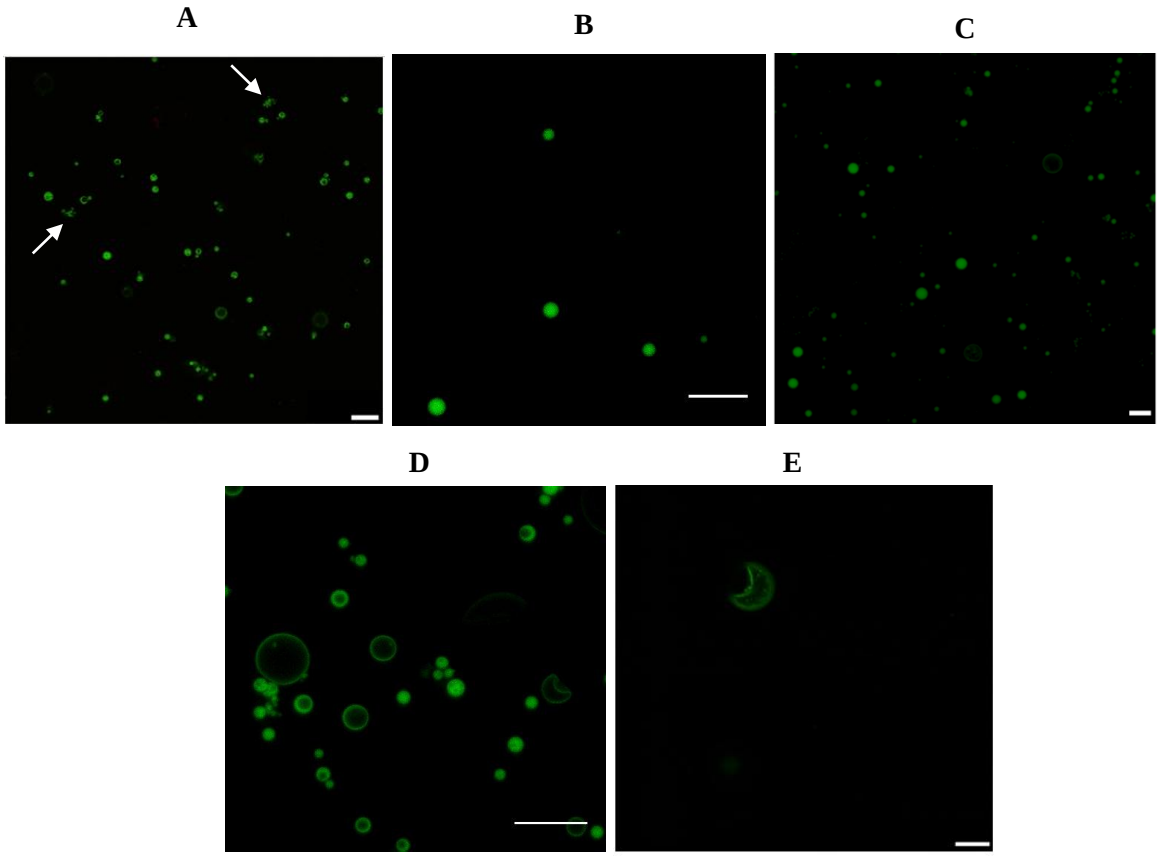

Figure 5.2 Physichochemical properties of coumarin-6-loaded PLGA MPs with different surface modifications were evaluated by confocal microscopy imaging. Three-dimensional projection images from 0.5 μm confocal slices of PLGA MPs labeled with coumarin-6 (green): (A), (D) PLGA PVA-C6-3 MPs, (B) PLGA CH-C6-3 MPs, (C), (E) PLGA ALG-C6-3 MPs. Representative images of three independent experiments are shown. Scale bars = 10 μm

5.2 Spectral characterization of coumarin-6

Coumarins are a family of molecules composed by a fused pyrone and benzene rings, presenting the pyrone carbonyl group at position 2 (92,93). Coumarins can exhibit high sensitivity to the environment properties such as local polarity, microviscosity and pH (92). They are known to have a high fluorescence in the green and blue regions of the spectrum and high quantum yield (92,94). 3-(2'-benzothiazolyl)-7-N,N-diethylaminocoumarin, also named coumarin-6, is a good example of this type of coumarins. The absorption and fluorescence spectra of coumarin-6 display a solvatochromic behaviour to the red region for increasing values of solvent polarity. To characterize the photophysical properties and localization of coumarin-6 into polymeric matrix of the PLGA-C6 MPs, the absorption

and fluorescence spectra of coumarin-6 were performed. In fact, these methods are excellent tools to access the impact of the microenvironment on the electronic states of the molecules (95). For each batch of PLGA-C6 MPs, the suspensions were diluted to 1:100, 1:125, 1:200, 1:250 and 1:500 (final concentration of PLGA in the suspensions: 0.50, 0.40, 0.25, 0.20 and 0.10 mg/mL, respectively) in ultrapure water, and the photophysical parameters of coumarin-6 were evaluated.

5.2.1 Spectral characterization of coumarin-6 – the stock solutions

According to the formulation process employed, PLGA was dissolved in DCM to form the oil phase. Coumarin-6 stock solution was also prepared in DCM and the photophysical properties of the probe in this organic solvent were characterized. **Figure 5.3 A and C** shows the absorption spectra for coumarin-6 solutions prepared in DCM, at different concentrations. As observed, the absorption occurs in the range of 400-490 nm, being observed two wavelength ranges with absorption maxima at 445-448 nm and 455-463 nm. These results suggest that more than one electronic transition is occurring due to some aggregation in coumarin-6 chemical structure. This phenomenon can be explained by the presence of certain sites in coumarin-6 that are interacting with DCM at different strengths. However, literature data suggest that coumarin-6 presents a maximum of absorption at 455 nm in DCM and no aggregation behavior has been reported (93).

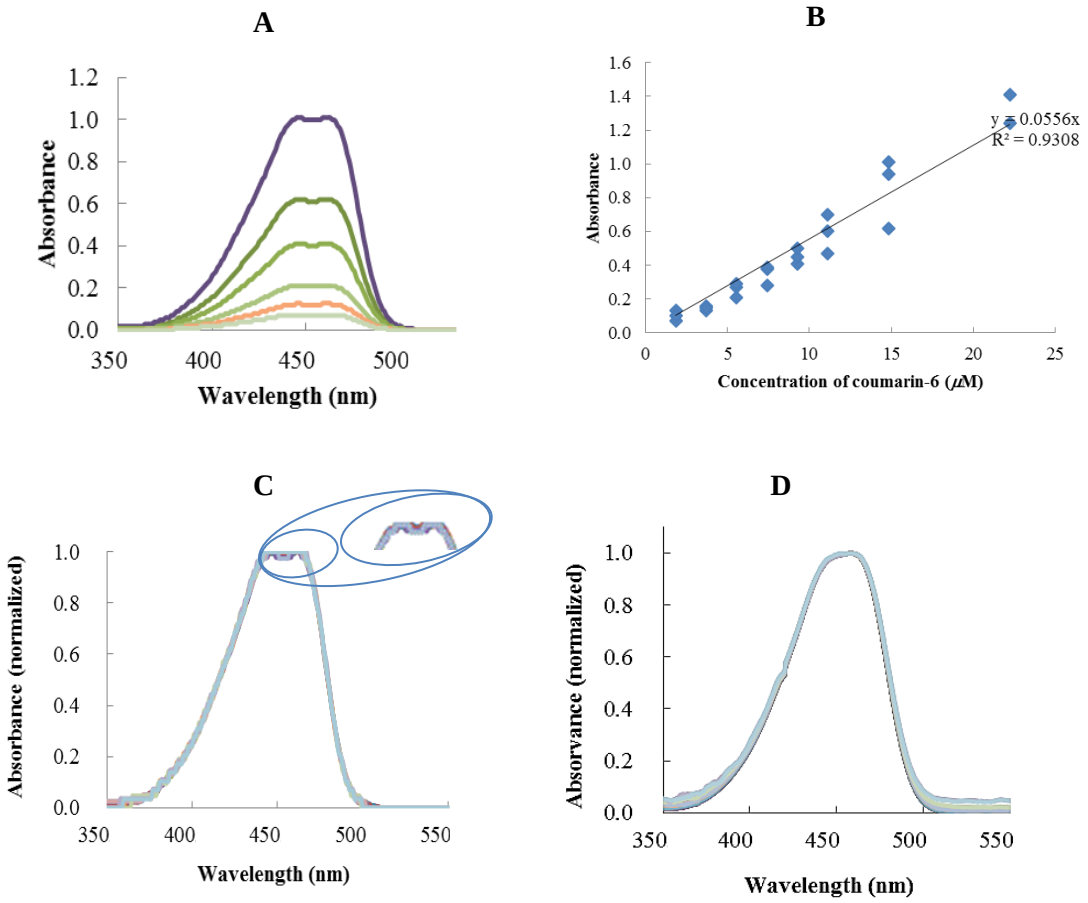

Figure 5.3 Coumarin-6 absorption spectra and calibration curve in stock solutions prepared in DCM and ethanol. (A) Coumarin-6 absorption spectra and (B) Calibration curve both obtained by the different solutions prepared from the coumarin-6 stock solution in DCM (in triplicate). Normalized absorption spectra of the different solutions prepared from (C) the coumarin-6 stock solution in DCM (detail of the two ranges of maximal absorption) and (D) coumarin-6 stock solution in ethanol. Concentrations of each solution of coumarin-6: 1.85 μM (light blue), 3.7 μM (orange), 5.56 μM (light green), 7.41μM (green), 9.26 μM (dark green), 11.1 μM (purple). Data correspond to $N \geq 3$, $n = 3$.

To avoid the use of a stock solution that could present coumarin-6 aggregates, a new stock solution was prepared using ethanol as solvent (**Figure 5.3 D**). Coumarin-6 in ethanol presents an absorption in the range of 390 - 490 nm and an absorption maximum at 458 nm, in agreement with previous studies (93). According to the spectral results obtained, it can be inferred that coumarin-6 is more soluble in ethanol than DCM. Since no aggregated species seemed to be present in this stock solution, coumarin-6 in ethanol was used during the formulation process of the PLGA-C6 MPs.

5.2.2 Spectral characterization of coumarin-6-loaded MPs

To characterize coumarin-6-loaded PLGA MPs, UV-Vis and fluorescence spectroscopy were initially employed. However, it was not possible to address the extent of incorporation of coumarin-6 into MPs using UV-Vis spectroscopy due to the lower sensitivity of this tecnhique (data not shown). To determine the parameters that resulted in optimal formulation conditions of coumarin-6-loaded PLGA MPs, two types of studies were performed. In the first set of experiments, the concentration of coumarin-6 loaded into MPs was kept constant and the concentration of MPs in suspension was varied. In the second set of experiments, the influence of coumarin-6 concentration was studied for each concentration of MPs in suspension. These studies allowed to determine the best probe-to-polymer ratio to be used in the formulation process.

Figure 5.4 shows the excitation and emission spectra for the different PLGA-C6 MPs

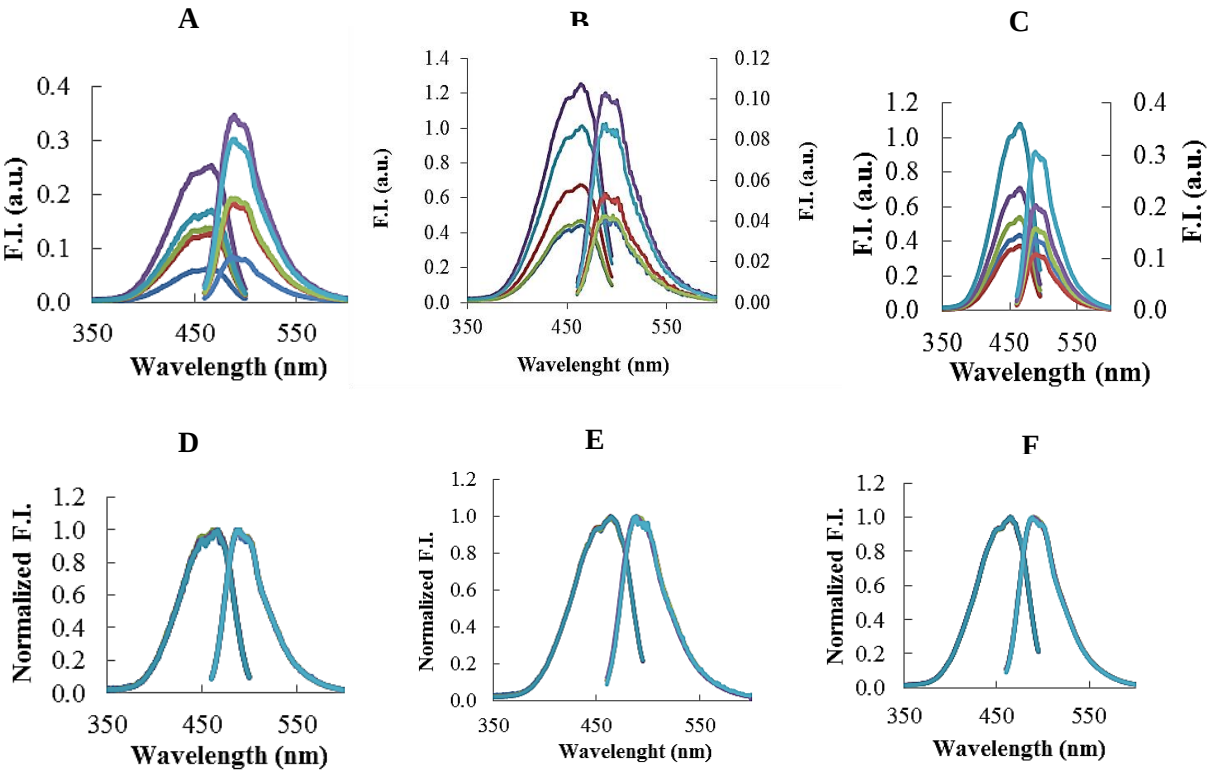

Figure 5.4 Coumarin-6 excitation and emission spectra in PLGA-C6 MPs labeled with 0.20 μg/mg of coumarin-6 for the different concentrations of MPs in suspension. Excitation and emission spectra of (A) PLGA PVA-C6 MPs, (B) PLGA CH-C6 MPs, and (C) PLGA ALG-C6 MPs and correspondent normalized excitation and emission spectra (D,E,F) . Data for the concentrations of PLGA in suspension 0.10 mg/mL, 0.20 mg/mL, 0.25 mg/mL, 0.40 mg/ml and 0.50 mg/mL are shown in blue, red, green, purple and light blue. Data correspond to N = 1, n = 1. F.I. Measurements were performed setting λ_{em}=510 nm during the acquisition of the excitation spectra and λ_{ex} = 445 nm during the acquisition of the emission spectra. Fluorescence Intensity (a.u).

containing 0.2 μg/mg of coumarin-6. In **Figure 5.4 B and C** the left YY axis represents the excitation and the right YY axis the emission. Excitation and emission spectra for PLGA MPs labeled with 0.04, 0.1, 0.4 and 1.00 μg/mg of coumarin-6 are shown in **Annex 1**. Overall data shows that increasing the MP concentration in the suspension results in increased fluorescence intensities (**Figure 5.4 A-C**). However, no spectral alterations were observed (**Figure 5.4 D-F**), displaying that changes in MP suspension content do not affect the partition of coumarin-6 between the hydrophobic polymeric matrix, MP surface and aqueous environment.

Comparison between the emission spectra of coumarin-6 when loaded in the different MPs shows that fluorescence intensity is lower in PLGA CH-C6-3 MPs and quite similar for the remaining ones (**Figure 5.5 A**). Moreover, no spectral alterations were detected when coumarin-6 was loaded in the different MPs suggesting that under these conditions the probe is essentially located in the hydrophobic polymeric matrix (**Figure 5.5 B**).

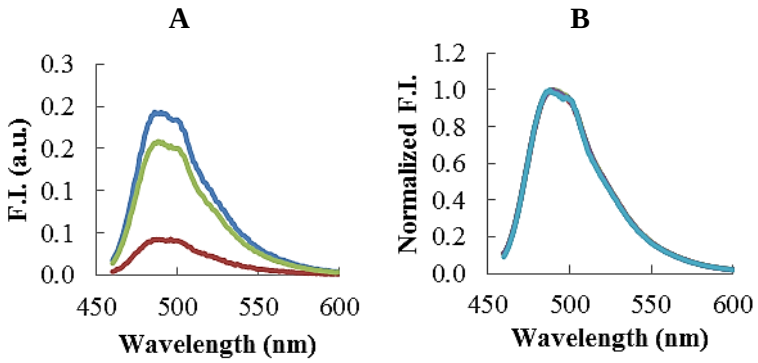

Figure 5.5 Coumarin-6 and emission spectra in PLGA-C6 MPs labeled with 0.20 μg/mg of coumarin-6 for MPs concentration 0.25 mg/mL, (A) non-normalized and (B) normalized. Data for PLGA PVA-C6-3 MPs, PLGA CH-C6-3 and PLGA ALG-C6-3 MPs is shown in blue, red and green (respectively). Data correspond to N = 1, n = 1. Measurements were performed setting λ_{ex} = 445 nm during the acquisition of the emission spectra. F.I. Fluorescence Intensity (a.u.).

To further characterize the different coumarin-6-loaded PLGA MPs, the variation of the fluorescence intensity maximum of coumarin-6 as a function of the concentration of PLGA-C6 MPs in suspension was analysed (**Figure 5.6**). As it would be anticipated, an increase in the fluorescence intensity maximum is observed upon increasing the concentration of the PLGA-C6 MPs, independently of their surface modification. It would be expected that for the same concentration of coumarin-6 used to label PLGA-C6 MPs, the fluorescence intensity maximum of the probe would change linearly with the concentration of PLGA-C6 MPs. This fact can be mainly confirmed for PLGA PVA-C6 MPs that present an almost linear trend of variation of the fluorescence intensity for all the concentrations of coumarin-6 studied. However, the variation is not perfectly linear for PLGA PVA-C6-3/4/5 MPs (0.2, 0.4 and 1.0 μg/mg of coumarin-6). For PLGA CH-C6 MPs and PLGA-ALG-C6 MPs, the variation in the fluorescence intensity maximum is also close to linear, but the data are more scattered. This might be mainly due to experimental errors during the dilution of the samples. Indeed, the PLGA-C6 MPs have a strong tendency to sediment and form non-homogenous solutions. Differences in the redispersion of the PLGA-C6 MPs could account for this scattered variation. Nonetheless, because the general trend is close to linear, one can assume that no significant

differences in the partition of the coumarin-6 between the polymeric medium and the aqueous solution are taking place upon dilution of the samples. It should be noted that for the higher coumarin-6 concentration, saturation of fluorescence intensity maximum is observed. In fact, fluorescence quantum yield of coumarin-6 in hydrophobic mediums such as DCM is 0.94 and in water is 0.03 (93). Thus, the saturaded behaviour could be explained by some probe adsorption onto the MPs surface or even in water, where the quantum yieald is lower.

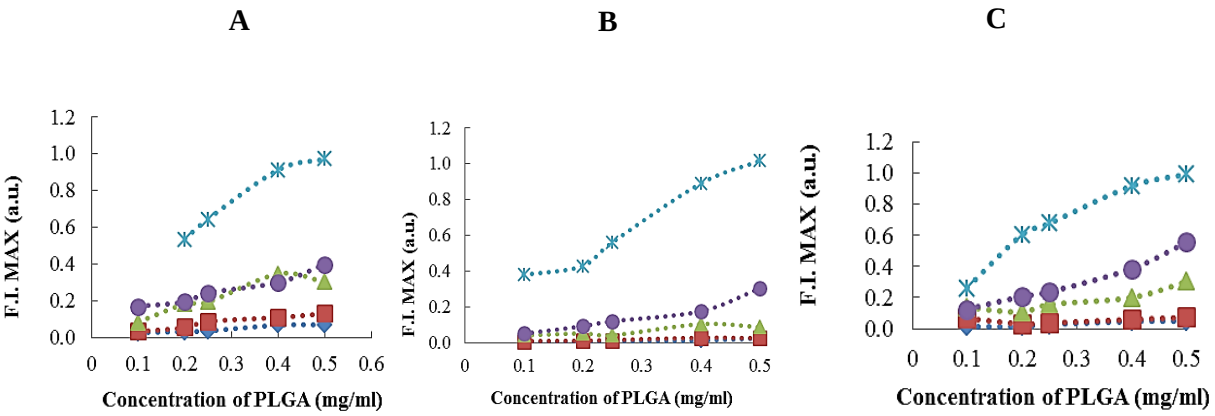

Figure 5.6 Variation of coumarin-6 fluorescence intensity maximum as a function of MPs concentration in the suspension in (A) PLGA PVA-C6 MPs, (B) PLGA CH-C6 MPs and (C) PLGA ALG-C6 MPs. Data for coumarin-6 concentration 0.04 μg/mg, 0.10 μg/mg, 0.20 μg/mg, 0.40 μg/mg and 1.00 μg/mg is shown in blue, red, green, purple and light blue, respectively. Data correspond to N = 1, n = 1. F.I. MAX, Fluorescence Intensity Maximum (a.u).

Comparison of the fluorescence properties of coumarin when loaded in different MPs showed that fluorescence intensity maximum increases with the increase of the concentration of the PLGA-C6-3/4 MPs suspension in a linear manner (**Figure 5.7**). Actually, for PLGA-C6 MPs labeled with 0.4 μg/mg of coumarin-6, there is a direct correlation between the increase of fluorescence intensity maximum and the concentration of MPs. Results further show differences upon changing the distinct surface-modifier polymers during MPs formulation. In fact, fluorescence intensity maximum values are lower for CH surface-modified MPs comparing with PVA and ALG formulations. In fact, fluorescence intensity maximum values of PVA and ALG formulations are generally similar.

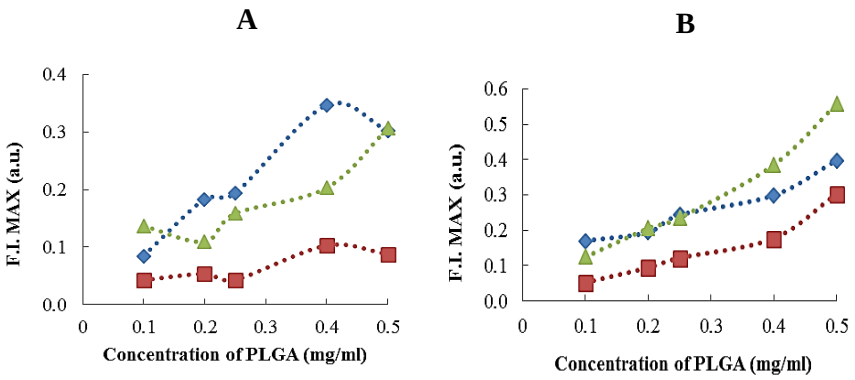

Figure 5.7 Variation of coumarin-6 fluorescence intensity maximum as a function of MPs concentration in the suspension. PLGA MPs were loaded with (A) 0.2 and (B) 0.4 μg coumarin-6/mg of PLGA. Data for PLGA PVA, PLGA CH and PLGA ALG MPs are shown in blue, red and green, respectively. Data correspond to N = 1, n = 1. F.I. MAX, Fluorescence Intensity Maximum (a.u).

Figure 5.8 A-C shows the emission spectra of coumarin-6 in PLGA-C6 MPs suspension with 0.25 mg/mL of PLGA concentration. Additional spectra obtained for PLGA-C6 MPs suspensions with MPs concentrations of 0.50, 0.40, 0.20 and 0.10 mg/mL are shown in **Annex 2**. Results demonstrate a red shift in the probe emission for increasing concentrations of coumarin-6. This behaviour is observed in the three different formulations studied (PVA, CH and ALG). Indeed, an *ap.* 15 nm shift (from 485 to 500 nm) in the maximum emission wavelenght is also observed when coumarin-6 concentration increases from 0.04 to 1.00 μg/mg, regardless of MP composition **(Figure 5.8 D-F)**. Additional spectra obtained for PLGA-C6 MP suspensions at different concentrations of 0.50, 0.40, 0.20 and 0.10 mg/mL are presented in **Annex 3.** These results suggest that coumarin-6 is predominantly localized in the polymeric matrix. However, for higher probe concentrations, the increase of λ_{em} might be explained by an exposure of the probe in the MPs surface or by increase of non-encapsulated molecules that remains in the water.

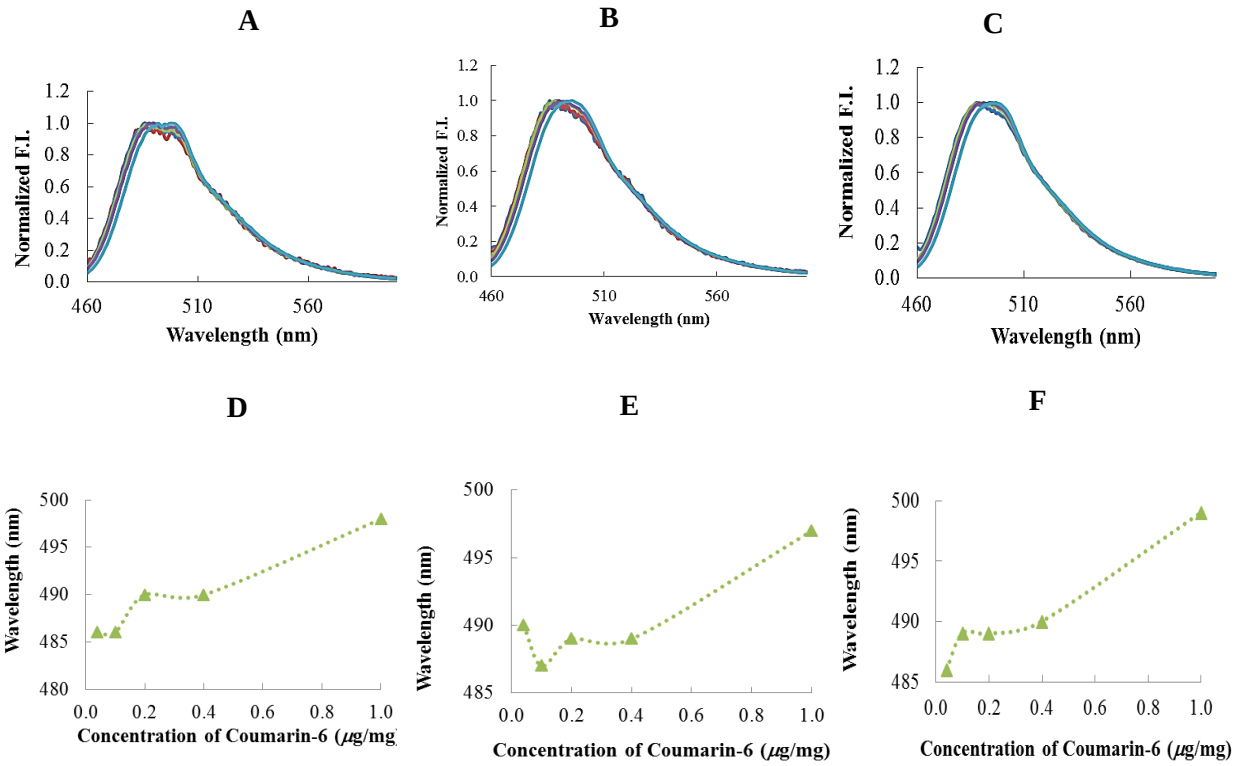

Figure 5.8 Coumarin-6 normalized spectra in (A) PLGA PVA-C6 MPs, (B) PLGA-CH-C6 MPs and (C) PLGA-ALG-C6 MPs labeled with 0.04 μg/mg (blue), 0.10 μg/mg (red), 0.20 μg/mg (green), 0.40 μg/mg (purple) and 1.00 μg/mg (light blue) of coumarin-6. Variation of $\lambda_{em\ max}$ in (D) PLGA PVA-C6 MPs, (E) PLGA-CH-C6 MPs, and (F) PLGA-ALG-C6 MPs as a function of coumarin-6 concentration. The concentration of the MPs in the suspension is 0.25 mg/mL for all panels. Data correspond to N = 1, n = 1. Measurements were performed setting λ_{ex} = 445 nm during the acquisition of the emission spectra. F.I. Fluorescence Intensity (a.u.).

Figure 5.9 shows the variation of the fluorescence intensity maximum as a function of the concentration of coumarin-6 used to label PLGA-C6 MPs. Data shows that the fluorescence intensity maximum increases almost linearly with the concentration of coumarin-6, except for lower probe concentrations in PLGA PVA-C6 MPs and PLGA ALG-C6 MPs. Experimental errors and the strong tendency to sediment may account for this variation.

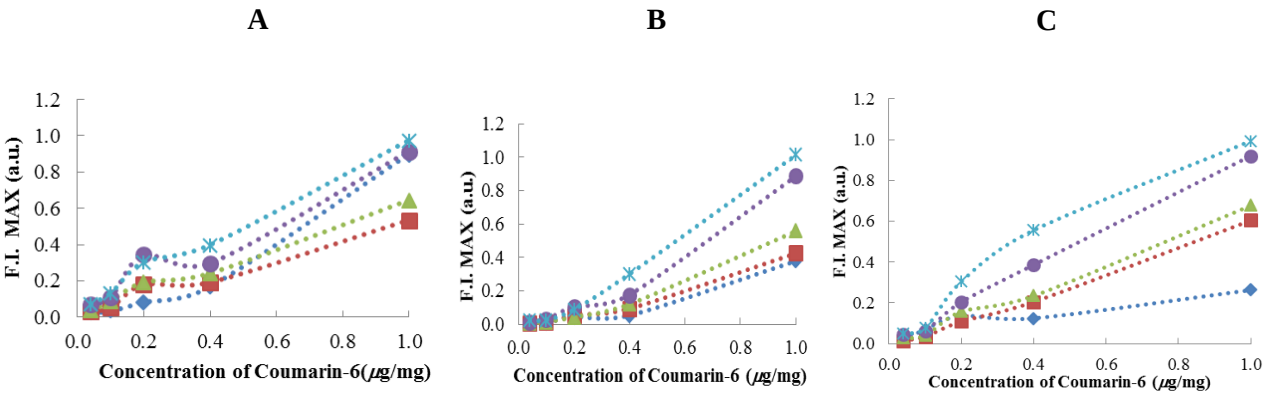

Figure 5.9 Variation of the coumarin-6 fluorescence intensity maximum as a function of probe concentration in (A) PLGA PVA-C6 MPs, (B) PLGA CH-C6 MPs and (C) PLGA ALG-C6 MPs. Data for the concentration of PLGA in suspension 0.10 mg/mL, 0.20 mg/ml, 0.25 mg/mL, 0.40 mg/mL and 0.50 mg/mL are shown in blue, red, green, purple and light blue. Data correspond to N = 1, n = 1. F.I. MAX, Fluorescence Intensity Maximum (a.u).

To further infer about the localization of coumarin-6 in the hydrophobic polymeric matrix of PLGA, the steady-state anisotropy of the probe was measured (**Figure 5.10)**. Significant differences were observed upon changing the concentration of the coumarin-6 (**Figure 5.10 A-C**). For lower coumarin-6 concentrations the anisotropy is very high, suggesting that the probe is highly restricted, most likely within the polymeric matrix of PLGA MPs. When the concentration of coumarin-6

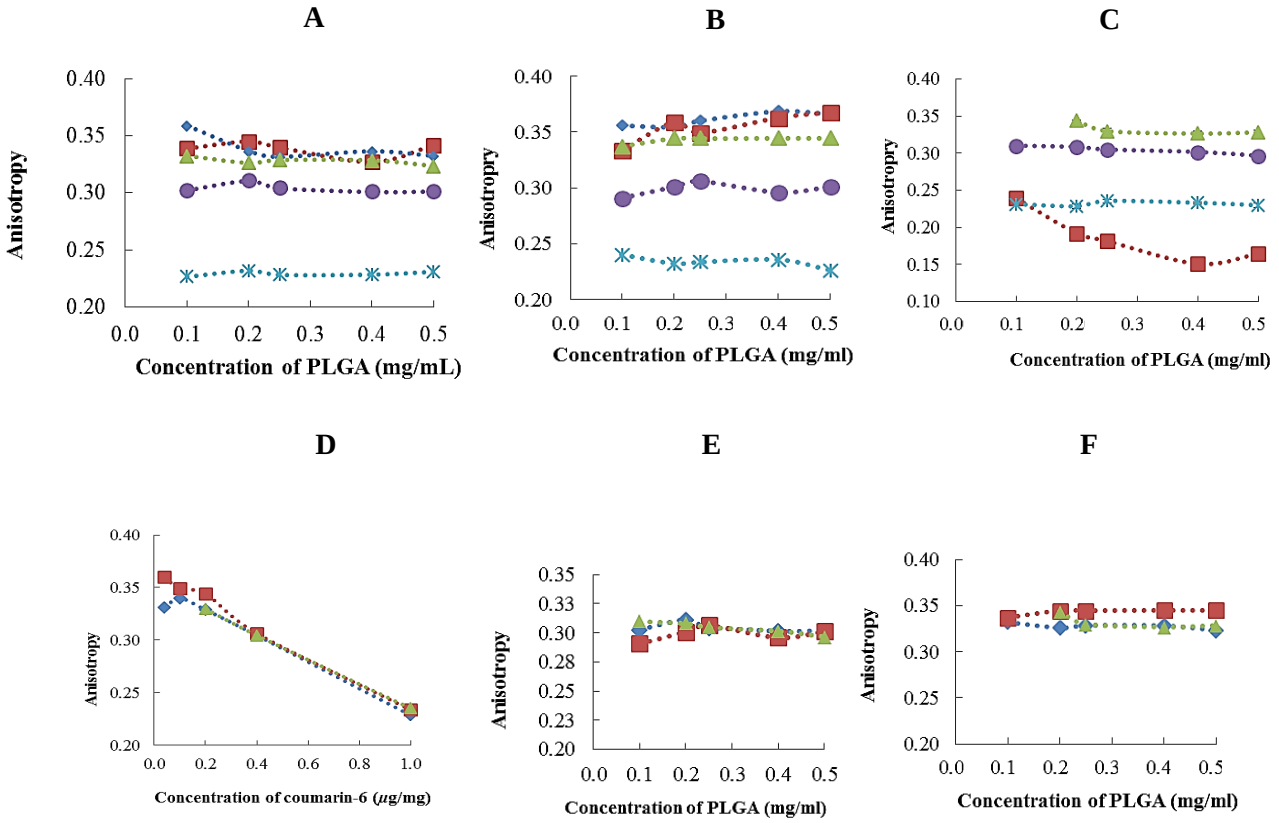

Figure 5.10 Variation of coumarin-6 anisotropy as a function of MPs concentration in suspension (A-C, E-F) or coumarin-6 concentration (D). (A) PLGA PVA-C6 MPs, (B) PLGA CH-C6 MPs and (C) PLGA ALG-C6 MPs were loaded with 0.04 μg/mg (blue), 0.10 μg/mg (red), 0.20 μg/mg (green), 0.40 μg/mg (purple) and 1.00 μg/mg (light blue). In (D) the concentration of the MPs suspension is 0.25 μg/mL. PLGA PVA MPs (blue), PLGA CH MPs (red) and PLGA ALG MPs (green) were loaded with (E) 0.20 μg/mg and (F) 0.40 μg/mg of coumarin-6. Data correspond to N = 1, n = 1.

increases a decrease in its fluorescence anisotropy is observed, probably due to a change in the environment of the probe. This might result from the exposure of the probe at the surface of the PLGA-C6 MPs, or even due to an increase in the population of the probe that is not encapsulated and remains in the aqueous environment. **Figure 5.10 D** shows the variation of the anisotropy as a function of the concentration of coumarin-6 ([PLGA]=0.25 mg/ml) for all the formulations. **Figure 5.10 E-F** shows the anisotropy in PLGA PVA-C6-3/4 MPs, PLGA CH-C6 MPs-3/4 and PLGA ALG-C6-3/4 MPs (labeled with 0.20 and 0.40 μg/mg of coumarin-6) as function of MP concentration. Overall, data suggest that no significant variation in coumarin-6 anisotropy was observed independently of MP composition.

5.3 Quantification of the Coumarin-6 entrappment

The ability of surface-modified MPs to entrap coumarin-6 was determined by direct method. To each batch of PLGA MPs containing 0.2 μg/mg of coumarin-6, the amount of entrapped probe was obtained through the dissolution of MPs in DCM and quantified by absorbance spectroscopy at 455 nm (**Table 5.3**). Results revealed that all the three types of surface-modified PLGA MPs are able to entrap the probe, although in different extensions (**Table 5.3**). PLGA PVA-C6-3 MPs showed the highest capacity to entrap the fluorescent probe, presenting E.E. and L.C. values around 47 % and 24 μg of coumarin-6 per mg of polymer, respectively. PLGA ALG-C6-3 MPs demonstrated a slightly lower E.E. % of 40 % and L.C. of 20 μg/mg. On the other hand, the ability of PLGA CH-C6-3 MPs to entrap the probe demonstrated to be significantly different from the other formulations ($p < 0.001$), presenting the lowest E.E. % of 9 % and a L.C. of 5 μg/mg. In fact, spectroscopy data (**Figure 5.7 A)** corroborates the E.E. and L.C. results showing that PLGA CH-C6 MPs displayed always the lowest fluorescence intensity maximum values. Despite the significant differences obtained for the entrapment ability of the different types of MPs, the direct method to quantify the amount of coumarin-6 entrapped should be improved by using different ratios of DCM:ethanol to dissolve the pellet in order to achieve the best proportion to solubilize coumarin-6. As demonstrated by spectral results (**Figure 5.3 C**), coumarin-6 form aggregates in DCM which clearly affect the method used to quantify the probe entrappment.

Alternative concentrations of coumarin-6 and consequently highest values for E.E. % and L.C. (μg/mg) were not explored once the main goal of producing fluorescent carriers to study the interaction between MPs and membrane models was achieved. Overall, independently from the loading values obtained, the entrapment of coumarin-6 into MPs would be considered successful once fluorescent MPs could be clearly visualized by confocal microscopy, with sufficient fluorescence intensity (**Figure 5.2**).

Table 5.3 Entrapment Efficiency (E.E. %) and Loading Capacity (μg/mg) of coumarin-6 used at an initial concentration 0.2 μg/ml to formulate surface-modified PLGA MPs with PVA (PLGA PVA-C6-3 MPs), CH (PLGA CH-C6-3 MPs) and ALG (PLGA ALG-C6-3 MPs) (mean ± SD; $N = 3$, $n = 3$). Statistical analysis: one way ANOVA and Tukey's post test. E.E and L.C., relative to the same coumarin-6 concentration *** $p < 0.001$.

Formulation	Concentration of coumarin-6 (μg/mg)	Efficiency of Entrapment, E.E. (%)	Loading Capacity, L.C. (μg/mg)
PLGA PVA-C6-3	0.2	47.4 ± 8.6	9.5E-02 ± 1.7E-02
PLGA CH-C6-3	0.2	9.5±5.4***	1.9E-02 ± 1.1E-02***
PLGA ALG-C6-3	0.2	39.6±7.9	7.9E-02 ± 1.6E-02

5.4 MPs-membrane interaction: impact of MPs surface properties

Confocal microscopy was used to study the interaction between PLGA MPs labeled with 0.2 μg/mg of coumarin-6 and GUVs containing different lipid compositions. Three different lipid mixtures were used to prepare GUVs: POPC, POPC/DPPC (1:1 mol/mol) and POPC/SM/Chol (1:1:1 mol/mol/mol). GUVs were labeled with Rho-DOPE, allowing the identification of the phase composition of mixtures. Rhodamine-based probes, especially Rhodamine-labeled lipids as Rhodamine-DOPE, have been generally used in fusion assays and in the study of membrane lateral organization (89). Moreover, this probe has been widely used to study the properties of mixtures displaying gel-fluid phase separations and l_d-l_o phase coexistence (89). It is known that Rhodamine-based probes are excluded from the l_o and gel phases and incorporated into the l_d phase, in GUVs (96). Thus, the bright areas correspond to the fluid phases and the dark areas correspond to gel and l_o phases. More specifically, the shape of the domain allows to distinguish the gel phase from the l_o phase. Studies have also shown that gel domains display dendritic/tubular shapes while l_o domains present circular shapes (66,84). GUVs obtained by electroformation displayed a nonhomogeneous size distribution ranging from 15 to 30 μm. Regarding the phase properties of the lipid mixtures (**Figure 25**), Rho-DOPE displays a homogeneous distribution along the entire POPC vesicles, being present only the fluid phase **(Figure 5.11 A-C)**. In **Figure 5.11 D-F,** GUVs exhibit fluid (bright areas) and gel (dark areas) phases, which according to the POPC/DPPC phase diagram, for a 1:1 mol/mol composition, was an expected result. In **Figure 5.11 H-I** it was possible to observe POPC/SM/Chol GUVs displaying fluid-fluid separation, revealed by the presence of bright areas (l_d phase), and also some dark areas that are thought to be l_o phase. On the l_o phase, the morphology of the domain can be considered as circular. However, results from **Figure 5.11 J** show that some POPC/SM/Chol (1:1:1 mol/mol/mol) GUVs also display fluid-gel phase separations revealed by the tubular morphology of the domain. This phenomenon can be explained by the improper addition of lipids during the preparation, leading to a different lipid proportion from 1:1:1 and some degree of heterogeneity of the GUV population in terms of lipid phases.

Concerning the study of MPs-membrane interaction, the results suggest that regardeless of the MPs composition, no specific MPs-membrane interactions occur with fluid homogenous POPC GUVs as shown by the absence of MPs internalization and/or overlay with the lipid bilayer (**Figure 5.11 A-C**). In contrast, for lipid mixtures displaying gel-fluid phases separation a clear internalization of MPs composed of CH and ALG was observed (**Figure 5.11 E,F**). The analysis of the 3D projection images and confocal slices (**Figure 5.11 E,F**) further suggests that MPs internalization occurs through interaction with gel domains and interface of gel-fluid phase. Moreover, the results further suggest that MPs surface modified with CH were also able to interact with POPC/SM/Chol mixtures, likely through contact with fluid ordered domains (**Figure 5.11 H**).

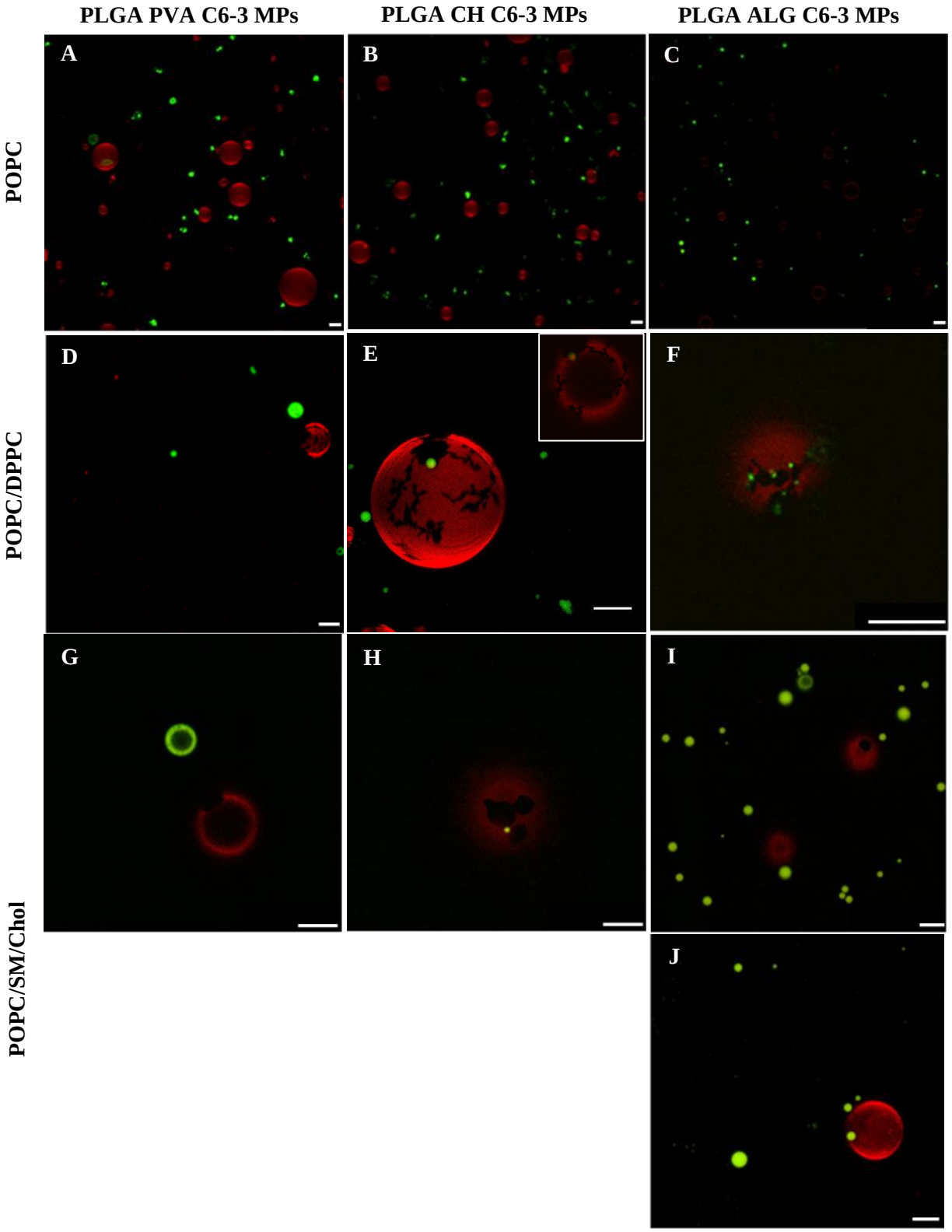

Figure 5.11 Confocal Microscopy images of GUVs labeled with Rho-DOPE (red), and PLGA-C6 MPs labeled with a concentration of 0.2 μg/mg of coumarin-6 (green). The concentration of the MPs in the suspension is 0.25 mg/mL for all panels. GUVs are composed by the following lipid mixtures: (A-C) POPC, (D-F) POPC/DPPC (1:1 mol/mol) and (G-J) POPC/SM/Chol (1:1:1 mol/mol/mol). Data for PLGA PVA-C6-3 MPs, PLGA CH-C6-3 MPs and PLGA ALG-C6-3 MPs are shown in (A,D,G), (B,E,H) and (C,F,I,J), respectively. In (E) is visible de detail of the confocal section which demonstrated that the MP is inside the GUV. Representative images of three independent experiments are shown. Scale bars = 10 μm**.**

CHAPTER 6: Discussion

Challenges on modern drug delivery are focused on the development of the so called "smart" and more effective preventive and/or therapeutic strategies (97). Nano and micro drug delivery systems have been explored as promising approaches for therapeutic strategies due to its ability to protect the therapeutic entity from proteolytic degradation in biological environment, enhance the targeted delivery to specific cells and improve drug bioactivity, minimizing side effects (6). Despite the high number of nano and micro particulate systems under research, there is still a lack of knowledge on the kinetics of these systems at the cellular level and how they interact with cell membranes. Recent studies have suggested that a thorough knowledge of the physicochemical features essential for the interaction between drug delivery systems and cells will allow the design of more effective and safe carriers (4–6). Accordingly, the study of the interaction of nano/micro drug delivery systems with cell membranes and membrane model systems has become an important research line (1,4,6,42,43,85). On the other hand, studies on cell membranes and membrane model systems have shown that biomembranes are functionally and structurally highly compartmentalized and their lipids have an active role on the cellular homeostasis (63–65). However, there is a lack of knowledge on how biomembrane properties influence the interactions with nano and micro systems. Exploiting these gaps by acquiring a deep expertise in different but complementary areas as nanotechnology, pharmaceutical technology, chemistry and biophysics will improve the success rate of the therapeutic entities that reaches the target site and also modulate the extent of undesirable effects (97).

This project aimed to develop biodegradable and biocompatible surface-modified PLGA microparticulate systems in order to evaluate the effect of their surface charge in the interaction with membrane model systems. Accordingly, PLGA MPs were prepared using the surface-modifier polymers CH and ALG, labeled with a fluorescent probe and physicochemically characterized. A thorough spectral study of the probe in its free form and entrapped into PLGA MPs was performed. Membrane model systems, more specifically GUVs, were also produced and used to monitor the possible interactions with PLGA MPs and to study the impact of different MP surface modifications on those interactions, using confocal microscopy.

6.1 Physicochemical characterization of the surface-modified microparticles and coumarin-6 spectral characterization

In vitro and *in vivo* MP behaviour depends on several physicochemical characteristics including size distribution, surface charge, hydrophobicity, chemical composition and morphology (48,50,54). Accordingly, PLGA MPs were characterized for their physicochemical properties mainly surface charge, size and shape.

The median sizes of unloaded and coumarin-6-loaded PLGA MPs ranged between 1.4±0.3 to 3.8±0.2 μm (**Table 5.1**). The size range obtained can be considered satisfactory to visualize MP under the confocal microscope once the minimum size of 200 nm has been reported (98). In fact, the differences observed in $D_{50\%}$ values of unloaded and coumarin-6-loaded PLGA MPs were mainly not statistically significant demonstrating that the different surface modifications and also the coumarin-6 loading did not have a significant impact on their median size values. Additionally, $D_{10\%}$ values for PLGA CH-C6-4 MPs, PLGA ALG-C6-4 MPs and PLGA ALG-C6-5 MPs demonstrated the presence

of one subpopulation in the nanometer size range. For PLGA ALG-C6-3 MPs, **Figure 5.1 B** demonstrated a subpopulation in micrometer size range. The origin of this subpopulation can be explained by different factors such as MP aggregation, insufficient solvent evaporation time and inconstant stirring during emulsion steps. In fact, the mechanic agitation of the homogenizer used was not completely constant. The homogenizer used (Ultraturrax) is a rotor-stator system composed of coaxial intermeshing rings with radial openings. During Ultraturrax homogenization, the fluid enters into the system and is accelerated and decelerated multiple times (99). Actually, during the mechanic agitation there is some air incorporation and foam formation, leading to loss of the stabilizer surfactant agent. Another factor that causes subpopulations is the drop-by-drop addition of the first aqueous phase to the oil phase or the first w/o emulsion to the external phase (100). However, while operator gets more experient, this addition becomes automatic and variability that can origin these sub population decreases. Therefore, adding drop-by-drop will not be a direct cause for these subpopulations.

Analyzing the dispersity, the span results of unloaded and coumarin-6-loaded PLGA MPs ranged from 1.1±0.2 to 4.8±1.1 (**Table 5.1**). Ito et *al.* reported that PLGA MPs prepared by the emulsion solvent method with spans lower than 1 are homogeneous populations (101). Accordingly, MP populations under study can be considered heterogeneous being this behavior independent of surface modification and probe loading. Despite the absence of flocculation phenomenon during the formulation process that suggests a stable formulation, the span values and also the $D_{10\%}$ demonstrated that MPs aggregate. Consequently, the studied MPs can be considered unstable.

Confocal results obtained were able to corroborate laser diffraction results. Confocal images (**Figure 5.2**) showed aggregated coumarin-6-loaded PLGA MPs with high size dispersion. Confocal studies also revealed the instability of coumarin-6-loaded PLGA PVA MPs and coumarin-6-loaded PLGA ALG MPs, which tend to collapse forming sickle-like shapes. Doshi et *al.* described the production of sickle-like shaped PLGA MPs through the shape variation of spherical PLGA MPs by their incubation with 2-propanol (102). Actually, the study demonstrated that the partial fluidization of PLGA caused by 2-propanol might induce MP collapse. Similarly, the incomplete DCM evaporation during the formulation of coumarin-6-loaded PLGA PVA MPs and PLGA ALG MPs could also be the cause for this phenomenon. Moreover, confocal studies showed a non-homogeneous labelling of PLGA PVA-C6-3 MPs and PLGA ALG-C6-3 MPs by coumarin-6 (**Figure 5.2**). These spots might correspond to DCM that was not completely evaporated or even surfactant on the surface resultant from unproper surfactant wash. Surprisingly, coumarin-6-loaded PLGA CH-C6 MPs that demonstrated the lowest ability to entrap coumarin-6 displayed an homogenous staining.

Although $D_{50\%}$ values did not demonstrated statistically significant differences, the formulation of PLGA MPs containing PVA as external surfactant presented the lowest size disparity. This finding is in agreement with other studies that demonstrated that PVA allows the production of PLGA NPs and MPs with uniform size distribution (15,103,104). Through intra- and/or intermolecular interactions with hydrophobic moieties, PVA fits spontaneously the droplet surface forming micelles in aqueous media. This phenomenon confers stability to the formulation process by decreasing the free energy at the interface between two phases, and avoiding the coalescence and flocculation of the emulsion droplets. Accordingly, PVA particles have lower particle sizes and lower polidispersity (105). On the other hand, CH and ALG formulations present higher size disparities. This observation can be explained by the higher viscosity of external phase of the secondary emulsion conferred by both polymers, which results in the formation of large emulsion droplets. In fact, a higher energy is needed to form droplets that will become solid MPs after solvent evaporation. Similar facts were previously observed in our laboratory (21,105,106). Moreover, the polymers CH and ALG are derived

from natural sources and consequently their own polydispersity is high. An alternative strategy to decrease the variability and also produce highly positive and negative PLGA MPs would be the coating of PLGA surface with cationic and anionic lipids, respectively (42).

As expected, non-fluorescent and coumarin-6-loaded PLGA MPs prepared with distinct surface-modifier polymers presented significantly different ($p < 0.001$) surface charges **(Table 5.2)**. Non-fluorescent and coumarin-6-loaded PLGA MPs containing PVA displayed ZP values ranging from -17.8±0.9 to -19.9±0.2 mV. Similar results were obtained in several studies either for non-labeled or labeled PLGA NPs and MPs (21,103,107,108). Non-fluorescent and coumarin-6-loaded PLGA MPs containing CH as surface modifier showed highly positive ZP values range between 50.8±2.7 and 58.7±3.4 mV. ZP results confirmed the presence of CH on the surface of MPs resultant from the linkage between protonated amino groups of CH and carboxylic end groups of PLGA (109). Similar surface-modified PLGA MPs prepared by Manca *et al.* using the emulsion solvent diffusion method show ZP values close to 40 mV for the same CH concentration (0.75 % (w/v)) used in this study. (110). Non-fluorescent and coumarin-6-loaded PLGA MPs containing ALG displayed a ZP ranging from -30.8±2.3 to -36.8±4.4 mV, confirming the adsorption of ALG to the surface. This highly negative surface charge is probably attained due to the presence of the ALG carboxyl groups at MP surface. Several studies corroborate the ZP results obtained for ALG surface-modified PLGA MPs by suggesting that the surface modification with ALG leads to negatively charged carriers. Florindo *et al.* demonstrated that antigen-loaded PLA NPs modified with ALG at the concentration of 0.75 % (w/v) exhibited surface charges that ranged from -50.8±2.4 to -50.0±4.5 mV (105), supporting the highly negative ZP values obtained for PLGA MPs containing the same amount of surface modifier. Contrary to the results obtained for the different surface-modified MPs ($p < 0.001$), ZP values seems to be independent of the coumarin-6 concentration used. Despite the high negative charge of probe at pH 5.7 according to its $pK_{a(coumarin-6)} = 0.8$, previous observations may indicate that coumarin-6 molecules should be mainly entrapped into polymer matrix not being available in sufficient amount to cause significant surface charge variations in coumarin-6-loaded PLGA MPs (111). However, significant differences on ZP values would be observed if a sufficient amount of coumarin-6 was present on MP surface. The absence of significant ZP differences can be justified by the trace concentration of coumarin-6 used during the formulation process comparing to other formulation components.

Although the MP surface modification with CH and ALG has successfully produced positively and negatively charged MPs, it was not possible to produce fluorescent or non-fluorescent PLGA PVA MPs with neutral surface charge (**Table 5.2**). Stolnik *et al.* reported that PLGA NPs without PVA coating have highly negative ZP values close to -45 mV due to the exposure of uncapped carboxyl groups of PLGA at NP surface (112). Accordingly, MP surface coating with amphiphilic polymers should lead to the reduction of uncapped carboxyl groups decreasing the ZP (107). In fact, it was demonstrated that increasing PVA concentration to values close to 5 % (w/v) can originate particles with surface charges close to neutrality (103). Thus, neutrality was not achieved for surface-modified PVA MPs probably due to the insufficient concentration of 2.5 % (w/v) PVA used. Therefore, a possible future strategy to reach this goal can be designed by increasing PVA concentration. An alternative approach to obtain particulate carriers with neutral surface charges may also take into account the MP surface modification with hydrophilic polymers such as PEG (113).

ZP measurement depends on the pH and ionic strength of dispersant as well as on temperature. ZP was initially measured in phosphate buffer pH 7.4 containing Ca^{2+} and Mg^{2+} (data not shown) to mimetize MP behavior at physiological extracellular conditions. However, all formulations presented surface charges close to neutrality, which can be explained by the effect of Ca^{2+} and Mg^{2+} cations in

the neutralization of negative charged MPs. Attending the main goals of this study to evaluate the impact of different surface charges on the interaction between surface-modified MPs and membrane model systems, and to predict the behavior of MPs and GUVs, ultrapure water at pH 5.7 was used to measure ZP. In the absence of any ions at pH 5.7, PLGA PVA MPs were slightly more negative, PLGA CH MPs were highly positive and PLGA ALG MPs were highly negative (**Table 5.2**). The aforementioned choice can be supported by Sahoo *et al.* that published the pH effect in PLGA NPs coated with PVA at different concentrations of 0.5, 1, 2 and 5 % (w/v) showing that ZP progressively changes to positive values at pH < 5 and above that pH attain negative values (103). On the other hand, PLGA and ALG are highly negative at physiological pH. Thereby, electrostatic repulsions between both polymers will definitely increase the desorption of ALG from MP surface (114). Accordingly, ALG desorption from the surface of negatively charged PLGA MPs can be prevented at pH 5.7 once PLGA is less negative and ALG is still anionic. A similar phenomenon might occur for CH surface-modified MPs since PLGA is highly negative and CH weakly positive at physiological pH, promoting CH desorption. Actually, CH is highly positively charged at pH 5.7 whereas at pH 7.4 it is close to neutrality (115). Consequently, CH desorption from PLGA MP surface will be vestigial at pH 5.7 due to the high electrostatic attraction between both polymers. In conclusion, all these evidences can explain the neutral ZP values (data not shown) obtained for non-fluorescent and fluorescent surface-modified PLGA MPs, at physiological pH.

Analysis of the fluorescence behavior of coumarin-6-loaded MPs revealed important features: i) coumarin-6-concentration dependent saturation of the fluorescence intensity of the probe, particularly for coumarin-6 concentration above 0.20 μg/mg (green), ii) red-shift in coumarin-6 emission spectra when coumarin-6 concentration increases from 0.04 to 1.00 μg/mg, regardless of MP composition and iii) decrease in the fluorescence anisotropy of coumarin-6 when MPs were loaded with 0.20, 0.40 and 1.00 μg/mg . Overall, these results indicate an alteration in the environment where coumarin-6 is localized, from less polar environment within the PLGA hydrophobic matrix, to a more polar environment at the surface of the MPs or even in the water. Apart from the behaviors above described, values from F.I. MAX (**Figure 5.5 A and Figure 5.7**) are lower for PLGA CH-C6 MPs and higher for PLGA PVA-C6 MPs and PLGA ALG-C6 MPs. The referred trend strongly corroborates with E.E. and L.C. results. So, PLGA CH-C6 MPs demonstrated the lowest tendency to entrap coumarin-6. In addition, values of $D_{50\%}$ and ZP were independent of the introduction of the probe. In conclusion, coumarin-6 spectral characterization demonstrated that the entrapment of the probe into the surface modified PLGA MPs leads to a probe/MPs stable system.

6.2 Impact of surface properties of the surface modified MPs in interactions with GUVs

The vesicles produced were labeled with Rho-DOPE. As Silva *et al.* described, the partition coefficient of Rho-DOPE between the l_o and the l_d phases in POPC/SM/Chol (1:1:1 mol/mol/mol) is 0.28±0.08 meaning that this probe has a high affinity to fluid disordered phases (116). Rho-DOPE displayed homogeneous distribution along the entire POPC vesicles, as expected for vesicles formed by a single lipid with very low melting temperature (T_m= -2˚C, (117)), and therefore fluid at the temperature employed in the present study. In contrast, POPC/DPPC (1:1 mol/mol) GUVs displayed gel-fluid phase separation, as expected for this mixture (118). For POPC/SM/Chol (1:1:1 mol/mol/mol) GUVs l_o-l_d should be presented in all GUVs produced. This is mainly evidenced by the presence of the dark circular domains along the vesicle. However, some vesicles displayed gel-fluid phase separation, as denoted by the dendritic/tubular dark regions observed. This phenomenon can be

explained by some experimental errors: i) lipids stock solutions could display concentration different from the one assayed, ii) the lipid proportions of each component were not mixed correctly and iii) experimental temperature different from 23 ˚C. Overall, those experimental errors could have contributed to a lipid proportion different from the ideal 1:1:1 proportion (**Figure 6.1**, purple point at the phase diagram).

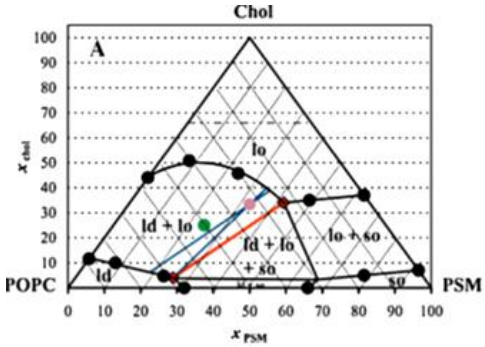

Figure 6.1 PSM/POPC/Chol phase diagram at 23 °C. experimental points are represented by circles (122).

GUVs produced have sizes ranging from 15 to 30 μm which is within the size range described for macrophage cells (119). It is well documented that these cells are able to phagocytize MPs with the same diameters as the ones produced in this study (4). The interactions observed for PLGA CH-C6-3 MPs and PLGA ALG-C6-3 MPs and POPC/DPPC GUVs seemed to happen essentially at the interface of the fluid-gel phases. From the literature, it is known that phase separation regions trigger packing defects at the membrane (84). In fact, the MPs affinity to this interface region could be related with packing defects that may allow the MPs integration on the membrane. In addition, at this region, the physico-chemical properties of the membrane could be altered (87). In this region, the ZP alteration can be present due to lipids interaction. This phenomenon can explain the presence of negative charges in coexistence with positive charges that trigger electrostatic attraction of PLGA CH-C6-3 MPs and PLGA ALG-C6-3 MPs, respectively. Results shown strongly corroborate that the interface of the gel-fluid phases is a preferential region for interaction of highly positive and highly negative PLGA MPs and GUVs.

In physiological terms, these observations can raise some questions. How important is the interaction between MPs and interface fluid-gel regions? Is there some relationship between these biophysical phases and the presence of membrane receptors? Are these phases involved in endocytic processes? These are some questions that have yet to be answered and that could be addressed in future studies. What is the impact of all these observations in the future development of MPs? By the project under study it was demonstrated that under the experimental conditions employed, highly negative and highly positively charged PLGA MPs presented higher interaction with membrane models at gel-fluid phases interface.

CHAPTER 7: Conclusion

The main goal of this study was to evaluate the interactions between polymeric microcarriers with different surface charges and GUVs with different biophysical properties. In general, this study was intended to give additional information fundamental for a future rational design of engineered nano/microsystems acting as therapeutic vectors.

Our studies revealed that non-fluorescent and fluorescent surface-modified PLGA MPs displayed median sizes ranging between 1.4±0.3 to 3.8±0.2 μm and presented high size dispersity. The surface modification and the introduction of the probe did not change significantly the median sizes. A clear distinction in terms of surface charge, once changing the surface modification, was attained under acidic pH = 5.7. In addition, coumarin-6 did not change significantly the surface charge. The instability of the surface-modified MPs was mainly revelead by its i) aggregation, ii) tendency to collapse forming sickle-like shapes (mainly the case of coumarin-6-loaded PLGA PVA MPs and coumarin-6-loaded PLGA ALG MPs) and iii) span values.

Spectral characterization revealed that the entrapment of the fluorescent dye coumarin-6 in PLGA MPs leads to a probe/MP stable system. Spectral properties were analyzed by fluorescence spectroscopy with five different probe concentrations and five concentrations of MPs in suspension. Results demonstrated that coumarin-6 is essently localized in the polymeric matrix since does not change its partion environment when changing the concentration of MPs in suspension. At higher concentrations (above 0.2 μg/mg), the increase of the non-encapsulated molecules localized in the surface of the MPs or even aqueous medium lead to a decrease of anisotropy values.

Studies on MPs-membranes interaction by confocal microscopy showed that highly positive PLGA CH-C6-3 MPs and highly negative PLGA ALG-C6-3 MPs interacted with GUVs and were mainly attracted to the gel phases and interface of fluid-gel phases. The packing defects in interface regions and also the ZP alteration could account for this phenomenon. These observations will help a more accurate design of PLGA MPs on drug delivery applications.

CHAPTER 8: Future Work Perspectives

As future work perspectives, the formulation method could be optimized in order to achieve homogeneous surface modified PLGA MPs populations (both unloaded and coumarin-6 loaded). It would be interesting to compare the behavior of MPs and NPs in order to study the size effect. Also, the ZP of the different GUVs could be measured in order to better understand the role of membrane charges in membrane-MP interactions.

In microscopy studies, the experimental conditions could be further optimized. Real time microscopy techniques could be used in order to acquire more accurate results. In this way, using the same method, several dilutions of the coumarin-6 loaded surface modified PLGA NPs/MPs suspension could be tested. This could allow a more precise selection of the PLGA-C6 MPs/GUVs favorable proportion to their interaction. In addition, microscopy studies could also be performed under physiological pH, to further extend this study to the normal extracellular medium condition found in biological cells.

Finally, at a later stage, it would be interesting to confirm the observations made using membrane models in more complex systems such as cellular models, using different types of cells.

References

1. Zhao F, Zhao Y, Liu Y, Chang X, Chen C. Cellular Uptake , Intracellular Traffi cking , and Cytotoxicity of Nanomaterials. Small. 2011;7(10):1322–37.
2. Jaspreet K. Vasir VL. Biodegradable nanoparticles for cytosolic delivery of therapeutics. Adv Drug Deliv Rev. 2007;59:718–28.
3. Sahay G, Alakhova DY, Kabanov A V. Endocytosis of nanomedicines. J Control Release [Internet]. Elsevier B.V.; 2010 Aug 3 [cited 2013 Dec 15];145(3):182–95. Available from: http://www.pubmedcentral.nih.gov/articlerender.fcgi?artid=2902597&tool=pmcentrez&rendertype=abstract
4. Tahara K, Tadokoro S, Kawashima Y, Hirashima N. Endocytosis-like uptake of surface-modified drug nanocarriers into giant unilamellar vesicles. Langmuir [Internet]. 2012;28(18):7114–8. Available from: http://www.ncbi.nlm.nih.gov/pubmed/22515197
5. Miguel P, Silva B De. Desenvolvimento de formulações de libertação modificada de ranitidina. Faculdade de Farmácia da Universidade do Porto; 2007.
6. Mozafari MR. Nanomaterials and Nanosystems for Biomedical Applications. Mozafari MR, editor. Monash University, Victoria, Australia: Springer; 2007.
7. Tran V, Benoît J, Venier-julienne M. Why and how to prepare biodegradable , monodispersed , polymeric microparticles in the field of pharmacy ? Int J Pharm [Internet]. Elsevier B.V.; 2011;407(1-2):1–11. Available from: http://dx.doi.org/10.1016/j.ijpharm.2011.01.027
8. Vilos C, Velasquez LA. Therapeutic strategies based on polymeric microparticles. J Biomed Biotechnol [Internet]. 2012 Jan [cited 2014 Aug 20];2012:672760. Available from: http://www.pubmedcentral.nih.gov/articlerender.fcgi?artid=3363323&tool=pmcentrez&rendertype=abstract
9. McCall RL, Sirianni RW. PLGA nanoparticles formed by single- or double-emulsion with vitamin E-TPGS. J Vis Exp [Internet]. 2013;(82):51015. Available from: http://www.ncbi.nlm.nih.gov/pubmed/24429733
10. Makadia HK, Siegel SJ. Poly Lactic-co-Glycolic Acid (PLGA) as Biodegradable Controlled Drug Delivery Carrier. Polymers (Basel). 2011;1377–97.
11. Rao JP, Geckeler KE. Polymer nanoparticles: Preparation techniques and size-control parameters. Prog Polym Sci [Internet]. Elsevier Ltd; 2011;36(7):887–913. Available from: http://dx.doi.org/10.1016/j.progpolymsci.2011.01.001
12. Gadad A.P., Vannuruswamy G., Sharath Chandra P, Dandagi P.M MVS. Study of different properties and applications of Poly lactid-co-glycolic acid (PLGA) nanotechnology: an overview. INDIAN DRUGS. 2012;(November):5–22.
13. Ramchandani M, Robinson D. In vitro and in vivo release of ciprofloxacin from PLGA 50 : 50 implants. 1998;54:167–75.
14. Amann LC, Gandal MJ, Lin R, Liang Y, Siegel SJ. In Vitro – In Vivo Correlations of Scalable PLGA-Risperidone Implants for the Treatment of Schizophrenia. Pharm Res. 2010;27(8):1730–7.
15. Panyam J, Labhasetwar V. Biodegradable nanoparticles for drug and gene delivery to cells and tissue. Adv Drug Deliv Rev [Internet]. 2003 Feb [cited 2013 Dec 15];55(3):329–47. Available from: http://linkinghub.elsevier.com/retrieve/pii/S0169409X02002284
16. F.X. Lacasse, M.C. Fillion, N.C. Phillips, E. Escher, J.N. McMullen PH. Influence of Surface Properties at Biodegradable Microshpere Surfaces effestcs on plasma protein adsorption and phagocytosis. 1997.

17. Youan BC, Hussain A, Nguyen NT. Evaluation of Sucrose Esters as Alternative Surfactants in Microencapsulation of Proteins by the Solvent Evaporation Method. AAPS PharmSci. 2003;5(2):1–9.
18. Lavisse S., Paci A. R V. In vitro echogenicity characterization of poly[lactide-coglycolide] (PLGA) microparticles and preliminary in vivo ultrasound enhancement study for ultrasound contrast agent application. Investig R adiology. 2005;40(8):536–44.
19. Yemisci M, Bozdag S. CM. Treatment of malignant gliomas with mitoxantrone-loaded poly(lactide-co-glycolide) microspheres. Neurosurgery. 2006;59(6):1296–302.
20. Peyre M., Sesardic D., Merkle H. P. GB, P J. An experimental divalent vaccine based on biodegradable microspheres induces protective immunity against tetanus and diphtheria. J Pharm Sci. 2003;92(5):957–66.
21. Danhier F, Ansorena E, Silva JM, Coco R, Le Breton A, Préat V. PLGA-based nanoparticles: an overview of biomedical applications. J Control Release [Internet]. Elsevier B.V.; 2012 Jul 20 [cited 2013 Dec 12];161(2):505–22. Available from: http://www.ncbi.nlm.nih.gov/pubmed/22353619
22. Zhu M, Nie G, Meng H, Xia T, Nel A, Zhao Y. Physicochemical properties determine nanomaterial cellular uptake, transport, and fate. Acc Chem Res [Internet]. 2013 Mar 19;46(3):622–31. Available from: http://www.ncbi.nlm.nih.gov/pubmed/22891796
23. Salvador A, Igartua M, Hernández RM, Pedraz JL. Designing improved poly lactic-co-glycolic acid microspheres for a malarial vaccine: incorporation of alginate and polyinosinic-polycytidilic acid. J Microencapsul [Internet]. 2014;2048:1–7. Available from: http://www.ncbi.nlm.nih.gov/pubmed/24697189
24. Bernkop-Schnürch A, Dünnhaupt S. Chitosan-based drug delivery systems. Eur J Pharm Biopharm [Internet]. 2012 Aug [cited 2014 Aug 9];81(3):463–9. Available from: http://www.ncbi.nlm.nih.gov/pubmed/22561955
25. Sinha VR, Singla AK, Wadhawan S, Kaushik R, Kumria R, Bansal K, et al. Chitosan microspheres as a potential carrier for drugs. Int J Pharm [Internet]. 2004 Apr 15 [cited 2014 Jul 11];274(1-2):1–33. Available from: http://www.ncbi.nlm.nih.gov/pubmed/15072779
26. Dash M, Chiellini F, Ottenbrite RM, Chiellini E. Chitosan—A versatile semi-synthetic polymer in biomedical applications. Prog Polym Sci [Internet]. Elsevier Ltd; 2011 Aug [cited 2014 Jul 9];36(8):981–1014. Available from: http://linkinghub.elsevier.com/retrieve/pii/S007967001100027X
27. Benediktsdóttir BE, Baldursson Ó, Másson M. Challenges in evaluation of chitosan and trimethylated chitosan (TMC) as mucosal permeation enhancers: From synthesis to in vitro application. J Control Release [Internet]. Elsevier B.V.; 2014;173(1):18–31. Available from: http://dx.doi.org/10.1016/j.jconrel.2013.10.022
28. Chandy T, Das GS, Rao GH. 5-Fluorouracil-loaded chitosan coated polylactic acid microspheres as biodegradable drug carriers for cerebral tumours. J Microencapsul [Internet]. 2000;17(5):625–38. Available from: http://www.ncbi.nlm.nih.gov/pubmed/11038121
29. Kang ML, Cho CS, Yoo HS. Application of chitosan microspheres for nasal delivery of vaccines. Biotechnol Adv [Internet]. Elsevier Inc.; 2009 [cited 2014 Aug 20];27(6):857–65. Available from: http://www.ncbi.nlm.nih.gov/pubmed/19583998
30. Casettari L, Castagnino E, Stolnik S, Lewis A, Howdle SM, Illum L. Surface characterisation of bioadhesive PLGA/chitosan microparticles produced by supercritical fluid technology. Pharm Res [Internet]. 2011 Jul [cited 2015 Jun 20];28(7):1668–82. Available from: http://www.ncbi.nlm.nih.gov/pubmed/21394661
31. Kawashima Y, Yamamoto H, Takeuchi H, Kuno Y. Mucoadhesive DL-lactide/glycolide copolymer nanospheres coated with chitosan to improve oral delivery of elcatonin. Pharm Dev

Technol. 2000;5(1):77–85.
32. Jain D, Bar-shalom D. Alginate drug delivery systems : application in context of pharmaceutical and biomedical research. Drug Dev Ind Pharm [Internet]. Informa Healthcare USA, Inc; 2014;1–9. Available from: http://dx.doi.org/10.3109/03639045.2014.917657
33. Goh CH, Wan P, Heng S, Chan LW. Alginates as a useful natural polymer for microencapsulation and therapeutic applications. Carbohydr Polym [Internet]. Elsevier Ltd.; 2012;88(1):1–12. Available from: http://dx.doi.org/10.1016/j.carbpol.2011.11.012
34. Sosnik A. Alginate Particles as Platform for Drug Delivery by the Oral Route : State-of-the-Art. Hindawi Publ Corp. 2014;2014.
35. Mata E, Igartua M, Patarroyo ME, Pedraz JL, Hernández RM. Enhancing immunogenicity to PLGA microparticulate systems by incorporation of alginate and RGD-modified alginate. Eur J Pharm Sci [Internet]. Elsevier B.V.; 2011 Sep 18 [cited 2015 May 14];44(1-2):32–40. Available from: http://www.ncbi.nlm.nih.gov/pubmed/21699977
36. Ungaro F, D'Angelo I, Coletta C, D'Emmanuele Di Villa Bianca R, Sorrentino R, Perfetto B, et al. Dry powders based on PLGA nanoparticles for pulmonary delivery of antibiotics: Modulation of encapsulation efficiency, release rate and lung deposition pattern by hydrophilic polymers. J Control Release. 2012;157(1):149–59.
37. Silva JM, Préat V, Florindo H. Encyclopedia of Biomedical Polymers and Polymeric Biomaterials Role of the Aliphatic Polyesters as Particulate Vaccine Delivery Systems Role of the Aliphatic Polyesters as Particulate Vaccine Delivery Systems.
38. Chithrani BD, Chan WCW. Elucidating the Mechanism of Cellular Uptake and Removal of Protein-Coated Gold Nanoparticles of Different Sizes and Shapes. Nano Lett. 2007;7:1542–50.
39. Akinc, Akin. Battaglia G. Exploiting Endocytosis for Nanomedicines. Cold Spring Harb Perspect Biol. 2013;5.
40. Zauner W, Farrow NA, Haines AMR. In vitro uptake of polystyrene microspheres : effect of particle size , cell line and cell density. 2001;71:39–51.
41. Bozavikov P, Rajshankar D, Lee W, Mcculloch CA. Particle size influences fibronectin internalization and degradation by fibroblasts. Elsevier. 2014;
42. Couvreur HÆP. Nanocarriers ' entry into the cell : relevance to drug delivery. Cell Mol Life Sci. 2009;66:2873–96.
43. Albanese A, Tang S. P. CCWW. The Effect of Nanoparticle Size , Shape , and Surface Chemistry on Biological Systems. Annu Rev Biomed Eng. 2012;1–16.
44. Tzlil S, Deserno M, Gelbart WM, Ben-shaul A. A Statistical-Thermodynamic Model of Viral Budding. Biophys J. 2004;86(April):2037–48.
45. Gao H, Shi W, Freund LB. Mechanics of receptor-mediated endocytosis. Proc Natl Acad Sci. 2005;102(27):3–8.
46. Zhang, Sulin. Li, Ju. Lykotrafitis, George. Bao, Gang. Suresh S. Size-Dependent Endocytosis of Nanoparticles. PMC. 2009;21:419–24.
47. Chaudhuri A, Battaglia G, Golestanian R. The effect of interactions on the cellular uptake of nanoparticles. Phys Biol. 2011;046002.
48. Yi X, Shi X, Gao H. Cellular Uptake of Elastic Nanoparticles. Phys Rev Lett. 2011;107.
49. Korn ED, Weisman R a. Phagocytosis of latex beads by Acanthamoeba III. Electron microscopic study of the initial events. J Cell Biol. 1967;34:219–27.
50. Fröhlich E. The role of surface charge in cellular uptake and cytotoxicity of medical nanoparticles. Int J Nanomedicine. 2012;5577–91.
51. Oyewumi MO, Kumar A, Cui Z. Nano-microparticles as immune adjuvants : correlating particle sizes and the resultant immune responses. Expert Rev Vaccines. 2010;9(9):1095–107.
52. Tabata Y, Ikada Y. Effect of the size and surface charge of polymer microspheres on their

phagocytosis by macrophage. Biomaterials. 1988;9(4):356–62.
53. Roser M, Fischer D KT. Surface-modified biodegradable albumin nano- and microspheres. II: effect of surface charges on in vitro phagocytosis and biodistribution in rats. Eur J Pharm Biopharm. 1998;46(3):255–63.
54. Yue Z, Wei W, Lv P, Yue H, Wang L, Su Z, et al. Surface Charge Affects Cellular Uptake and Intracellular Trafficking of Chitosan-Based Nanoparticles. Biomacromolecules. 2011;12:2440–6.
55. Longfa Kou, Jin Sun, Yinglei Zhai ZH. The endocytosis and intracellular fate of nanomedicines: Implication for rational design. Asian J Pharm Sci. 2013;8:1–10.
56. Lao F, Chen L, Li W, Ge C, Qu Y, Sun Q, Zhao Y, Han D CC. Fullerene nanoparticles selectively enter oxidation-damaged cerebral microvessel endothelial cells and inhibit JNK-related apoptosis. ACS Nano. 2009;3(11):3358–68.
57. Arnida, Janát-Amsbury MM, Ray a, Peterson CM, Ghandehari H. Geometry and surface characteristics of gold nanoparticles influence their biodistribution and uptake by macrophages. Eur J Pharm Biopharm [Internet]. Elsevier B.V.; 2011 Apr [cited 2014 Jul 9];77(3):417–23. Available from: http://www.pubmedcentral.nih.gov/articlerender.fcgi?artid=3379889&tool=pmcentrez&rendertype=abstract
58. Venkataraman S, Hedrick JL, Yuin Z, Yang C, Lai P, Ee R, et al. The effects of polymeric nanostructure shape on drug delivery ☆. Adv Drug Deliv Rev [Internet]. Elsevier B.V.; 2011;63(14-15):1228–46. Available from: http://dx.doi.org/10.1016/j.addr.2011.06.016
59. Champion J, Mitragotri S. Role of target geometry in phagocytosis. Proc Natl Acad Sci [Internet]. 2006 [cited 2014 Aug 20];103:4930–4. Available from: http://www.pnas.org/content/103/13/4930.short
60. Hutter E, Boridy S, Labrecque S, Lalancette-he M, Kriz J. Microglial Response to Gold Nanoparticles. ACS Nano. 2010;4(5):2595–606.
61. Ispas C, Andreescu D, Patel A, Goia D V., Andreescu S, Wallace KN. Toxicity and developmental defects of different sizes and shape nickel nanoparticles in zebrafish. Environ Sci Technol. 2009;43(16):6349–56.
62. Chiu Y-L, Ho Y-C, Chen Y-M, Peng S-F, Ke C-J, Chen K-J, et al. The characteristics, cellular uptake and intracellular trafficking of nanoparticles made of hydrophobically-modified chitosan. J Control Release [Internet]. 2010 Aug 17 [cited 2014 Sep 1];146(1):152–9. Available from: http://www.ncbi.nlm.nih.gov/pubmed/20580915
63. Cooper GM. The Cell. Second Edi. University B, editor. Sunderland: Sinauer Associates; 2000.
64. Williams EE. Membrane Lipids : What Membrane Physical Properties are Conserved during Physiochemically-Induced Membrane Restructuring ? AMER ZOOL. 1998;290:280–90.
65. Deleu M, Crowet J-M, Nasir MN, Lins L. Complementary biophysical tools to investigate lipid specificity in the interaction between bioactive molecules and the plasma membrane: A review. Biochim Biophys Acta [Internet]. Elsevier B.V.; 2014 Aug 28 [cited 2014 Sep 2]; Available from: http://www.ncbi.nlm.nih.gov/pubmed/25175476
66. Sonnino S, Prinetti A. Membrane Domains and the " Lipid Raft " Concept. Curr Med Chem. 2013;20:4–21.
67. Meer G Van, Voelker DR, Feigenson GW. Membrane lipids : where they are and how they behave. Nat Publ Gr. 2008;9(February).
68. Heimburg T. Thermal Biophysics of Membranes. WILEY-VCH Verlag GmbH & Co. KGaA, Weinheim; 2007.
69. Singer SJ, Nicolson GL. The Fluid Mosaic Model of the Structure of Cell Membranes. Science

(80-). 1972;175:720–31.
70. Simons K, Ikonen E. Functional rafts in cell membranes. Nature. 1997;387:569–72.
71. Kusumi A, Nakada C, Ritchie K, Murase K, Suzuki K, Murakoshi H, et al. Paradigm shift of the plasma membrane concept from the two-dimensional continuum fluid to the partitioned fluid: high-speed single-molecule tracking of membrane molecules. Annu Rev Biophys Biomol Struct [Internet]. 2005 Jan [cited 2014 Jul 17];34:351–78. Available from: http://www.ncbi.nlm.nih.gov/pubmed/15869394
72. Simons K. Cell Membranes : The Lipid Perspective. Elsevier. 2011;19:1543–8.
73. Chiantia S, London E. Sphingolipids and Membrane Domains: Recent Advances. Sphingolipids: Basic Science and Drug Development, Handbook of Experimental Pharmacology. 2013. p. 33–55.
74. Yeagle P. The Membranes of Cells. San Diego: Academic Press; 1993. 349 p.
75. Eze MO. Phase Transitions in Phospholipid Bilayers: Lateral Phase Separations Play Vital Roles in Biomembranes. Biochem Educ. 1991;19(Cmc):204–8.
76. Gennis RB. Biomembranes: Molecular Structure and Function. New York, USA: Springer-Verlag; 1989.
77. Mouritsen OG. Life- As a Matter of Fat: The emerging science of lipidomics. Heidelberg, Germany: Springer-Verlag; 2005.
78. Aresta-Branco F, Cordeiro AM, Marinho HS, Cyrne L, Antunes F, de Almeida RFM. Gel Domains in the Plasma Membrane of *Saccharomyces cerevisiae*. J Biol Chem [Internet]. 2011;286(7):5043–54. Available from: http://www.jbc.org/lookup/doi/10.1074/jbc.M110.154435
79. Mouritsen OG, Zuckermann MJ. What 's So Special About Cholesterol ? Lipids. 2004;39(11):1101–13.
80. Rao M, Mayor S. Active organization of membrane constituents in living cells. Curr Opin Cell Biol [Internet]. Elsevier Ltd; 2014;29:126–32. Available from: http://dx.doi.org/10.1016/j.ceb.2014.05.007
81. Simons K, Toomre D. Lipid rafts and signal transduction. Nat Rev Mol Cell Biol [Internet]. 2000 Oct;1(1):31–9. Available from: http://www.ncbi.nlm.nih.gov/pubmed/11413487
82. Walde P, Cosentino K, Engel H, Stano P. Giant vesicles: preparations and applications. Chembiochem [Internet]. 2010 May 3 [cited 2014 Jul 12];11(7):848–65. Available from: http://www.ncbi.nlm.nih.gov/pubmed/20336703
83. van Swaay D, deMello A. Microfluidic methods for forming liposomes. Lab Chip [Internet]. 2013 Mar 7 [cited 2014 Sep 1];13(5):752–67. Available from: http://www.ncbi.nlm.nih.gov/pubmed/23291662
84. Wesołowska O, Michalak K, Maniewska J, Hendrich AB. Giant unilamellar vesicles - a perfect tool to visualize phase separation and lipid rafts in model systems. Acta Biochim Pol [Internet]. 2009 Jan;56(1):33–9. Available from: http://www.ncbi.nlm.nih.gov/pubmed/19287805
85. Zhang S, Nelson A, Beales PA. Freezing or Wrapping : The Role of Particle Size in the Mechanism of Nanoparticle − Biomembrane Interaction. Biophys J. 2012;
86. Matter S, Poveda A, Mateo CR. Immobilization and characterization of giant unilamellar vesicles (GUVs) within porous silica glasses. R Soc Chem. 2012;8:408–17.
87. Zupancic E, Carreira AC, Almeida RFM De, Silva LC. Biophysical Implications of Sphingosine Accumulation in Membrane Properties at Neutral and Acidic pH. J Phys Chem. 2014;118:4858−4866.
88. Valeur B. Molecular Fluorescence: Principles and Applications. Wiley-VCH Verlag GmbH; 2001.
89. Castro BM, Almeida RFM De, Fedorov A, Prieto M. The photophysics of a Rhodamine head

labeled phospholipid in the identification and characterization of membrane lipid phases. Chem Phys Lipids [Internet]. Elsevier Ireland Ltd; 2012;165(3):311–9. Available from: http://dx.doi.org/10.1016/j.chemphyslip.2012.02.007
90. Company EK. New coumarin dyes with rigidized structure for flashlamp-pumped dye lasers. Opt Commun. 1975;13(3):3–6.
91. Lakowicz JR. Principles of Fluorescence Spectroscopy. Third Edit. Baltimore, Maryland, USA: Springer; 2006.
92. Wagner BD. The Use of Coumarins as Environmentally-Sensitive Fluorescent Probes of Heterogeneous Inclusion Systems. Molecules. 2009;14:210–37.
93. A A-MB, M AS, S AM, Abo IMM, F ME-SL, K SAM. Photophysics and dynamics of coumarin laser dyes and their analytical implications. Proc Indian Acad Sci (Chem Sci). 1992;104(2):185–96.
94. Moreira LM, Melo MM de, Martins PA, P.Lyon J, Romani A paula, Codognoto L, et al. Photophysical Properties of Coumarin Compounds in Neat and Binary Solvent Mixtures: Evaluation and Correlation Between Solvatochromism and Solvent Polarity Parameters. J Braz Chem Soc. 2014;25(5):873–81.
95. Li D, Zhang J, Anpo M, Xue M, Liu Y. Photophysical and photochemical properties of Coumarin-6 molecules incorporated within MCM-48. Mater Lett. 2005;59:2120–3.
96. Klymchenko AS, Kreder R. Fluorescent probes for lipid rafts: from model membranes to living cells. Chem Biol [Internet]. 2014 Jan 16 [cited 2014 Oct 8];21(1):97–113. Available from: http://www.ncbi.nlm.nih.gov/pubmed/24361047
97. Alvarez-Lorenzo C, Concheiro A. Smart drug delivery systems: from fundamentals to the clinic. Chem Commun (Camb) [Internet]. 2014 Jul 25 [cited 2015 Apr 18];50(58):7743–65. Available from: http://www.ncbi.nlm.nih.gov/pubmed/24805962
98. Wikipédia. Microscopia confocal [Internet]. Available from: https://pt.wikipedia.org/wiki/Microscopia_confocal
99. Weiss J. Emulsion Processing - Homogenization. Emulsion Workshop. Amherst, MA;

100. Taghipour, B. M. Yakhchali, I. Haririan, A.M. Tamaddon, S. Samani M. The effects of technical and compositional variables on the size and release profile of bovine serum albumin from PLGA based particulate systems. Res Pharm Sci. 9:407–20.
101. Ito F, Makino K. Preparation and properties of monodispersed rifampicin-loaded poly (lactide-co-glycolide) microspheres. Elsevier. 2004;39:17–21.
102. Doshi N, Zahr AS, Bhaskar S, Lahann J, Mitragotri S. Red blood cell-mimicking synthetic biomaterial particles. Proc Natl Acad Sci. 2009;106(51):21495–9.
103. Sahoo SK, Panyam J, Prabha S, Labhasetwar V. Residual polyvinyl alcohol associated with poly (D , L -lactide-co- glycolide) nanoparticles affects their physical properties and cellular uptake. J Control Release. 2002;82:105–14.
104. Ma W, Kaushal S, Bouvet M, Kruse C, Grotjahn D, Ichim T, et al. PLGA nanoparticle-mediated delivery of tumor antigenic peptides elicits effective immune responses. Int J Nanomedicine. 2012;1475–87.
105. Florindo HF, Pandit S, Gonçalves LMD, Videira M, Alpar O, Almeida AJ. Antibody and cytokine-associated immune responses to S. equi antigens entrapped in PLA nanospheres. Biomaterials. 2009;30(28):5161–9.
106. Florindo HF, Pandit S, Gonçalves LMD, Alpar HO, Almeida a J. Streptococcus equi antigens adsorbed onto surface modified poly-epsilon-caprolactone microspheres induce humoral and cellular specific immune responses. Vaccine [Internet]. 2008 Aug 5 [cited 2015 Jun

23];26(33):4168–77. Available from: http://www.ncbi.nlm.nih.gov/pubmed/18599166
107. Hawley AE, Illum L DS. Preparation of biodegradable, surface engineered PLGA nanospheres with enhanced lymphatic drainage and lymph node uptake. Pharm Res. 1997;14:657–61.
108. Panyam J, Sahoo SK, Prabha S, Bargar T, Labhasetwar V. Fluorescence and electron microscopy probes for cellular and tissue uptake of poly(D,L-lactide-co-glycolide) nanoparticles. Int J Pharm. 2003;262(1-2):1–11.
109. Sanna V, Roggio AM, Siliani S, Piccinini M, Marceddu S, Mariani A, et al. Development of novel cationic chitosan- and anionic alginate – coated poly (d , l -lactide- co - glycolide) nanoparticles for controlled release and light protection of resveratrol. Int J Nanomedicine. 2012;5501–16.
110. Manca M-L, Mourtas S, Dracopoulos V, Fadda AM, Antimisiaris SG. PLGA, chitosan or chitosan-coated PLGA microparticles for alveolar delivery? A comparative study of particle stability during nebulization. Colloids Surf B Biointerfaces [Internet]. 2008 Apr 1 [cited 2015 Jun 20];62(2):220–31. Available from: http://www.ncbi.nlm.nih.gov/pubmed/18023977
111. Barooah N, Mohanty J, Pal H, Bhasikuttan AC. Stimulus-Responsive Supramolecular pKa Tuning of Cucurbit[7]uril Encapsulated Coumarin 6 Dye. AJ Phys Chem B. 2012;116:3683−3689.
112. Stolnik S, Garnett M., Davies M., Illum L, Bousta M, Vert M, et al. The colloidal properties of surfactant-free biodegradable nanospheres from poly(β-malic acid-co-benzyl malate)s and poly(lactic acid-co-glycolide). Colloids Surfaces A Physicochem Eng Asp. 1995;97(3):235–45.
113. Silva J, Vandermeulen G, Oliveira V, Pinto S, Rodrigues C, Salgado A, et al. Development of functionalized nanoparticles for vaccine delivery to dendritic cells: a mechanistic approach. Nanomedicine (Lond). 2014;9(17):2639–56.
114. Pongsawatmanit R, Harnsilawat T, McClements DJ. Influence of alginate, pH and ultrasound treatment on palm oil-in-water emulsions stabilized by beta-lactoglobulin. Colloids Surfaces A Physicochem Eng Asp. 2006;287(1-3):59–67.
115. An JH, Dultz S. Adsorption of tannic acid on chitosan-montmorillonite as a function of pH and surface charge properties. Appl Clay Sci. 2007;36(4):256–64.
116. Silva LC, de Almeida RFM, Castro BM, Fedorov A, Prieto M. Ceramide-domain formation and collapse in lipid rafts: membrane reorganization by an apoptotic lipid. Biophys J. 2007;92(2):502–16.
117. Lipids AP. Phase Transition Temperatures for Glycerophospholipids [Internet]. 2016 [cited 2016 Sep 25]. Available from: https://avantilipids.com/tech-support/physical-properties/phase-transition-temps/
118. Pinto SN, Fernandes F, Fedorov A, Futerman AH, Silva LC, Prieto M. A combined f uorescence spectroscopy , confocal and 2-photon microscopy approach to re-evaluate the properties of sphingolipid domains. BBA - Biomembr [Internet]. Elsevier B.V.; 2013;1828(9):2099–110. Available from: http://dx.doi.org/10.1016/j.bbamem.2013.05.011
119. Sapin A, Garcion E, Clavreul A, Lagarce F, Benoit JP MP. Development of new polymerbased particulate systems for anti-glioma vaccination. Int J Pharm. 2006;309((1-2)):1–5.
120. Holthuis JCM, Levine TP. Lipid traffic: floppy drives and a superhighway. Nat Rev Mol Cell Biol [Internet]. 2005 Mar [cited 2014 Dec 8];6(3):209–20. Available from: http://www.ncbi.nlm.nih.gov/pubmed/15738987
121. Davis A. Chapter 2: Cells 101: Business Basics [Internet]. Inside the Cell. [cited 2015 Aug 1]. Available from: http://publications.nigms.nih.gov/insidethecell/chapter2.html
122. Goñi FM, Alonso A, Bagatolli L a., Brown RE, Marsh D, Prieto M, et al. Phase diagrams of lipid mixtures relevant to the study of membrane rafts. Biochim Biophys Acta - Mol Cell Biol Lipids [Internet]. Elsevier B.V.; 2008;1781(11-12):665–84. Available from:

http://dx.doi.org/10.1016/j.bbalip.2008.09.002

Annexes

Annex 1

Excitation and emission spectra of coumarin-6 in PLGA PVA-C6-1/2/4/5 MPs, PLGA CH-C6-1/2/4/5 MPs and PLGA ALG-C6-1/2/4/5 MPs suspensions with MPs concentrations of 0.50 mg/mL, 0.40 mg/mL, 0.25 mg/mL, 0.20 mg/mL and 0.10 mg/mL.

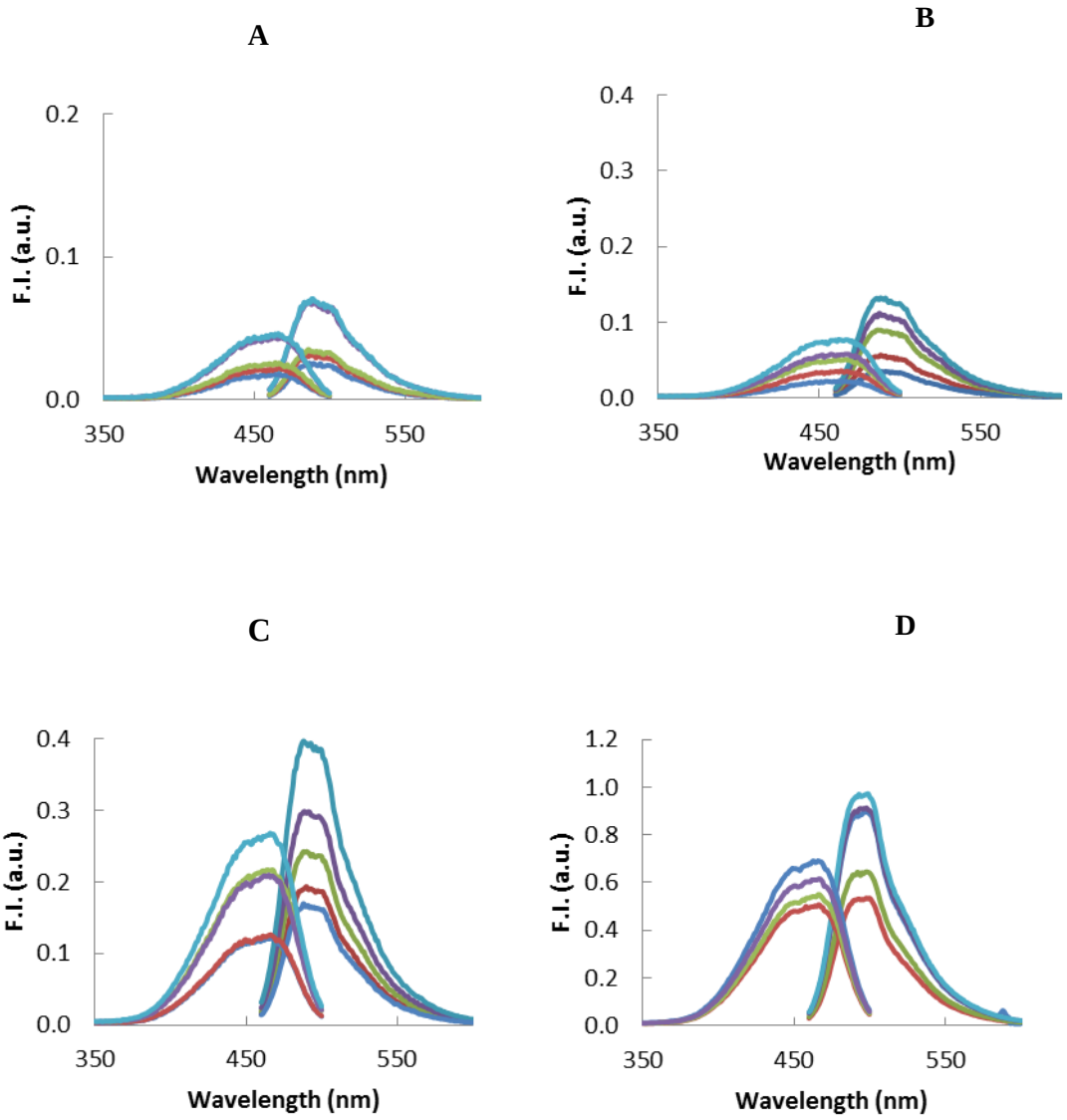

Figure A.1 Coumarin-6 excitation and emission spectra in PLGA PVA-C6 MPs labeled with 0.04, 0.1, 0.4 and 1.00 μg/mg of coumarin-6 for the different concentrations of MPs in suspension. Excitation and emission spectra of (A) PLGA PVA-C6-1 MPs, (B) PLGA PVA-C6-2 MPs, and (C) PLGA PVA-C6-4 MPs and (D) PLGA PVA-C6-5 MPs. Data for the concentrations of PLGA in suspension 0.10 mg/mL, 0.20 mg/mL, 0.25 mg/mL, 0.40 mg/mL and 0.50 mg/mL are shown in blue, red, green, purple and light blue. Data correspond to N = 1, n = 1. Measurements were performed setting λ_{em}=510 nm during the acquisition of the excitation spectra and λ_{ex} = 445 nm during the acquisition of the emission spectra. F.I. Fluorescence Intensity (a.u).

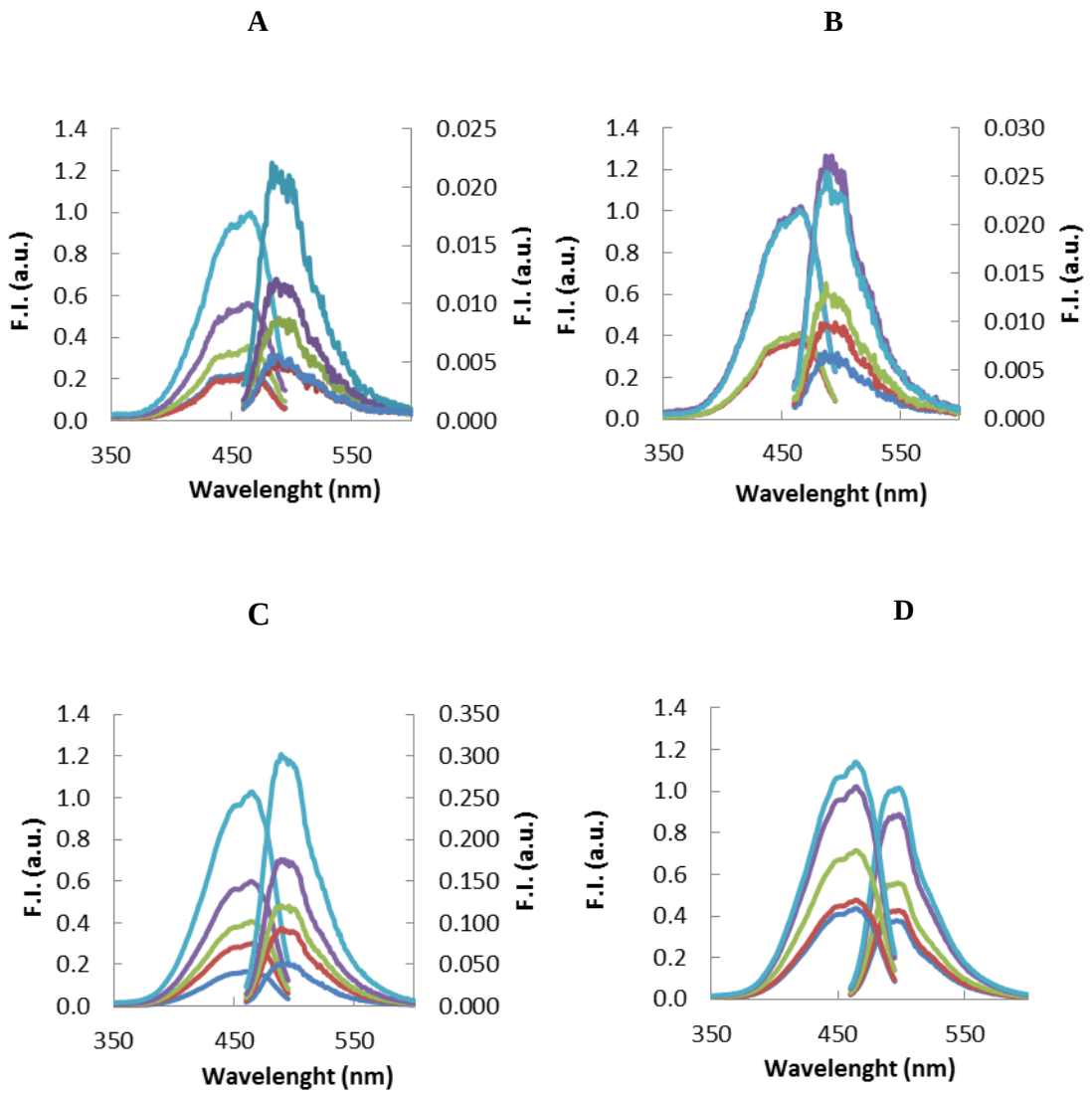

Figure A.2 Coumarin-6 excitation and emission spectra in PLGA CH-C6 MPs labeled with 0.04, 0.1, 0.4 and 1.00 μg/mg of coumarin-6 for the different concentrations of MPs in suspension. Excitation and emission spectra of (A) PLGA CH-C6-1 MPs, (B) PLGA CH-C6-2 MPs, and (C) PLGA CH-C6-4 MPs and (D) PLGA CH-C6-5 MPs. Data for the concentrations of PLGA in suspension 0.10 mg/mL, 0.20 mg/mL, 0.25 mg/mL, 0.40 mg/mL and 0.50 mg/mL are shown in blue, red, green, purple and light blue. Data correspond to N = 1, n = 1. Measurements were performed setting λ_{em}=510 nm during the acquisition of the excitation spectra and λ_{ex} = 445 nm during the acquisition of the emission spectra. F.I. Fluorescence Intensity (a.u).

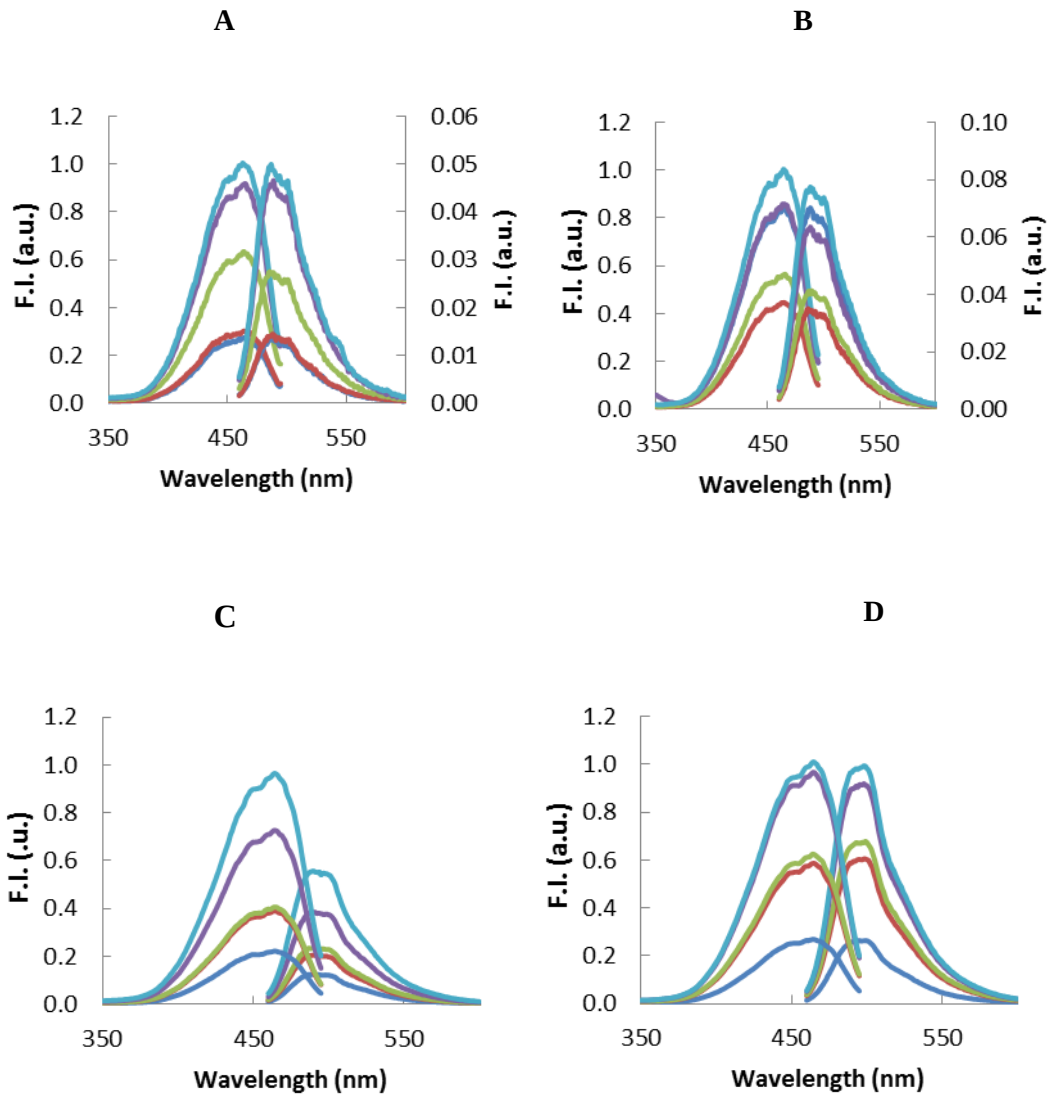

Figure A.3 Coumarin-6 excitation and emission spectra in PLGA ALG-C6 MPs labeled with 0.04, 0.1, 0.4 and 1.00 μg/mg of coumarin-6 for the different concentrations of MPs in suspension. Excitation and emission spectra of (A) PLGA ALGC6-1 MPs, (B) PLGA ALG-C6-2 MPs, and (C) PLGA ALG-C6-4 MPs and (D) PLGA ALG-C6-5 MPs. Data for the concentrations of PLGA in suspension 0.10 mg/mL, 0.20 mg/mL, 0.25 mg/mL, 0.40 mg/mL and 0.50 mg/mL are shown in blue, red, green, purple and light blue. Data correspond to N = 1, n = 1. Measurements were performed setting λ_{em}=510 nm during the acquisition of the excitation spectra and λ_{ex} = 445 nm during the acquisition of the emission spectra. F.I. Fluorescence Intensity (a.u).

Normalized excitation and emission spectra of coumarin-6 in PLGA PVA-C6-1/2/4/5 MPs, PLGA CH-C6-1/2/4/5 MPs and PLGA ALG-C6-1/2/4/5 MPs suspensions with MPs concentrations of 0.50 mg/mL, 0.40 mg/mL, 0.25 mg/mL, 0.20 mg/mL and 0.10 mg/mL.

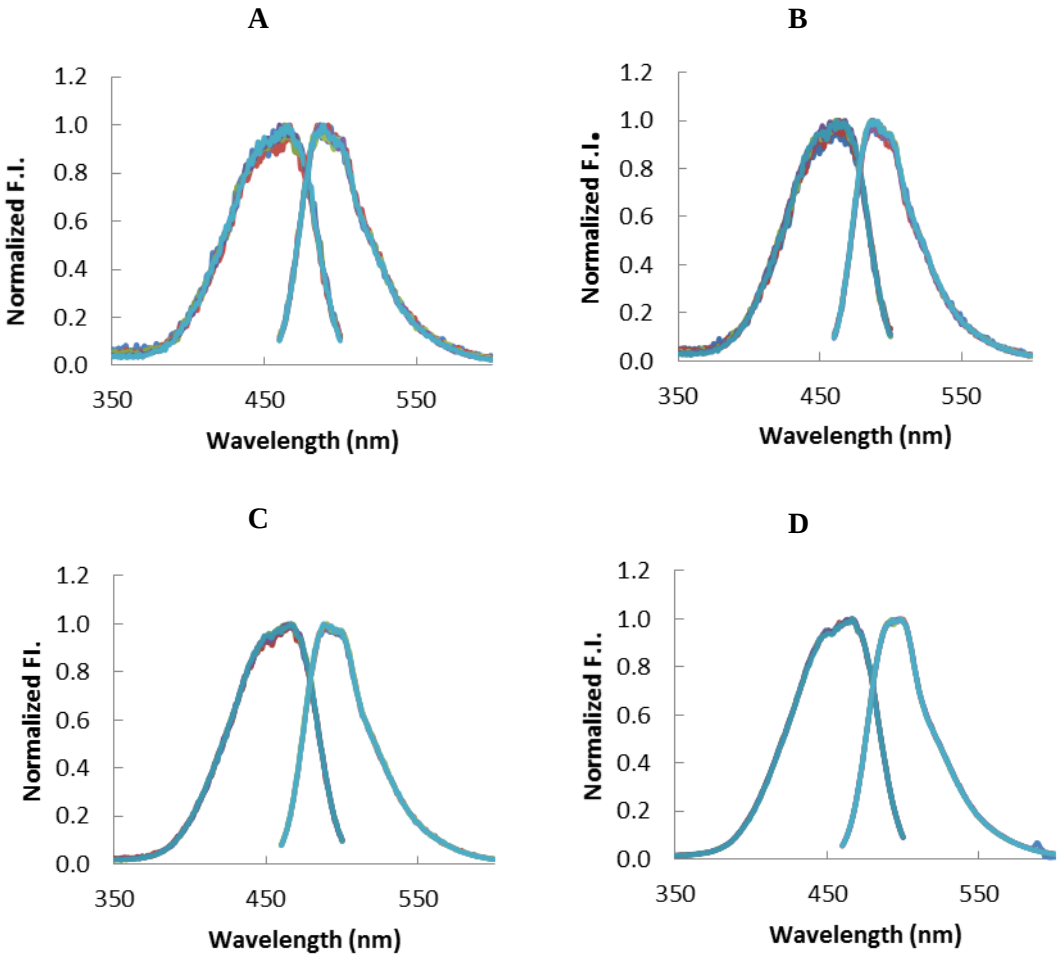

Figure A.4 Coumarin-6 normalized excitation and emission spectra in PLGA PVA-C6 MPs labeled with 0.04, 0.1, 0.4 and 1.00 μg/mg of coumarin-6 for the different concentrations of MPs in suspension. Excitation and emission spectra of (A) PLGA PVA-C6-1 MPs, (B) PLGA PVA-C6-2 MPs, and (C) PLGA PVA-C6-4 MPs and (D) PLGA PVA-C6-5 MPs. Data for the concentrations of PLGA in suspension 0.10 mg/mL, 0.20 mg/mL, 0.25 mg/mL, 0.40 mg/mL and 0.50 mg/mL are shown in blue, red, green, purple and light blue. Data correspond to N = 1, n = 1. Measurements were performed setting λ_{em}=510 nm during the acquisition of the excitation spectra and λ_{ex} = 445 nm during the acquisition of the emission spectra. F.I. Fluorescence Intensity (a.u).

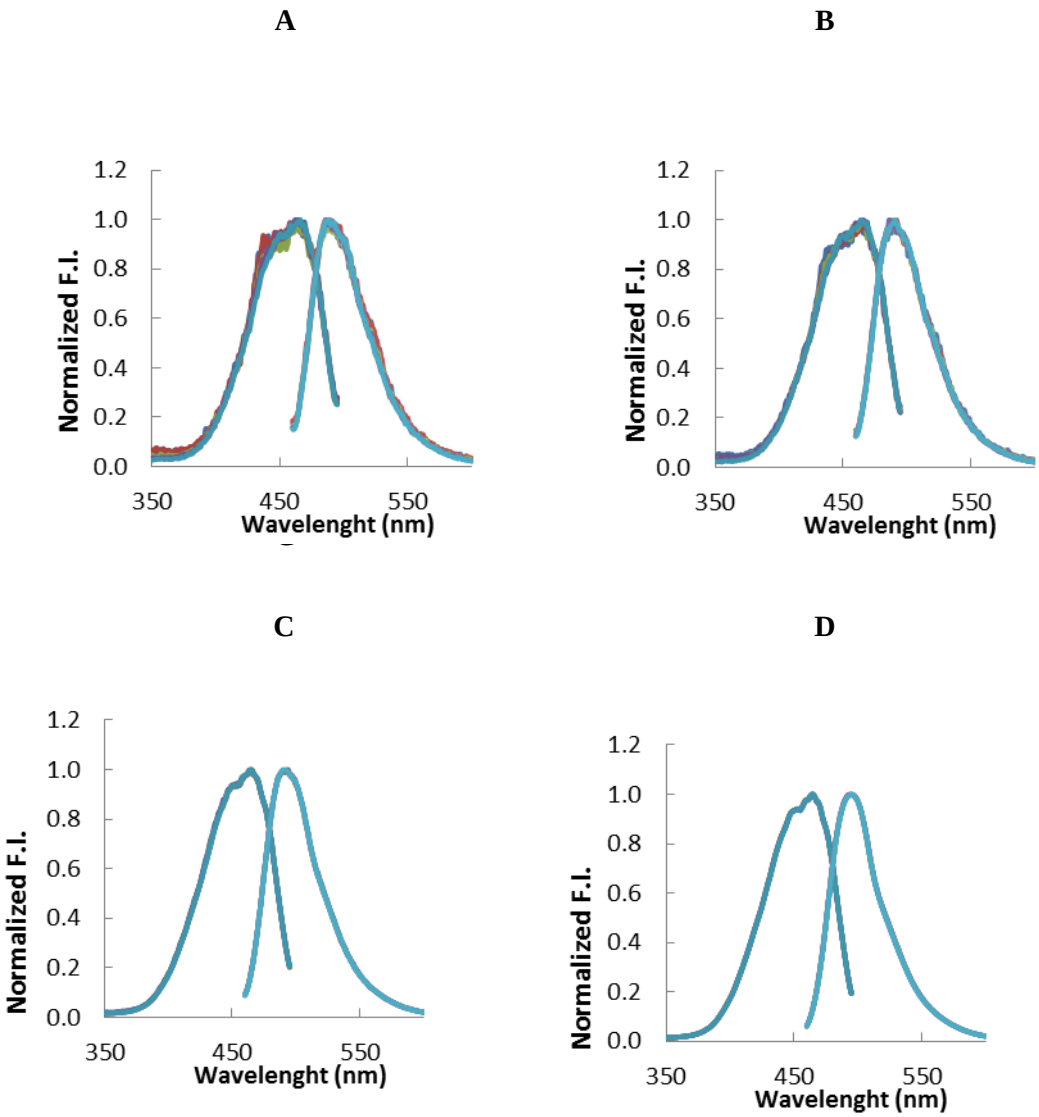

Figure A.5 Coumarin-6 normalized excitation and emission spectra in PLGA CH-C6 MPs labeled with 0.04, 0.1, 0.4 and 1.00 μg/mg of coumarin-6 for the different concentrations of MPs in suspension. Excitation and emission spectra of (A) PLGA CH-C6-1 MPs, (B) PLGA CH-C6-2 MPs, and (C) PLGA CH-C6-4 MPs and (D) PLGA CH-C6-5 MPs. Data for the concentrations of PLGA in suspension 0.10 mg/mL, 0.20 mg/mL, 0.25 mg/mL, 0.40 mg/mL and 0.50 mg/mL are shown in blue, red, green, purple and light blue. Data correspond to N = 1, n = 1. Measurements were performed setting λ_{em}=510 nm during the acquisition of the excitation spectra and λ_{ex} = 445 nm during the acquisition of the emission spectra. F.I. Fluorescence Intensity (a.u).

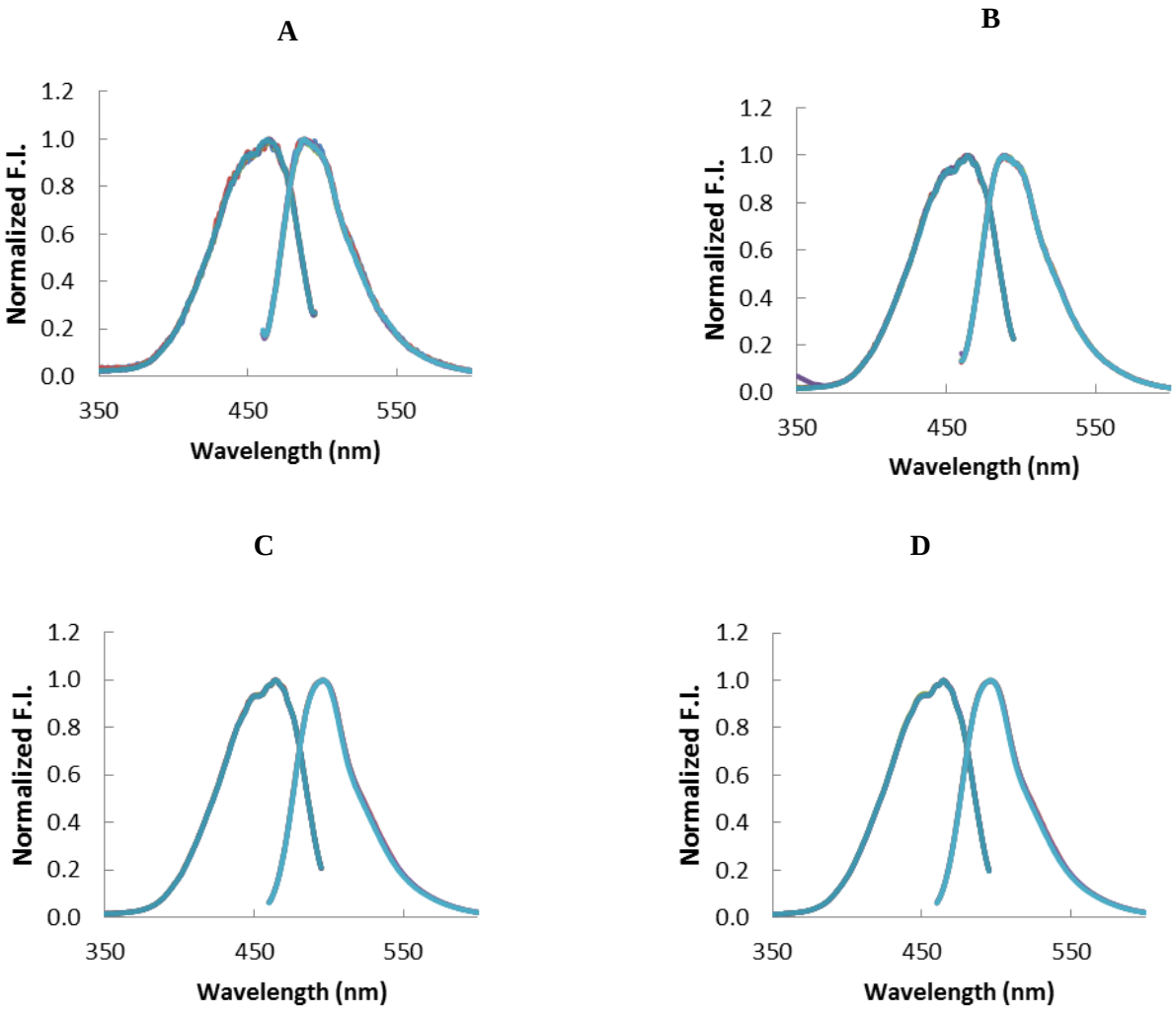

Figure A.6 Coumarin-6 normalized excitation and emission spectra in PLGA ALG -C6 MPs labeled with 0.04, 0.1, 0.4 and 1.00 μg/mg of coumarin-6 for the different concentrations of MPs in suspension. Excitation and emission spectra of (A) PLGA ALG-C6-1 MPs, (B) PLGA ALG -C6-2 MPs, and (C) PLGA ALG -C6-4 MPs and (D) PLGA ALG -C6-5 MPs. Data for the concentrations of PLGA in suspension 0.10 mg/mL, 0.20 mg/mL, 0.25 mg/mL, 0.40 mg/mL and 0.50 mg/mL are shown in blue, red, green, purple and light blue. Data correspond to N = 1, n = 1. Measurements were performed setting λ_{em}=510 nm during the acquisition of the excitation spectra and λ_{ex} = 445 nm during the acquisition of the emission spectra. F.I. Fluorescence Intensity (a.u).

Annex 2

Emission spectra of PLGA PVA-C6-1/2/4/5 MPs, PLGA CH-C6-1/2/4/5 MPs and PLGA ALG-C6-1/2/4/5 MPs suspensions with MPs concentrations of 0.50 mg/mL, 0.40 mg/mL, 0.25 mg/mL, 0.20 mg/mL and 0.10 mg/mL.

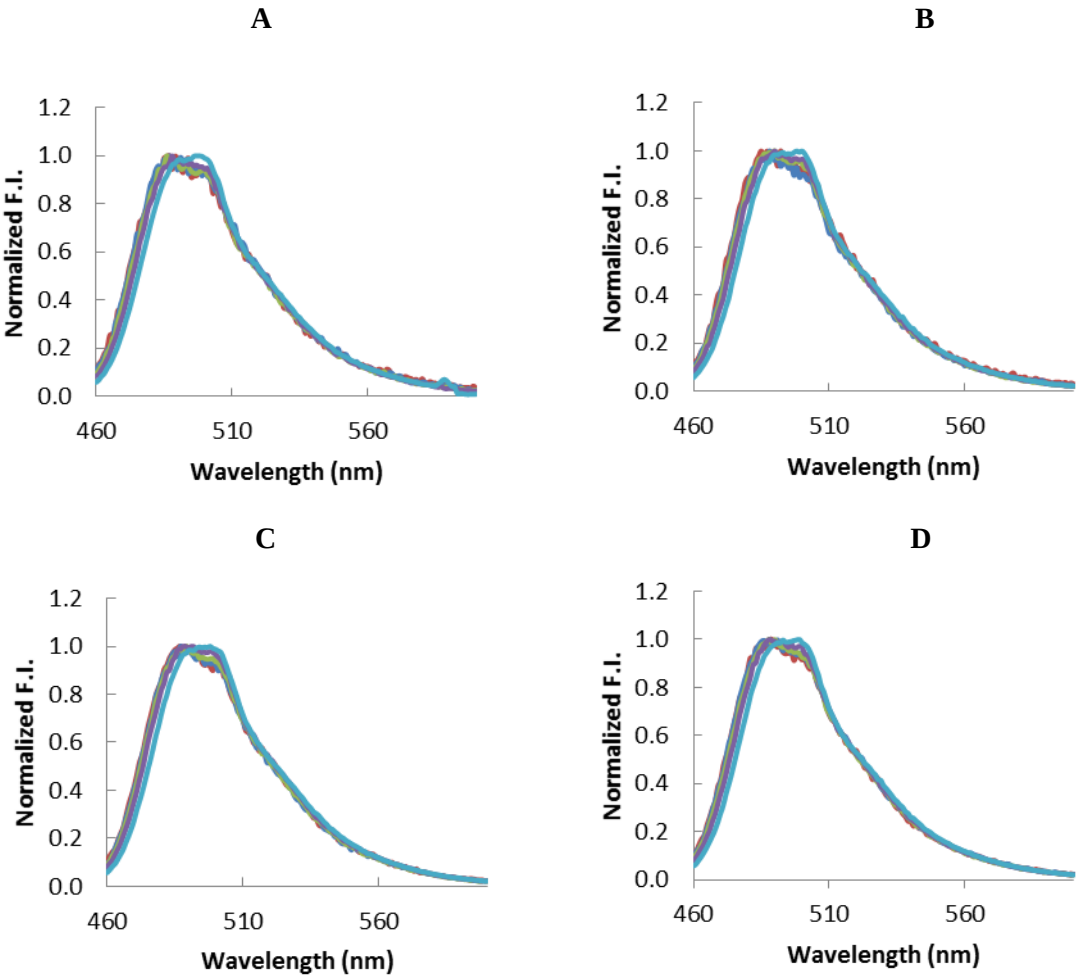

Figure A.7 Coumarin-6 normalized spectra in PLGA PVA-C6 MPs suspensions with concentration of MPs (A) 0.1 μg/mL, (B) 0.2 mg/mL, (C) 0.4 mg/mL and (D) 0.5 mg/mL labeled with coumarin-6 different concentrations of coumarin-6. Data for the concentrations of coumarin-6 0.04 μg/mg, 0.1 µg/mg, 0.2 μg/mg, 0.4 μg/mg and 1 μg/mg are shown in blue, red, green, purple and light blue. Data correspond to N = 1, n = 1. Measurements were performed setting λ_{ex} = 445 nm during the acquisition of the emission spectra. F.I. Fluorescence Intensity (a.u.).

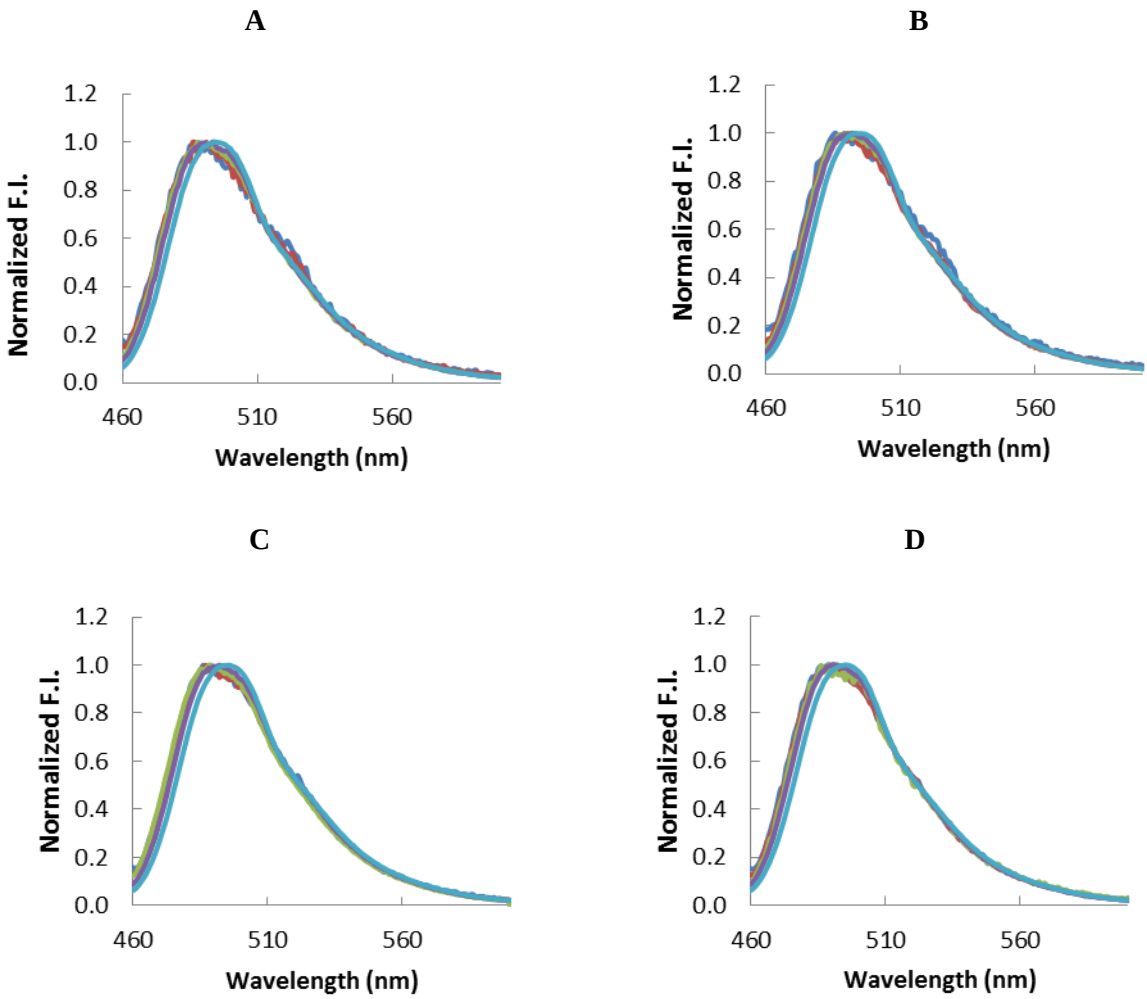

Figure A.8 Coumarin-6 normalized spectra in PLGA CH-C6 MPs suspensions with concentration of MPs (A) 0.1 μg/mL, (B) 0.2 mg/mL, (C) 0.4 mg/mL and (D) 0.5 mg/mL labeled with coumarin-6 different concentrations of coumarin-6. Data for the concentrations of coumarin-6 0.04 μg/mg, 0.1 μg/mg, 0.2 μg/mg, 0.4 μg/mg and 1 μg/mg are shown in blue, red, green, purple and light blue. Data correspond to N = 1, n = 1. Measurements were performed setting λ_{ex} = 445 nm during the acquisition of the emission spectra. F.I. Fluorescence Intensity (a.u.).

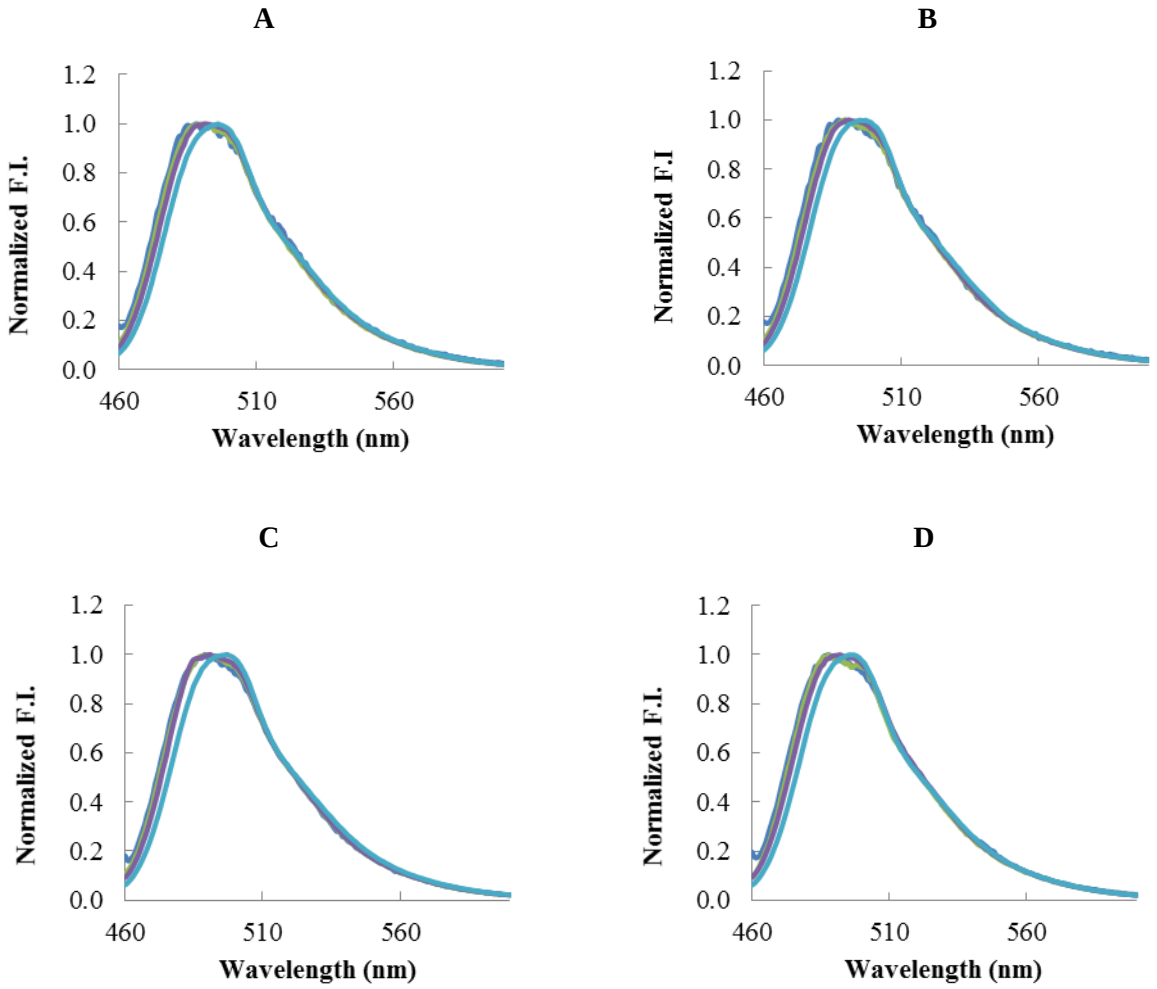

Figure A.9 Coumarin-6 normalized spectra in PLGA ALG-C6 MPs suspensions with concentration of MPs (A) 0.1 μg/mL, (B) 0.2 mg/mL, (C) 0.4 mg/mL and (D) 0.5 mg/mL labeled with coumarin-6 different concentrations of coumarin-6. Data for the concentrations of coumarin-6 0.04 μg/mg, 0.1 μg/mg, 0.2 μg/mg, 0.4 μg/mg and 1 μg/mg are shown in blue, red, green, purple and light blue. Data correspond to N = 1, n = 1. Measurements were performed setting λ_{em}=510 nm during the acquisition of the excitation spectra and λ_{ex} = 445 nm during the acquisition of the emission spectra. F.I. Fluorescence Intensity (a.u.).

Annex 3

Variation of the $\lambda_{em\ max}$ of PLGA PVA-C6 MPs, PLGA CH-C6 MPs and PLGA ALG-C6 MPs as a function of concentration of coumarin-6

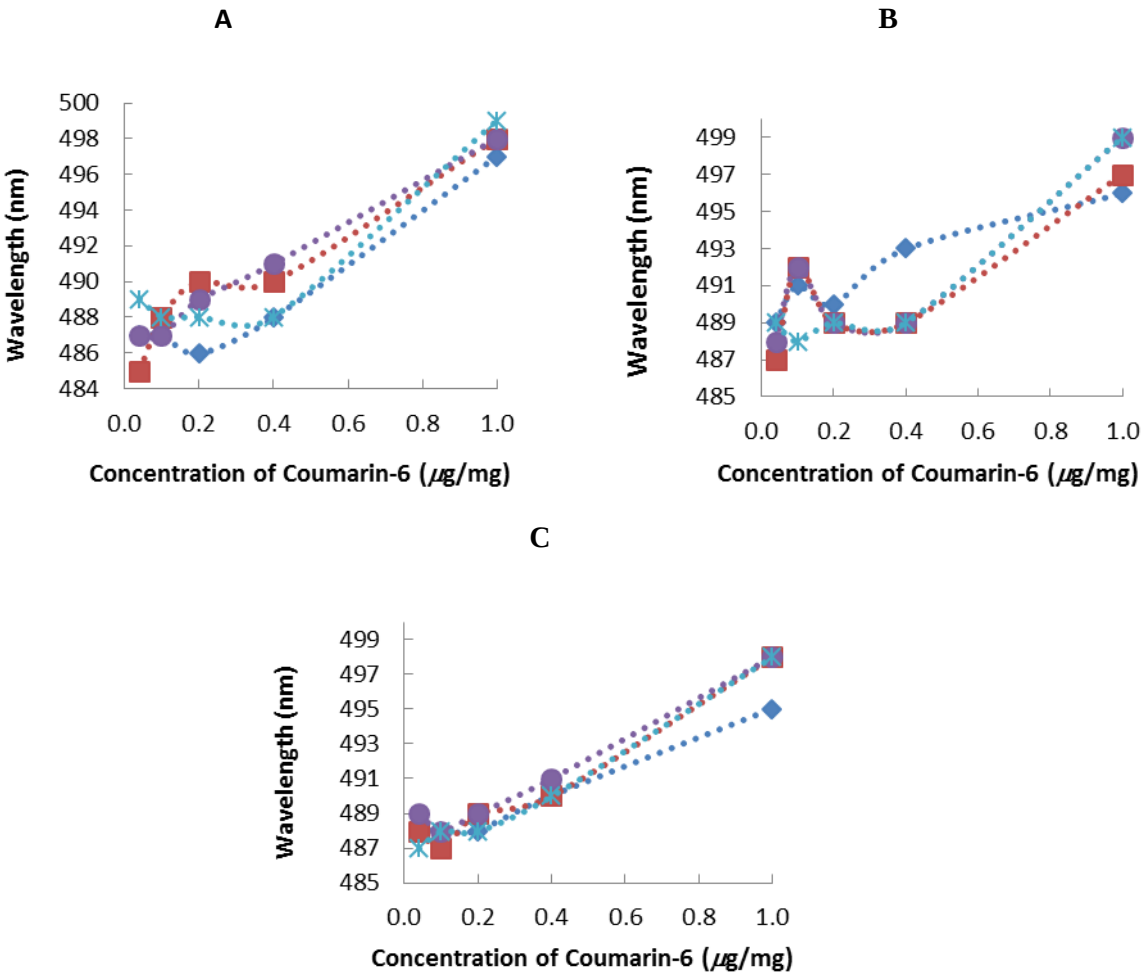

Figure A.10 Variation of λ_{em} with the concentration of coumarin-6 in (A) PLGA PVA-C6 MPs, (B) PLGA CH-C6 MPs and (B) PLGA ALG-C6 MPs. Data for the concentrations of MPs in suspension 0.10 mg/mL, 0.20 mg/mL, 0.40 mg/mL and 0.50 mg/mL are shown in blue, red, green, purple and light blue. Data correspond to N = 1, n = 1.